Global Modelling of Secondary Aerosol

Ananth Ranjithkumar

Submitted in accordance with the requirements for the degree of Doctor of Philosophy

University of Leeds
School of Earth and Environment

March 3rd, 2022

Declaration of Authorship

The candidate confirms that the work submitted is his own, except where work which has formed part of jointly authored publications has been included. The contribution of the candidate and the other authors to this work has been explicitly indicated below. The candidate confirms that appropriate credit has been given within the thesis where reference has been made to the work of others.

The contents of Chapter 2 are from a jointly authored publication in *Atmospheric Chemistry and Physics, 2021*, titled "**Constraints on global aerosol number concentration, SO_2 and condensation sink in UKESM1 using ATom measurements**" (Ranjithkumar et al., 2021). Co-authors Christina Williamson, Agnieska Kupc, Andrew Rollins and Charles Brock helped with collecting and understanding the observations used in this study. Co-authors Hamish Gordon and Ken Carslaw helped with the scientific guidance and editing of the manuscript. My role involved running the model simulations, performing the analysis of the model and observation data, and the writing of the manuscript.

Chapter 3 focuses on research work which is yet to be submitted for publication, titled "Climatic effect of new particle formation" (Ranjithkumar et al 2022, to be submitted). Co-authors Hamish Gordon and Ken Carslaw helped with scientific guidance and reviewing of the manuscript. Co-Author Xuemei Wang helped with the implementation of an ion-induced pure biogenic nucleation scheme into the model. The candidate carried out the necessary simulations, analysis and drafting of the manuscript.

The analysis in Chapter 4 pertains to a jointly authored publication titled "**Large contribution to secondary organic aerosol from isoprene cloud chemistry**" (Lamkaddam et al., 2021). The Co-authors carried out the experimental work which improves our understanding of aqueous phase isoprene chemistry. My role was to implement the experimental findings into a climate model (UKESM1) and quantify the global importance of isoprene cloud chemistry.

Acknowledgements

Firstly, I would like to thank my supervisors: Prof. Ken Carslaw and Dr. Hamish Gordon for their guidance and support during my PhD. I am grateful for the opportunity they gave me to pursue my PhD at Leeds, which for the most part has been a lot of fun, I made so many new friends and I had a blast.

I want to acknowledge that this research has been supported by the H2020 Marie Sklodowska-Curie Actions Grant (grant number 764991. CLOUD-MOTION). I would like to thank the CLOUD consortium for exposing me to a diverse group of talented people from whom I learnt so much. Giving me the opportunity to be part of the project and participate in the experiment at CERN was insightful and a character-building experience.

I would like to thank every member of the aerosol group, for being a fun group to be a part of. I especially would like to thank Amy Peace and Ben Silver for being great friends and making my time at Leeds enjoyable.

Abstract

Secondary aerosols are an important part of the climate system that affects the earth's radiation budget by scattering and absorbing solar radiation, and by influencing the microphysical properties of clouds. In this thesis, the UK Earth system model (UKESM1) is used to evaluate aerosol sources and sinks, and highlight their importance and deficiencies in reproducing aerosol and precursor vapor profiles, and we evaluate their influence on global climate.

Understanding the vertical distribution of aerosol helps to reduce the uncertainty in the aerosol life cycle and therefore in the estimation of the direct and indirect aerosol forcing. In Chapter 2, the UKESM1 model is compared to ATom (Atmospheric Tomography Mission) aircraft observations in terms of joint biases in the vertical profile of three variables related to new particle formation: total particle number concentration (N_{Total}), sulphur dioxide (SO_2) mixing ratio and the condensation sink. The N_{Total}, SO_2 and condensation sink are interdependent quantities and have a controlling influence on the vertical profile of each other; therefore, analysing them simultaneously helps to avoid getting the right answer for the wrong reasons. The simulated condensation sink in the baseline model is within a factor of 2 of observations, but the N_{Total} and SO_2 show much larger biases mainly in the tropics and high latitudes. A series of model sensitivity tests were carried out, to identify atmospheric processes that have the strongest influence on overall model performance. We find that perturbations to boundary layer nucleation, sub-3nm aerosol particle growth, cloud droplet pH and DMS emissions reduce the boundary layer and upper tropospheric model bias simultaneously. A simulation including all these modifications to the baseline version of UKESM1 has a much better SO_2 and

condensation sink vertical profile which agrees very well with observations, however the N_{Total} profile still shows large deviations especially in the upper troposphere-tropics (bias is a factor of ~4). The biases in N_{Total} could not be reduced further with the parameter perturbations used in this study and we hypothesize that there could be a structural issue with how nucleation, gas/particle transport or aerosol scavenging are handled in the model.

In Chapter 3, we quantified the importance of nucleation or new particle formation (NPF) as a source of aerosol and its influence on global climate. We estimate that nucleation causes a planetary cooling of 2.45 W/m^2, which exceeds the global warming effect of all atmospheric methane. A planet without nucleation would have 33% fewer cloud droplets, 8% reduction in liquid water path and 3% reduction in cloud fraction. NPF also damps cloud responses to changes in primary aerosol emission. In a preindustrial environment, NPF was found to damp the radiative effect of doubling fire emissions by a factor of 20.

In Chapter 4 Using UKESM1, we studied the importance of secondary organic aerosol produced from aqueous phase isoprene chemistry (aqSOA). We estimate that isoprene cloud chemistry contributes to 20% of the global SOA budget. The radiative effect of aqSOA varies regionally, which is about $-0.5W/m^2$ and $-0.3W/m^2$ over parts of South America and Africa respectively. AqSOA is predominant at lower altitudes with its concentration reaching 50 $\mu g/m^3$ at 2 km altitude. The default version of UKESM does not have a gas and aqueous phase SOA production mechanisms from isoprene, and the SOA yield from monoterpenes is scaled up a factor of 2 to account for deficiencies such as the lack of anthropogenic SOA and semi-volatile SOA. We

compare a simulation with gas and aqueous phase isoprene SOA mechanisms incorporated into UKESM1, against the default UKESM1 simulation with no isoprene SOA (but has a monoterpene SOA scaling factor of 2). Gas and aqueous Isoprene SOA simulation accounts for -0.11 W/m^2 of the earth's radiation budget globally (when compared to the default UKESM1 simulation), with regional effects of up to -2.0 W/m^2 over South America, Africa, and Australia.

Table of Contents

List of Tables

List of Figures

Abbreviations

N_{Total} : Total aerosol number concentration

SO_2: sulphur dioxide

CLOUD: Cosmics leaving outdoor droplets

ATom: Atmospheric Tomography mission

DMS: dimethyl sulphide

COS: carbonyl sulphide

UKESM: United Kingdom Earth System Model

CDNC: Cloud droplet number concentration

LWP: Liquid Water Path

SOA: Secondary Organic Aerosol

NPF: New particle formation

ARI: Aerosol radiation interactions

ACI: Aerosol Cloud Interactions

OA: Organic Aerosol

LWC: Liquid water content

t_{gas}SOA: SOA formed from monoterpenes in the gas phase

i_{gas}SOA: SOA formed from isoprene in the gas phase

aqSOA: SOA formed from isoprene in the aqueous phase

HOMs: Highly oxygenated organic molecules

Chapter 1 - Introduction

1.1 Introduction

An aerosol is a suspension of liquid or solid particles in a gas, with particle diameters in the range of a few nanometers up to a few micrometers. Understanding the chemistry and physics of different atmospheric aerosol particles is crucial to evaluate the impact they have on global climate and human health. Atmospheric aerosol particles can originate either from natural processes in the earth system, or from anthropogenic activity. Aerosol particles affect the global energy balance by directly scattering and absorbing solar radiation, and indirectly by their ability to act as cloud condensation nuclei (CCN), which changes the microphysical properties of clouds. The direct and indirect effect of aerosols on global climate have been identified as the largest source of uncertainty in the assessment of anthropogenic radiative forcing (Bellouin et al., 2020). The direct radiative effect by aerosol particles is dependent on factors like their size, shape and refractive index, which influence their ability to scatter and absorb solar radiation. The indirect effect is dependent on aerosol particles behaving as CCN or forming CCN, which is influenced by the particle's hygroscopicity and size distribution. The number concentration of various atmospheric aerosol particles is dependent on the sources; primary emissions and secondary sources (new particle formation and particle growth), sinks (scavenging, wet and dry deposition) and transport (convection and advection) through the atmosphere.

The sources of aerosols in the atmosphere are either natural or anthropogenic. Aerosols in the atmosphere can be characterised more broadly as primary and

secondary aerosols. Primary aerosol particles are emitted from the Earth's surface and, secondary aerosol particles are formed from gas-to-particle conversion ('nucleation') of gaseous precursors and condensation of gaseous precursors onto pre-existing aerosol. These gaseous precursors are usually low volatility compounds formed via the gas-phase oxidation of precursors. Improving our understanding and representation of both primary and secondary aerosols in models helps to reduce the uncertainty in the aerosol forcing and therefore improves the accuracy of climate projections.

1.2 Aerosol Sources and types

The main constituents of atmospheric aerosols particles are organic species, black carbon (BC), inorganic species (like sulphate, nitrate, ammonia, sea salt) and mineral species (like dust). Aerosol particles can originate from urban, marine, volcanic, stratospheric and biogenic sources, and they can have different chemical and physical properties depending on the type of environment they originate from. Natural sources include emissions from ocean, soils, fires, vegetation, and volcanoes. Anthropogenic emissions are largely from anthropogenic fires, agricultural activity, and the combustion of fossil fuels and biofuels.

1.2.1 Secondary sulphate and nitrate aerosol

Sulphur and nitrogen-containing atmospheric species originate from both natural and anthropogenic sources, and these compounds can participate in the formation of secondary aerosols. Sulphur-containing compounds like SO_2, dimethyl sulphide (DMS) and carbonyl sulphide (OCS) are important precursors for aerosol formation and growth in the atmosphere. SO_2 emitted directly over most land regions originates primarily from anthropogenic activity (McDuffie et al., 2020), DMS is mainly emitted by from phytoplankton in marine regions (Lovelock et al., 1972), and COS is most

abundant sulphur-containing compound in the atmosphere (Bandy et al., 1992; Brühl et al., 2012; Mihalopoulos et al., 1991; Montzka et al., 2007) formed mainly from biomass burning (Crutzen et al., 1979) and from the oxidation of DMS or carbon disulphide emitted from the ocean (Kettle et al., 2002). These precursor gases are oxidised in the atmosphere forming compounds like H_2SO_4 which have a low vapor pressure. Sulphuric acid molecules can cluster together with water molecules (via nucleation, described in section 1.3.1) forming molecular clusters which then grow to form aerosol particles (via condensation, described in section 1.3.2).

Nitrogen-containing compounds in the atmosphere like ammonia, amines and nitric acid also participate in secondary aerosol formation. Ammonia is found to participate in the H_2SO_4-H_2O cluster formation as well, and is found to increase the rate of formation of the cluster by up to a factor of 1000 under atmospheric conditions (Kirkby et al., 2011). Amines are found to further enhance the NH_3-H_2SO_4-H_2O molecular cluster formation by up to a factor of 1000 (Almeida et al., 2013). Nitric acid is also capable of nucleating with ammonia to form new atmospheric particles (Wang et al., 2020).

1.2.2 Secondary organic aerosol

Biogenic volatile organic compounds (BVOCs) like monoterpenes emitted from the terrestrial biosphere can participate in the formation of aerosol particles. Their emissions are dependent on the type of vegetation, soil humidity, temperature, CO_2 concentration and solar radiation (Guenther et al., 2012). These BVOCs can be oxidised by ozone and hydroxyl radical to form oxidation products with different volatilities (Donahue et al., 2011). A class of these oxidation products which are highly oxygenated (knows as highly oxygenated organic molecules or HOMs), has a very low volatility and can form new particles and grow pre-existing aerosols to larger

sizes, thereby forming secondary organic aerosol (SOA). Globally, a majority of the SOA is of biogenic origin, with anthropogenic sources being equally as important at northern mid latitudes (De Gouw and Jimenez, 2009). Studies also show that SOA formation is enhanced in the presence of high NOx concentrations and high anthropogenic primary organic aerosol which aides in the conversion of HOMs to the particle phase (Carlton et al., 2010; Heald et al., 2011; Hoyle et al., 2011).

1.2.3 Primary Aerosol

Sea spray is a prominent primary aerosol source, produced by bubble bursting at the sea surface caused by breaking waves. The sea spray emission flux to the atmosphere depends on the wind speed, atmospheric stability, temperature and composition of sea water. The composition of sea spray particles is mainly sea salt and marine primary organic matter, with the latter found mainly in smaller particles (< 200nm) (Leck and Bigg, 2008; Russell et al., 2010). There are significant uncertainties associated with the source and composition of sea spray aerosol which directly translates into uncertainties in the marine aerosol number concentration (Regayre et al., 2020). Marine ecosystems are also an important source of precursor vapours like DMS, which is oxidised to form sulphuric acid and methane sulphonic acid (MSA) which can form new aerosol particles and grow sea spray aerosol to larger sizes.

Mineral dust aerosol is formed via the disintegration of aggregates following creeping and saltation of larger soil particles over arid surfaces like desert regions (Chen et al., 2018; Ginoux et al., 2012). The dust emission flux into the atmosphere depends on the wind speed and many soil related factors like moisture, texture and vegetation cover. Anthropogenic sources of dust also exist which includes road dust and mineral dust due to land use change, which are poorly quantified.

Primary aerosol can also be generated from the burning of biomass via the incomplete combustion of organic matter. Biomass burning aerosol can be divided into organic carbon and black carbon, with black carbon having a very high carbon content. Biomass burning can happen naturally or anthropogenically and can also result in volatile organic compounds and SO_2 being emitted, which can act as precursor vapour for aerosol formation. Black carbon, unlike sulphate aerosol, absorbs sunlight and has a net warming effect on the planet (Samset et al., 2014). Black carbon deposited on snow lowers the snow albedo and enhances snow and ice melting (Hansen and Nazarenko, 2004; Warren and Wiscombe, 1980). The warming effect of BC can also impact clouds by influencing atmospheric stability and relative humidity (Ackerman et al., 2000; Johnson et al., 2004).

1.3 Aerosol Processes

The climatic importance of aerosols discussed in section 1.1 justifies the need to better understand atmospheric processes that control the aerosol size distribution and its radiative effect. In the subsections below we give a brief description of relevant atmospheric processes.

1.3.1 Nucleation

Nucleation or new particle formation (NPF) is an atmospheric process by which low-volatility vapour molecules form molecular clusters, which can then grow to form aerosol particles (McMurry and Friedlander, 1979; Vehkamäki and Riipinen, 2012). NPF occurs in two stages. the first stage involves the formation of a critical nucleus during the phase transformation from vapor to a liquid or solid. The second stage involves the growth of the critical nucleus to a larger size (>3nm), that competes with its removal by pre-existing aerosol. There is a decrease in enthalpy and entropy when nucleation occurs. For nucleation to occur spontaneously, the free energy barrier

needs to be overcome ($\Delta G > 0$). Another limitation to the growth of the molecular clusters is the elevated vapor pressure over their surface (Kelvin effect). The mechanism of nucleation has been widely investigated and, classical nucleation theory is a well-known theoretical framework that considers the thermodynamics and kinetics of nucleation. Classical nucleation theory however makes assumptions to estimate the Gibbs free energy barrier, as an example it doesn't consider the possibility of acid-base stabilization of the nucleated cluster. The best way to improve upon classical nucleation theory is to directly measure the Gibbs free energy changes in cluster formation, density, and surface tension of newly formed particles. Experiments in the past (Hanson and Lovejoy 2006, froyd and Lovejoy 2003, 2004) have conducted thermodynamic measurements of prenucleated sulfuric acid charged and uncharged clusters. However, the concentrations and lifetimes of nucleated clusters were extremely low, therefore the measurements of the change Gibbs free-energy from monomer to critical clusters is challenging and is an area for future research.

Our molecular understanding of NPF has evolved significantly over the last decade. Past studies show that ions, organic compounds, nitric acid, iodic acid, amines and ammonia play a role in NPF (He et al., 2021; Pierce, 2017; Wang et al., 2020). Nucleation has been observed extensively in the free-troposphere, coastlines, urban areas and forest (Kerminen et al., 2018a). Experimental studies like the CLOUD (Cosmics Leaving OUtdoor Droplets) experiment are dedicated to better understand nucleation with several research papers published dedicated to understanding novel nucleation mechanisms in the atmosphere (Dunne et al., 2016; Kirkby et al., 2011, 2016; Riccobono et al., 2014; Tröstl et al., 2016). Nucleation has been shown to

contribute to half of the CCN in the present-day atmosphere and about 2/3rd of the particles in the pre-industrial climate (Gordon et al., 2017; Merikanto et al., 2009).

1.3.2 Condensation and Coagulation

Condensation is a process whereby low volatility vapor molecules condense onto aerosol particles and grows these particles to larger sizes. Various pre-cursor vapour molecules can have different rates of condensation onto aerosol particle surfaces, which drives particle growth at varying rates. As an example, regions like the amazon rain forest and boreal forests see substantial biogenic emissions, whose oxidation products primarily drives aerosol growth in the region. The oxidation products from biogenic compounds can have a range of volatilities (Donahue et al., 2011) which influences their partitioning into the aerosol phase. Aerosol particles that can get activated to form cloud droplets at a given vapor supersaturation are called cloud condensation nuclei (CCN). The supersaturation of the vapor and the chemical composition of the dry aerosol determines the activation size above which aerosols get activated to form cloud droplets.

Aerosol particles can also come into contact with each other as a consequence of Brownian motion or their motion due to hydrodynamic, gravitational, electrical or other forces. Aerosol particles can collide with each other and coagulate to form larger aerosol particles. The growth of nucleated particles droplets is driven by condensation, and coagulation is an important atmospheric process when aerosol concentrations are high, especially near source regions and is the main sink for nucleated aerosol particles (Pierce and Adams, 2007). Observations of nucleation, condensational growth and coagulation of aerosol particles have been reported in past studies (Kerminen et al., 2018a; Kulmala and Kerminen, 2008; Lee et al., 2019; Williamson et al., 2019) and influences aerosol concentrations globally.

1.3.3 In-Cloud Aerosol Processing/ Cloud processing

Cloud processing is defined here to be the aerosol particle growth caused by the uptake and chemical reaction of gases whilst the particles exist as water droplets in non-precipitating clouds. Soluble atmospheric species can dissolve and react within a cloud droplet affecting its composition. The dissolution process involves mass transfer from the gas phase to the aqueous phase, and some of dissolved molecules can react further to form oxidation products inside the cloud droplet. As an example, SO_2 is oxidised in the aqueous phase within a cloud droplet to form sulphate which adds to the aerosol mass when the droplet evaporates. Some of the chemical reactions occurring within a cloud droplet can be strongly dependent on the pH of the aqueous phase. Global models like the UK Earth system model (UKESM) represent the cloud droplet pH as a constant value rather than it being parametrised. This can lead to biases in aerosol mass and size distribution (Ranjithkumar et al., 2021). Aerosols can also coagulate with liquid cloud droplets, which leads to an increase of soluble and insoluble material within a cloud droplet (Pierce and Adams, 2007). Cloud droplets can also coagulate with each other. Thus, cloud processing can regulate the aerosol size distribution, mixing state, and chemical composition of aerosol particles.

1.3.4 Wet Deposition

Wet deposition is the main sink for soluble species in the atmosphere. This includes processes like auto conversion (drizzle drops formed by self-collection of cloud droplets), accretion (growth of rain drops by collecting cloud droplets) and the scavenging that occurs by precipitating rain drops. If cloud droplets grow to become raindrops, the cloud starts precipitating and the aerosol matter within the falling raindrops are scavenged. However, if the rain droplets are too small (i.e 10μm to 20μm), the reevaporation of these droplets could also occur, thereby releasing the

aerosol particles back into the atmosphere. Wet deposition has been identified as a key atmospheric process that contributes to CCN uncertainty in clean remote regions (Lee et al., 2013).

1.3.5 Dry Deposition

Dry deposition, like wet deposition is a sink for aerosol particles in the atmosphere. However wet deposition is dependent on the presence of precipitating clouds, which are subject to significant spatial and temporal variation. In the absence of wet deposition, dry deposition becomes an important sink for aerosol particles, whereby turbulence and gravitational sedimentation results in aerosols being deposited onto the Earth's surface. Dry deposition is dependent on particle radius and the characteristics of the earth's surface, and complex dry deposition schemes taking this into account are increasingly being implemented into climate models (Mulcahy et al., 2020; Petroff and Zhang, 2010). Sedimentation (gravitational settling of aerosols) is also an important sink for aerosols that also redistributes aerosol particles vertically, thereby affecting the vertical profile of aerosol particles.

1.4 Anthropogenic climate change and aerosols

The changes to greenhouse gases have been the main driver of climate change since pre-industrial times (1850). Human activity is the main source of these greenhouse gases in the atmosphere. The atmospheric concentration of greenhouse gases has continued to increase since 1850, with their annual mean in 2019 being, 410ppm for CO_2, 332ppb N_2O and 1866 ppb for CH_4 (IPCC, 2021). Longwave radiation from the earth is absorbed by these gases and warms the planet. Figure 1a taken from the recent IPCC AR6 report (IPCC, 2021) shows the temperature time series over the past 2000 years, from which we observe an unprecedented increase in temperature over the past 100 years. Figure 1b shows the observed temperature record and, simulations with

and without anthropogenic activity. The simulation with both anthropogenic activity and natural factors included match the observed temperature record, with the simulation without anthropogenic activity not matching observations.

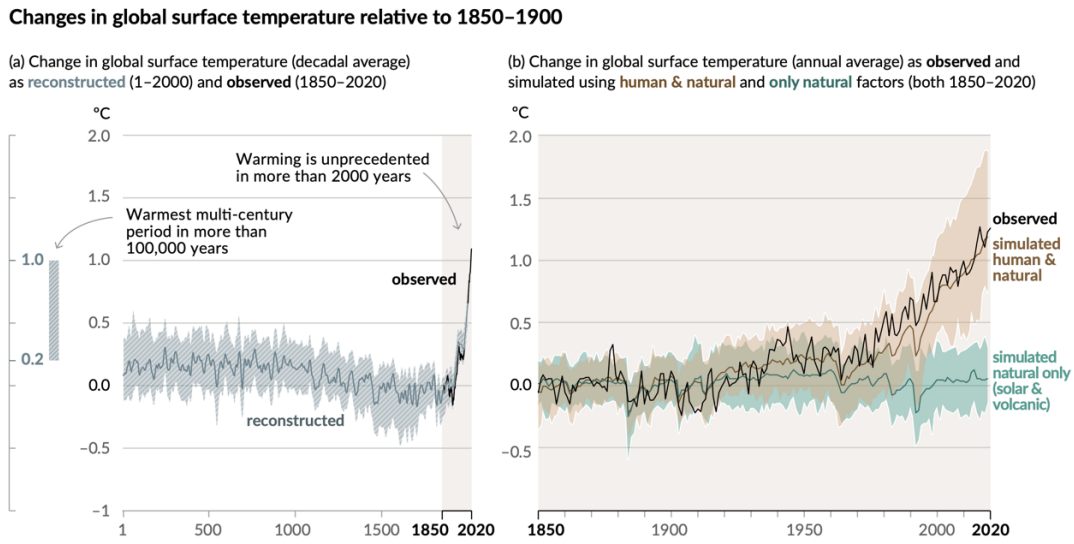

Figure 1: Global temperature change over the last 2000 years and causes of global warming; a) Change in the global surface temperature (decadally averaged) in the last 2000 years relative to the 1850-1900. The vertical bar on the left is the estimated temperature during the warmest multicentury period in the last 100,000 years. The grey shaded area shows the most likely range of the temperature record, b) Changes in global surface temperature since 1850 (annually averaged), the black line represents the observations and is compared to simulations from the coupled model intercomparison project (CMIP6) which included both human and natural drivers of climate change (brown) and simulations with only natural drivers (green). (image taken from IPCC AR6 report)

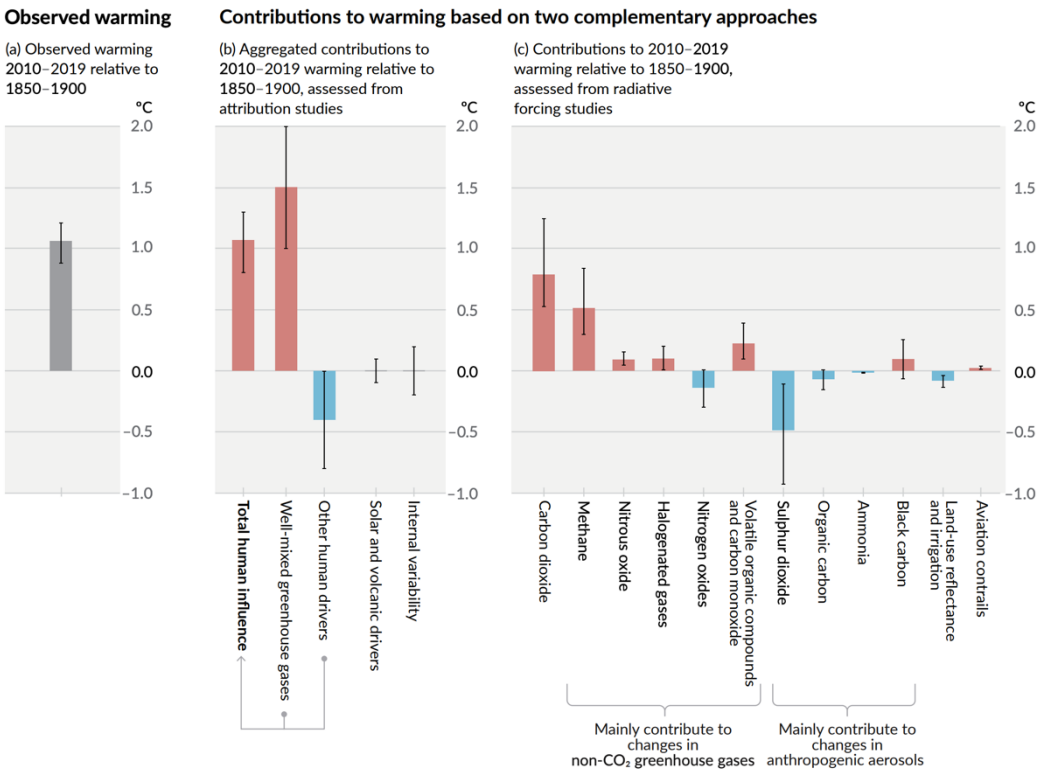

Figure 2: Contributions to global warming: a) Observed global warming in 2010-2019 relative to 1850-1900. b) Temperature change since pre-industrial times attributed to well-mixed greenhouse gases; "other human drivers" include aerosols, land use change and ozone; Solar and volcanic drivers, and internal climate variability. c) The temperature change contributions split into individual components of human activity which includes green-house gas emissions, aerosols and their precursors, land use changes and aviation contrails. (Image taken from IPCC AR6 report)

Since 1970 the global surface temperatures has increased more than any other 50-year period in the last 2000 years. The temperatures in the last decade (2010-2020) exceeds the most recent multi-century warming period (~6500 years ago, 0.2 to 1°C relative to period, 1850-1990). Figure 2 breaks down the contribution of the various drivers of climate change, which include greenhouse gases, aerosols, land use change and contrails. We have talked about how greenhouse gases play a role in warming the planet; however, the warming effect is offset by the cooling effect aerosols have on global climate. The likely range of human-induced global surface temperature increase since pre-industrial times is 0.8^0C to 1.3^0C. Well mixed greenhouse gases

contribute about 1^0C to 2^0C of warming, aerosols and their precursors contribute to a 0^0C to 0.8^0C cooling, natural drivers (solar radiation and volcanic activity) contribute about -0.1^0C to $+0.1^0$C and internal variability accounts for about -0.2^0C to $+0.2^0$C (IPCC, 2021).

The cooling effect aerosols have on global climate (IPCC, 2021) makes it an exciting avenue of research which is the focus of this thesis. Aerosols can scatter and absorb solar radiation (aerosol-radiation interactions, ARI) and act as a seed for cloud droplets and affect the microphysical properties of clouds (aerosol-cloud interactions, ACI).

1.5 Aims of this thesis

The aim of this thesis is to determine the climatic significance of secondary aerosol, and to better understand the microphysical processes involved in its formation. We split this thesis into 3 parts, each helping shed more light on our understanding of secondary aerosol using a climate model,

Firstly, we wanted to understand the current state of UKESM1 in reproducing aerosol vertical profiles and identify which atmospheric processes have a controlling influence on the model's biases. We identified the role of nucleation and condensational growth which helps reduce model biases. Secondly, we then explore the role of nucleation in the climate system. Lastly, we highlight the role of a missing source of secondary organic aerosol in the model, from isoprene gas and aqueous phase chemistry.

In Chapter 2, the global climate model UKESM1 was used to examine its accuracy when compared to observations. We explored the following research questions,

- What is the current state of UKESM1 in reproducing vertical profiles of three variables related to new particle formation: total particle number concentration, SO_2 and condensation sink?
- How sensitive is the model to perturbations in various atmospheric processes?
- Are there scientifically justifiable ways to reduce model biases and suggest improvements to UKESM1?

In Chapter 3, UKESM1 was used to examine the representation and role of nucleation (which was identified in Chapter 2 as an important process that helps reduce model biases) in the climate system. We examined the following,

- What is the impact of nucleation on aerosol concentration?
- What is its impact on atmospheric variables like liquid water path and cloud fraction?
- What is the radiative effect, and aerosol forcing contribution of nucleation?
- What is the role played by nucleation in damping the radiative effect of primary aerosol emission?

In Chapter 4, we examine the role of organic oxidation products which participate in nucleation and particle growth via condensation (which were identified in Chapter 2 as atmospheric processes that could help reduce model biases). We specifically examine the importance of a missing source of secondary organic aerosol in the model from isoprene gas and aqueous phase chemistry. The research questions we explored are,

- How important is SOA generated from aqueous phase isoprene cloud chemistry to the global SOA budget?
- What are the implications of SOA from isoprene gas phase and aqueous phase chemistry to global climate?

Chapter 2 : Constraints on global aerosol number concentration, SO_2 and condensation sink in UKESM1 using ATom measurements

Ananth Ranjithkumar[1], Hamish Gordon[2,1], Christina Williamson[3,4], Andrew Rollins[3], Kirsty Pringle[1], Agnieszka Kupc[4,5], Nathan Luke Abraham[6,7], Charles Brock[4], Ken Carslaw[1]

[1]School of Earth and Environment, University of Leeds, LS2 9JT, United Kingdom
[2]Engineering Research Accelerator and Centre for Atmospheric Particle Studies, Carnegie Mellon University, Pittsburgh, PA, 15213, USA
[3] Cooperative Institute for Research in Environmental Sciences, University of Colorado, Boulder, CO 80309, USA
[4]NOAA Chemical Sciences Laboratory, Boulder, CO 80305, USA
[5]Faculty of Physics, Aerosol Physics and Environmental Physics, University of Vienna, 1090 Vienna, Austria
[6]National Centre for Atmospheric Science, UK
[7]Department of Chemistry, University of Cambridge, Cambridge, UK

2.1 Abstract

Understanding the vertical distribution of aerosol helps to reduce the uncertainty in the aerosol lifecycle and therefore in the estimation of the direct and indirect aerosol forcing. To improve our understanding, we use measurements from four deployments of the Atmospheric Tomography (ATom) field campaign (ATom1-4) which systematically sampled aerosol and trace gases over the Pacific and Atlantic Oceans with near pole-to-pole coverage. We evaluate the UK Earth system model (UKESM1) against ATom observations in terms of joint biases in the vertical profile of three variables related to new particle formation: total particle number concentration (N_{Total}), sulphur dioxide (SO_2) mixing ratio and the condensation sink. The N_{Total}, SO_2 and condensation sink are interdependent quantities and have a controlling influence on the vertical profile of each other, therefore analysing them simultaneously helps to avoid getting the right answer for the wrong reasons. The simulated condensation sink in the baseline model is within a factor of 2 of observations, but the N_{Total} and SO_2

show much larger biases mainly in the tropics and high latitudes. We performed a series of model sensitivity tests to identify atmospheric processes that have the strongest influence on overall model performance. The perturbations take the form of global scaling factors or improvements to the representation of atmospheric processes in the model, for example by adding a new boundary layer nucleation scheme. In the boundary layer (below 1 km altitude) and lower troposphere (1-4 km) inclusion of a boundary layer nucleation scheme (Metzger et al., 2010) is critical to obtaining better agreement with observations. However, in the mid (4-8 km) and upper troposphere (>8 km), sub-3 nm particle growth, pH of cloud droplets, DMS emissions, upper tropospheric nucleation rate, SO_2 gas scavenging rate and cloud erosion rate play a more dominant role. We find that perturbations to boundary layer nucleation, sub 3 nm growth, cloud droplet pH and DMS emissions reduces the boundary layer and upper tropospheric model bias simultaneously. In a combined simulation with all 4 perturbations, the SO_2 and condensation sink profiles are in much better agreement with observations but the N_{Total} profile still shows large deviations, which suggests a possible structural issue with how nucleation or gas/particle transport or aerosol scavenging is handled in the model. These perturbations are well-motivated in that they improve the physical basis of the model and are suitable for implementation in future versions of UKESM1.

2.2 Introduction

Aerosols affect the global energy balance by directly scattering and absorbing solar radiation, and indirectly by their ability to act as cloud condensation nuclei (CCN), which changes the microphysical properties of clouds (Albrecht, 1989; Twomey, 1977). The direct and indirect effect aerosols have on climate has been identified as

the largest source of uncertainty in the assessment of anthropogenic forcing (Bellouin et al., 2020; Carslaw et al., 2013; Myhre et al., 2013). The direct radiative forcing by aerosol particles is dependent on the scattering and absorption of solar radiation, which in turn is dependent on aerosol properties like their size, shape and refractive index. The indirect radiative forcing is dependent on aerosol particles forming or behaving as CCN (or ice nuclei), which is controlled by the hygroscopicity and aerosol size distribution at cloud base (1– 3 km). There are still gaps in our knowledge of atmospheric processes that control the spatial, temporal and size distribution of aerosols in the atmosphere. Atmospheric aerosol concentrations depend on their sources; primary (emissions) and secondary (new particle formation and particle growth), their sinks (scavenging, wet and dry deposition) and transport through the atmosphere (Merikanto et al., 2009). Thus, the different atmospheric processes that have a controlling influence on the aerosol distribution throughout the atmosphere must be better understood.

Global-scale measurements of aerosol microphysical properties are needed to evaluate general circulation models (GCMs). Satellite measurements have extensive global coverage, but they cannot detect particles smaller than about 100 nm diameter. In-situ aircraft measurements give more detailed information about the full size distribution, chemical composition and radiative properties of aerosol particles. In past studies (Dunne et al., 2016; Ekman et al., 2012; Watson-Parris et al., 2019) global models have been compared against measurement campaigns such as CARIBIC (Civil Aircraft for Regular Investigation of the Atmosphere Based on an Instrument) (Heintzenberg et al., 2011), ACE1 (First Aerosol characterization experiment) (Clarke et al., 1998), PEM Tropics (Pacific Exploratory missions - Tropics) (Clarke et al., 1999), ARCTAS (Arctic Research of the composition of the troposphere from

aircraft and satellites) (Jacob et al., 2010), PASE (Pacific Atmosphere Sulphur experiment) (Faloona et al., 2009), INTEX-A (Intercontinental chemistry transport experiment – North America) (Singh et al., 2006) and VOCALS (VAMOS Ocean-Cloud-Atmosphere-Land Study) (Wood et al., 2011). Each of these campaigns had goals to help us understand particle size distribution in the upper troposphere, the particle production rate in cloud outflow regions, Arctic atmospheric composition, sulphur processing, tropospheric composition over land and clouds/precipitation in the south-eastern Pacific respectively. The measurements from these campaigns were used to identify atmospheric processes that help constrain the particle size distribution in global climate models like MIT-CAM3 (Ekman et al., 2012) and ECHAM-HAM (Watson-Parris et al., 2019) with observations.

In this work, we compare in-situ aircraft observations conducted as part of the NASA Atmospheric Tomography Mission (ATom) (Wofsy et al., 2018) to a global climate model (UKESM1) to better quantify the model biases in particle number concentration, SO_2 and the condensation sink. The ATom campaigns provide a representative continuous data set of daytime aerosol, gas and radical concentrations and properties by continuously sampling the atmosphere vertically and spatially over a vast region of the marine free troposphere. This single global dataset was obtained between 2016 and 2018 during four campaigns sampling each of the four seasons. During these campaigns, a large aerosol and gas instrument payload was deployed on the NASA DC-8 aircraft for systematic sampling of the atmosphere spanning altitudes between 0.2 km and 12 km, and spatially it encompasses Pacific and Atlantic oceans with near pole-to-pole coverage. This data has been used recently (Williamson et al., 2019) to highlight the importance of new particle formation to CCN concentration in the upper and free troposphere, and highlights severe deficiencies in the ability of

state of the art global chemistry climate models to capture new particle formation, particle growth and aerosol vertical transport accurately.

The ATom data have also been used in previous work to address biases in the vertical profile of sea salt and black carbon in the Community Earth System Model (CESM) and to better understand the in-cloud removal of aerosols by deep convection (Yu et al., 2019). Black carbon lifetime and differences in black carbon loading between the Pacific and Atlantic Basins have also been researched using ATom measurements (Katich et al., 2018; Lund et al., 2018). Other studies used the measurements to address uncertainties associated with the life cycle of organic aerosol in the remote troposphere (Hodzic et al., 2020a) and to investigate the mechanisms of new particle formation in the tropical upper troposphere (Kupc et al., 2020). The measurements have also shed light on the global distribution of biomass burning aerosol (Schill et al., 2020), brown carbon (Zeng et al., 2020) and DMS oxidation chemistry (Veres et al., 2020).

Although the ATom dataset is extensive and provides important information about aerosol number and gas concentrations (Williamson et al., 2019; Wofsy et al 2018), there are some challenges when comparing it to a GCM. A single data point sampled represents a point in the atmosphere defined by the latitude, longitude, altitude and time the data was collected. The UKESM1 output is, however, an average over a broad horizontal grid box of ~135km across, and it is usually temporally averaged over a month. In previous studies (Lund et al., 2018; Samset et al., 2018; Schutgens et al., 2016) it has been shown that sampling errors can be minimized by averaging the observations over time and model errors can be reduced by using 4D model fields with high temporal resolution. In the first part of this paper, we evaluate UKESM1 at

three-hour time resolution against observations and highlight some of the biases that exist in the model in different regions of Earth.

In the second part of this paper, we focus on trying to understand and reduce these biases. We focus on processes related to new particle formation, as this is the dominant source of aerosol number concentration globally (Gordon et al., 2017; Yu and Luo, 2009). Some model developments and a series of sensitivity simulations are performed to determine the source of the model-measurement bias. As well as resolving a bug in the model, we also address some of the deficiencies in the nucleation mode microphysics and the dependence of coagulation sink on particle diameter. The sensitivity tests comprise model simulations in which we perturb various parameters that control different atmospheric processes, one at a time.

In order to obtain physically motivated reductions in model bias, we evaluate the model simultaneously against three observed quantities related to new particle formation: total particle number concentration (N_{Total}), SO_2 mixing ratio and condensation sink. The condensation sink is a measure of how rapidly condensable vapor molecules (in UKESM1, sulphuric acid and secondary organic aerosol material) and newly formed molecular clusters are removed by the existing aerosol surface area. It is a loss term for new particles, while SO_2 is effectively a production term because it controls sulphuric acid vapour concentrations. Assessing the influence of model processes on only one of these quantities in one-at-a-time sensitivity tests can result in misleading or incomplete conclusions about model performance, because different atmospheric processes affect N_{Total}, SO_2 and the condensation sink to varying degrees and can be independent of each other. As an example, an atmospheric process like in-cloud production of sulphate aerosol can increase the condensation sink, which will

decrease the gas concentration of precursors such as sulphuric acid, H_2SO_4, for new particle formation, and then in turn decrease N_{Total}. Perturbing atmospheric processes can also have a direct effect on the SO_2 mixing ratio and affects H_2SO_4 concentration which controls new particle formation (NPF), and we know from past studies (Gordon et al., 2017) that new particle formation is the source of about half of the CCN in the atmosphere. Improving the model-observation match to only one of N_{Total}, SO_2 and the condensation sink can result in a poorer match for the other two quantities. Therefore, it is important to identify atmospheric processes that reduce N_{Total}, SO_2 and condensation sink biases simultaneously.

2.3 The ATom Dataset

The main goal of the ATom campaign was to improve our scientific understanding of the chemistry and climate processes in the remote atmosphere over marine regions. In relation to aerosols, the campaign helps to quantify the abundance, distribution, composition and optical properties of aerosol particles in the remote atmosphere. This can help determine the source of these particles and evaluate the mechanism for formation and growth of new particles to form CCN. The whole campaign used the NASA DC-8 research aircraft and was subdivided into four series of flights, ATom1 (August – September 2016), ATom2 (January – February 2017), ATom3 (September – October 2017) and ATom4 (April – May 2018). The flight path for each of the ATom deployments is shown in Figure 3. Measurements were made between ~0.18 km and ~12 km altitude, from the Antarctic to the Arctic, over the Atlantic and Pacific oceans. All of the data are publicly available (Wofsy et al., 2018).

We used the SO_2 data from ATom4 (the SO_2 data from ATom1-3 were not sensitive at concentrations less than 100ppt) and the particle number concentration data from

ATom1, ATom2, ATom3 and ATom4. The instruments used to measure the aerosol size distribution from 2.7 nm to 4.8 μm are a nucleation-mode aerosol size spectrometer (NMASS) (Williamson et al., 2018), an ultra-high-sensitivity aerosol size spectrometer (UHSAS) and a laser aerosol spectrometer (LAS). The NMASS consists of five continuous laminar flow condensation particle counters (CPCs) in parallel, with each CPC operated at different settings so as to detect different size classes (Brock et al., 2019; Williamson et al., 2018). During ATom 1, the cut-off sizes (probability of the particles at cut-off size to be detected is greater than 50%) for each of the CPCs were 3.2 nm, 8.3 nm,14 nm, 27 nm and 59 nm. From ATom 2 to ATom 4 (more CPCs were present in addition to the CPCs from ATom1), additional cut-off sizes of 5.2, 6.9, 11, 20 and 38 nm were present. This setup helps establish the aerosol size distribution for particles smaller than 59 nm. The UHSAS measures particle number concentrations for particles with diameter between 63 nm and 1000 nm (Kupc et al., 2018). The LAS efficiently measures particles between 120 nm and 4.8 μm. The POPS instrument was operated as a backup to detect coarse-mode particles (Gao et al., 2016).

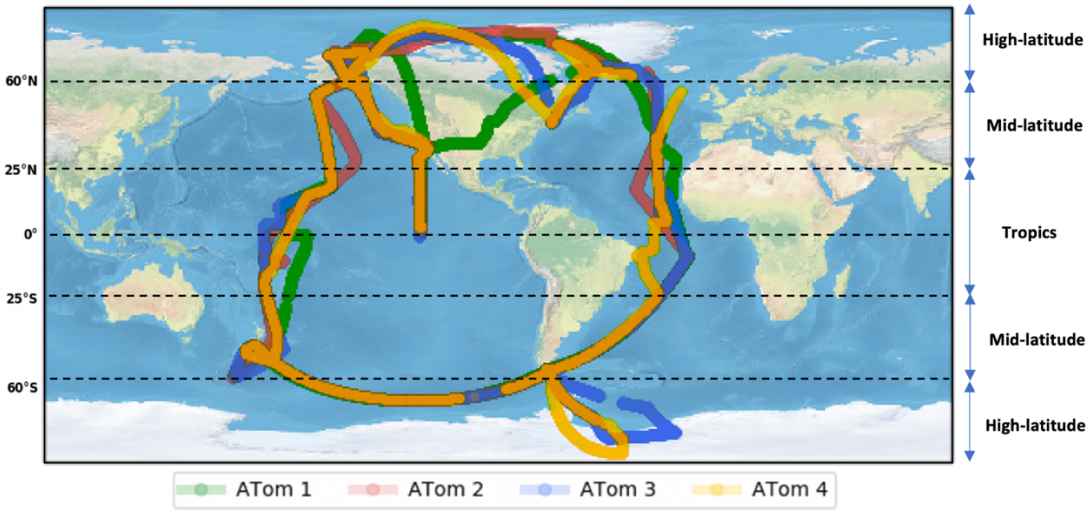

Figure 3: Flight tracks for NASA DC-8 for the 4 ATom campaigns: ATom1 (August – September 2016, green), ATom2 (January – February 2017, red), ATom3 (September – October 2017, blue) and ATom4 (April – May 2018, yellow)

The SO_2 measurements were obtained using the laser-induced fluorescence instrument (Rollins et al., 2016). SO_2 mixing ratios at high altitudes are quite low (between 1-10 parts per trillion). It is difficult to measure SO_2 mixing ratio at low pressure with high precision. This instrument is capable of retrieving precise measurements of SO_2 concentration at pressures as low as 35 hPa making this instrument operable up to altitudes of 20km. The instrument has a detection limit of 2 ppt (at a 10s measurement interval), and an overall uncertainty of $\pm$(16%+0.9ppt).

2.4 Model Description

The model used in this work is a modified version of the United Kingdom Earth system Model version 1 (UKESM1) (Mulcahy et al., 2020; Sellar et al., 2019) in its atmosphere-only configuration (with fixed sea surface temperatures). The model version used in this study has prescribed biogenic emissions rather than it being calculated interactively. The DMS emission flux is also scaled by a factor of 1.7 to account for a missing primary marine organic (PMO) source from oceans (this scaling factor is absent in the original version of UKESM1 with PMO aerosol incorporated into the model). The latest HadGEM3 global coupled (GC) climate configuration of the UK Met office was used to develop UKESM1. HadGEM3 consists of the core physical dynamical processes of the atmosphere, land, ocean and sea ice systems (Ridley et al., 2018; Storkey et al., 2018; Walters et al., 2017). The UK's contribution to the Coupled Model Intercomparison Project Phase 6 (CMIP 6) (Eyring et al., 2015) is comprised of model simulations from the HadGEM3 and UKESM1 models.

Atmospheric composition is simulated with the chemistry-aerosol component of UKESM1 which is the UK Chemistry and Aerosol model (UKCA) (Morgenstern et al., 2009; O'Connor et al., 2014; Archibald et al., 2020). The anthropogenic, biomass burning , biogenic and DMS land emissions used by the model are taken from Hoesly et al 2018, Van Marle et al 2017, Sindelarova et al 2014 and Spiro et al., 1992 respectively. The aerosol scheme within UKCA is referred to as the Global Model of Aerosol Processes, GLOMAP-mode, (Mann et al., 2010; Mulcahy et al., 2020). It uses a two-moment pseudo-modal approach and simulates multicomponent global aerosol which includes sulphate, black carbon, organic matter and sea spray. Dust is simulated separately using a difference scheme (Woodward, 2001). GLOMAP-mode includes aerosol microphysical processes of new particle formation, condensation, coagulation, wet scavenging, dry deposition and cloud processing. The aerosol particle size distribution is represented using 5 log-normal modes: nucleation soluble, Aitken soluble, accumulation soluble, coarse soluble and Aitken insoluble, with their size ranges shown in Table A1 (Appendix A). UKCA is coupled to other modules in UKESM1 to handle tracer transport by convection, advection and boundary layer mixing. Originally in GLOMAP-mode, sulphate and secondary organic formation was driven by prescribed oxidant fields (Mann et al., 2010). However, in this study the UKCA chemistry and aerosol modules are fully coupled (Mulcahy et al., 2020).

The model can be run in different configurations (Walters et al., 2017), in this work we use the N96L85 configuration which is 1.875^{o} x 1.25^{o} longitude-latitude, corresponding to a horizontal resolution of approximately 135km. The model has 85 vertical levels up to an altitude of 85 km from the Earth's surface, with 50 levels between 0 and 18km, and 35 levels between 18 and 85 km. To compare the model against observations, we run the model in a nudged configuration over the period

during which the ATom campaigns took place (2016-2018). In this configuration, horizontal winds and potential temperature in the model are relaxed towards fields from the ERA–interim reanalysis fields (Dee et al., 2011; Telford et al., 2008). This helps to reproduce the same meteorological conditions at the exact time and location the measurements were performed, and to reduce model biases compared to free-running configurations (Kipling et al., 2013; Zhang et al., 2014). A relaxation time constant of 6 hours is chosen (equal to the temporal resolution of the reanalysis fields), and the nudging is applied between model levels 12 and 80. When comparing the model data to observations, the output fields from the model are retrieved at high temporal resolution (3-hourly output) at the same times as the observations. This is done to reduce model sampling errors (Schutgens et al., 2016). The diagnostics fields that we use for our analysis are total particle number concentration (N_{Total}), sulphur dioxide (SO_2) mixing ratio and condensation sink. These 4D diagnostics fields occupy significant disk space, and due to storage space constraints, we developed an online interpolator to process the model fields as and when they are output to give the value of the required diagnostics at the exact time and location where the measurement was obtained. To reduce sampling errors, 5-minute averages of the measurements were used in this study. The interpolated diagnostic fields occupy less storage space and are retained for our analysis while the original large model field file is erased.

2.5 Evaluation of the baseline model

Figure 4 shows the simulated longitudinal mean fields of total particle number concentration (N_{Total}), SO_2 mixing ratio and condensation sink from the atmosphere-only configuration of UKESM1. The particle number concentrations are much lower at the surface than the free and upper troposphere, mainly due to the stronger production rate of new particles via binary homogenous nucleation at higher altitudes.

The highest zonal mean N_{Total} concentration ($8x10^4$ particles/cm^3 at STP) occurs at an altitude range of 12 to 16 km. At an altitude of 15 km, most of the particles are present in the intertropical latitude band (25^0N – 25^0S). The SO_2 mixing ratio is maximum (>1000ppt) at the surface in the northern hemisphere because there are significant SO_2 sources from land as a consequence of industrial activity. In the southern hemisphere, the SO_2 source is mainly from the oxidation of dimethyl sulphide emitted from the ocean. The SO_2 mixing ratio at high altitudes is substantial, with a simulated mixing ratio of ~50 pptv (at 15 km) in the tropics. A secondary peak in the mixing ratio of SO_2 occurs at 30 km altitude from the oxidation of carbonyl sulphide (we include the stratosphere up to 30km altitude in *Figure 4* for completeness and the troposphere is the main focus of this study). The condensation sink is directly related to the number of large particles present in the atmosphere, which provides a surface for the condensation of condensable vapours like H_2SO_4. Large particles are typically present at a lower altitude; this leads to a higher condensation sink close to the surface, where its maximum value (when longitudinally averaged) is ~0.01 s^{-1} (i.e., lifetime of condensable vapours before condensation is ~100 s). The minimum in the condensation sink is around 5 x 10^{-5} s^{-1}, in the upper troposphere. A low condensation sink at a higher altitude increases the lifetime and mixing ratio of condensable vapours like H_2SO_4 which is an important factor in the rapid formation of new particles at these altitudes.

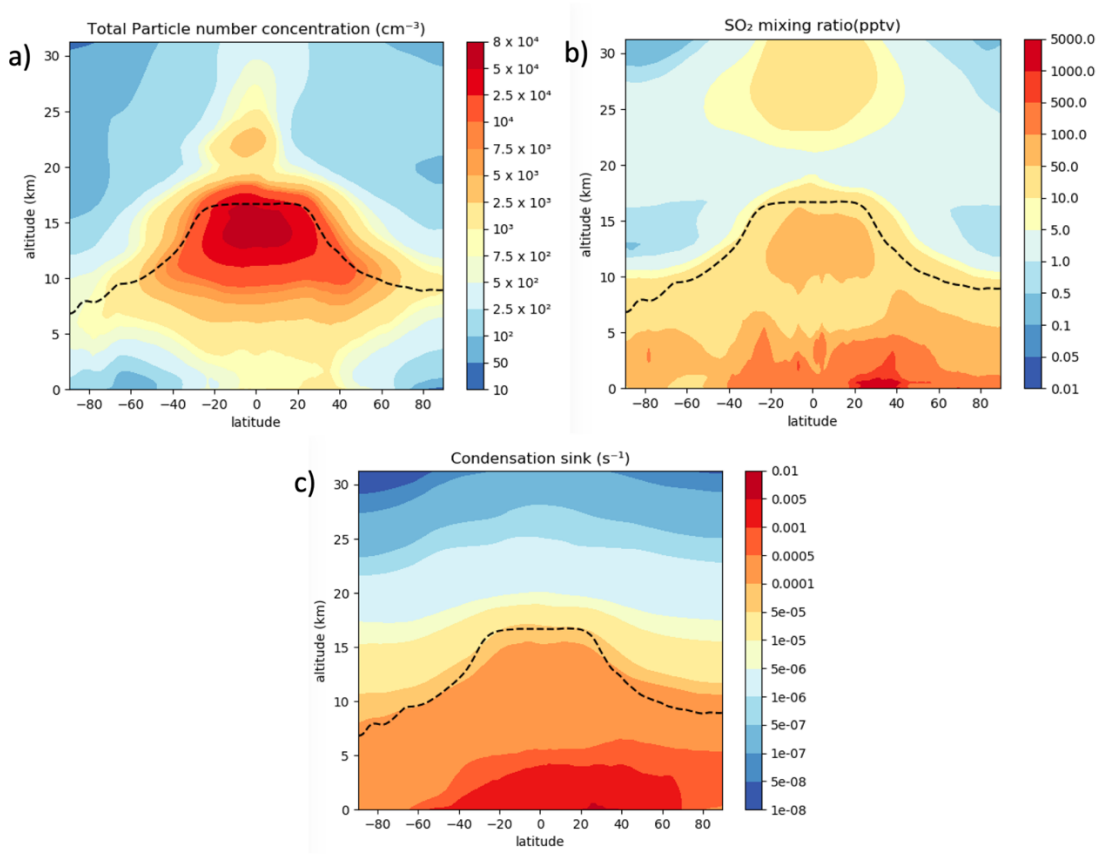

Figure 4: Global longitudinal mean vertical profile of the simulated a) total particle number concentration (N_{Total}), b) SO_2 mixing ratio and c) condensation sink from the default version of our model. In this figure, we show altitudes up to 30km, and our model top is 85km, but our analysis focuses on the troposphere. The black dashed line represents the tropopause height.

To compare the model with ATom data, we use high temporal resolution 4D model output data along the flight track. The default version of the model shows substantial biases when compared to observations (Appendix Figure A1, A2 and A3). On investigating these biases, we discovered a bug in the subroutine in which the tendency in H_2SO_4 concentration in the chemistry scheme was calculated. The chemistry and aerosol processes in the model are handled using the operator splitting technique, where the usual timestep for chemical reactions is 1 hour and the algorithm that handles the chemistry introduces sub-steps where necessary. Microphysical processes (nucleation, condensation and coagulation) are treated on a separate 4-minute-long sub-timestep within the 1-hour chemistry timestep. The H_2SO_4

concentration is updated on every microphysics time step, and this was incorrectly implemented: the production of sulphuric acid from SO_2 on the microphysics time step was missing and the sulphuric acid was being produced only at the beginning of every chemistry time step. This resulted in an excess H_2SO_4 concentration at the beginning of every chemistry time step, but no production of H_2SO_4 later in the timestep. Nucleation is a very non-linear process, and so the high initial H_2SO_4 concentration resulted in an excessive number of small particles being produced via nucleation. We resolved this bug and used this corrected version, which we refer to as the 'baseline' version, as the starting point for our sensitivity analysis in Section 2.7. The released version of UKESM1, which we started with, does not contain the bug-fix and was used in CMIP6 experiments (Eyring et al., 2015). In this study we refer to this version of the model as the 'default' version. Figures 3, 4 and 5 focus exclusively on how the baseline version of the model performs against observations and a comparison of how the default and baseline version perform against observations are shown in the Appendix figures A1, A2 and A3.

The SO_2 instrument was only flown on the ATom4 campaign, in spring 2018, while the vertical profiles of N_{Total} and Condensation sink are produced using all of the ATom campaigns, in all four seasons. However, we compare like with like, in that, for example, SO_2 observations in spring are compared only with SO_2 model data at three-hourly time resolution in spring. We perform our analysis using the available data, however our analysis could benefit from more SO_2 data. We also can see from the that the vertical profiles of N_{Total} and condensation sink for just ATom 4 (Appendix figure A4) show similar biases as Figure 5 and Figure 7, which have data from all the ATom campaigns aggregated together.

Figure 5 compares the simulated and measured vertical profile of N_{Total} and the model-measurement normalised mean bias factor (NMBF) (defined in equation ((1)) (Yu et al., 2006) for the baseline simulation. The global data is divided into three regions: the tropics (25N-25S), mid-latitudes (25N – 60N, 25S - 60S) and high latitudes (60N - 90N, 60S – 90S). The baseline version of UKESM1 is shown in green and the ATom measurements in black. The magnitude of the model bias is quantified by the value 1+|NMBF|, which is the factor by which the model over- or underestimates the observations.

$$NMBF = \begin{cases} \frac{\sum M_i}{\sum O_i} - 1 = \frac{\bar{M}}{\bar{O}} - 1, & if \bar{M} \geq \bar{O} \\ 1 - \frac{\sum O_i}{\sum M_i} = 1 - \frac{\bar{O}}{\bar{M}}, & if \bar{M} < \bar{O} \end{cases} \qquad (1)$$

where M indicates Model and O is the observation. A positive NMBF indicates that the model prediction is higher than the measurements and a negative value indicates that the model is lower than the measurements.

The default model substantially overpredicts N_{Total} (Figure A1) in the upper troposphere (>8 km), with a factor of 10-15 overestimate at an altitude of 12 km in the tropics. In the lower free troposphere (between 1 km and 3 km) and boundary layer (<1 km), the model agrees well (NMBF ~ 0) with observations in the tropics. However, the model underestimates the observations by a factor of 3 in the mid and high latitudes. The baseline (bug-fixed) version of the model shows biases a factor 5-10 lower in the upper troposphere than the default version, for the reasons explained above.

Figure 6 shows the vertical profile of SO_2 mixing ratio in the model. The baseline model is positively biased by approximately a factor 2-6 in the boundary layer regions

of the tropics and midlatitudes. In the tropical upper troposphere, the model overpredicts SO_2 by up to a factor 2-6, while the biases in the upper tropospheric mid and high latitudes are negligible. We speculate that the small differences in biases we see between the baseline and default version (Figure A2) are due to cloud adjustments, which can affect the SO_2 concentration and condensation sink. Adjustments arise because changes in N_{Total} can affect cloud drop concentration and liquid water path, and can therefore change the SO_2 lost in aqueous chemical processing in clouds.

Figure 7 shows the vertical profile of the condensation sink in the atmosphere. The condensation sink simulated by the baseline version of the model shows positive and negative biases within a factor of 2 of the observations. Larger particles in the atmosphere contribute to the condensation sink and a higher concentration of these large particles would result in more available surface area for condensable vapours to condense. The bias when comparing the model to observations can be explained by uncertainties in primary aerosol/gas emissions or other atmospheric processes. From the vertical profile it appears that the model either transports larger aerosol particles to the free troposphere or removes too little in precipitation.

To explore any longitudinal differences, we also plotted the observations and model data in the Pacific and Atlantic Ocean to briefly explore whether the model shows differing trends in these regions (Appendix Figure A5). From the figure we can see that the model shows biases of similar magnitude in the Pacific and Atlantic when compared to observations. The model shows biases of up to 10, 5 and 2 for the N_{Total}, SO_2 and condensation sink respectively in the Pacific and Atlantic. We also note that we have lumped northern and southern hemispheric data for the mid and high latitudes. The magnitudes of N_{Total}, SO_2 and condensation sink are different in both hemispheres and we illustrate that in Appendix Figure A6. The vertical profiles of all

three variables show similar biases in both the northern and southern midlatitudes. In the high latitudes we see more substantial interhemispheric differences. The most notable are, a) N_{Total} shows a factor of 5 underprediction in the northern high latitude boundary layer, with southern high latitude boundary layer showing good agreement with observations, b) The model predicts less than 1pptv SO_2 mixing ratio in the southern high latitudes with observation showing a mixing ratio of ~10ppt. We explore ways to reduce these biases in Section 2.7 and 2.8.

From Figure 5Figure 6 Figure 7 an immediate result of the baseline model evaluation is that the too-high particle number concentration in the free and upper troposphere at tropical and mid-latitudes is qualitatively consistent with too-high SO_2 mixing ratios, but inconsistent with the too-high condensation sink. The possible reasons for the biases in N_{Total}, SO_2 and condensation sink is explored later in section 2.6.

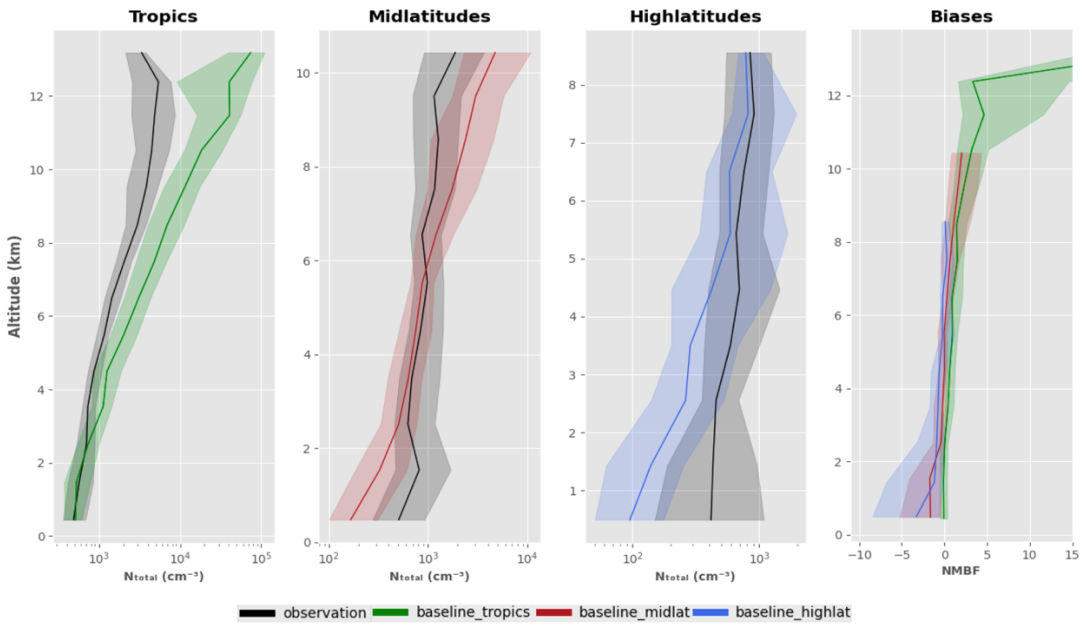

Figure 5: The first three columns show the vertical profile of the total particle number concentration (at standard temperature and pressure (STP)) as observed (ATom1-4) and in the simulated data from the baseline (bug-fixed) configuration of UKESM in the Tropics (25°N-25°S), mid-latitudes (25°N-60^{0}N and 25°S-60°S) and high latitudes (60°N-90°N and

60°S-90°S). The fourth column shows the NMBF of the baseline simulation in the tropics, mid-latitudes and high latitudes. The bold line represents the median and the shaded region represents the corresponding interquartile range (25th and 75th percentile) in a 1km altitude bin.

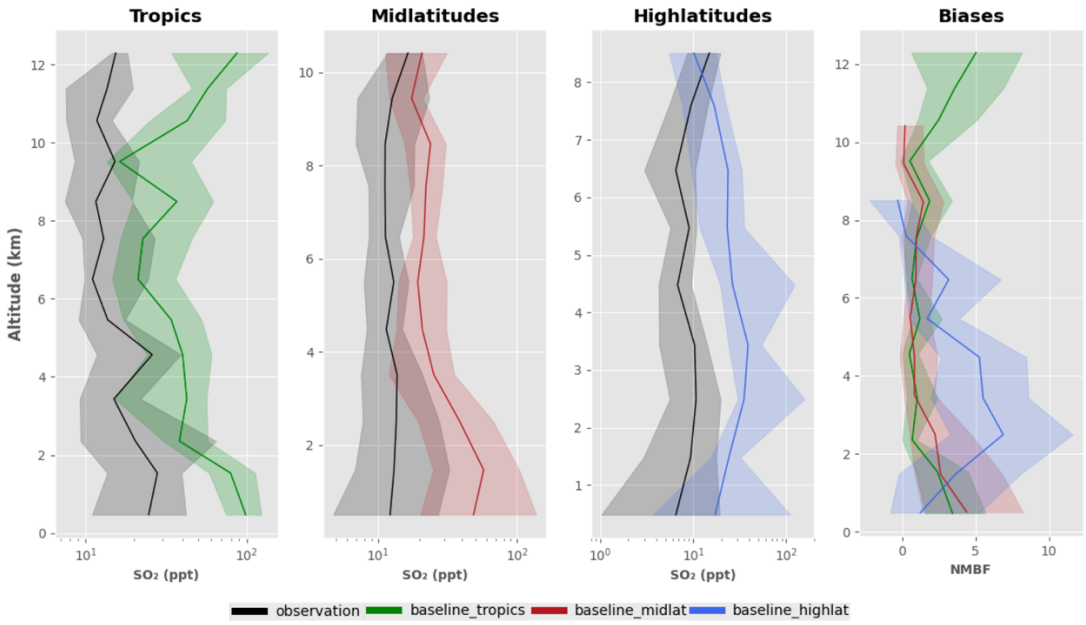

Figure 6: The first three columns show the vertical profile of the SO_2 (at standard temperature and pressure (STP)) as observed (ATom4 (April – May 2018)) and the simulated data from the baseline (bug-fixed) configuration of UKESM in the tropics (25°N-25°S), mid-latitudes (25°N-60°N and 25°S-60°S) and high latitudes (60°N-90°N and 60°S-90°S). The fourth column shows the NMBF of the baseline simulation in the tropics, mid-latitudes and high latitudes. The bold line represents the median and the shaded region represents the corresponding interquartile range (25th and 75th percentile) in a 1 km altitude bin.

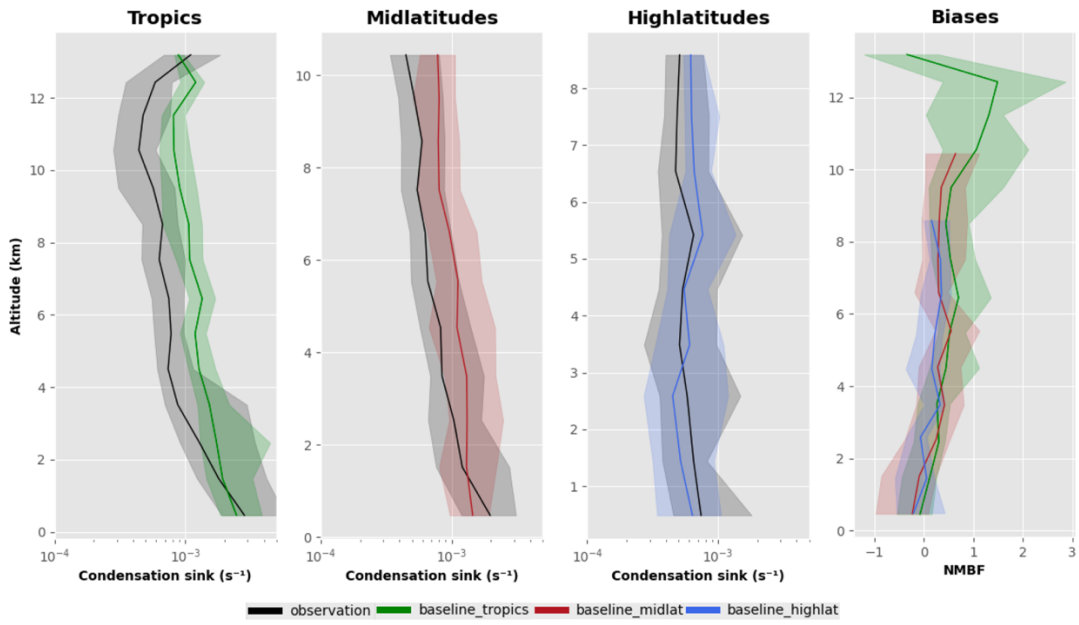

Figure 7: The first three columns show the vertical profile of the condensation sink (at standard temperature and pressure (STP)) as observed (ATom1-4) and in the simulated data from the baseline (bug-fixed) configuration of UKESM in the Tropics (25°N-25°S), mid-latitudes (25°N-60^{0}N and 25°S-60°S) and high latitudes (60°N-90°N and 60°S-90°S). The fourth column shows the NMBF of the baseline simulation in the tropics, mid-latitudes and high latitudes. The bold line represents the median and the shaded region represents the corresponding interquartile range (25th and 75th percentile) in a 1km altitude bin.

2.6 Model sensitivity simulations and improvements to model microphysics

To investigate the potential causes of the model biases, we have identified several atmospheric processes that are expected to influence the vertical profile of the N_{Total}, SO_2 and condensation sink. The model simulations that we performed include a combination of direct perturbations to atmospheric processes and changes in model microphysics. The perturbations were applied globally, and we analyse model performance at different regions in the troposphere. A more complete method of sensitivity analysis is to consider the joint effect of a combination of parameters on model performance, which has been done in the past with perturbed parameter ensemble studies (Lee et al., 2013; Regayre et al., 2018). The one-at-a time sensitivity tests that we carry out here help to determine which processes have the largest effect

on model biases and this information can be used in ensemble studies in the future. The atmospheric processes which we have selected for this study along with the motivation for why we picked them is described from Section 2.6.1 to 2.6.5 and also summarised in Table 1. A more detailed analysis of the effect of these model simulations on model biases is described in Section 2.7 and a three-way comparison of N_{Total}, SO_2 and condensation sink biases is explored in Section 2.8.

Table 1: Overview of the atmospheric processes that we have chosen for one-at-a-time sensitivity tests and the magnitude of the perturbation/scaling applied.

Atmospheric process/parameter	**Perturbation to parameter in UKESM1**
pH of cloud droplets	pH = 6 & 7 (default pH = 5)
Boundary layer nucleation (Metzger et al., 2010)	BL_nuc & BL_nuc/10
Condensation sink	condsink*5 & condsink*10
Primary marine organic emissions	primmoc & primmoc*5
Coagulation sink dependence on particle diameter	sub_3nm_growth represented using (Lehtinen et al., 2007)
DMS emissions	Seadms=1.0 (default = 1.7)
Binary H_2SO_4-H_2O nucleation rate	Jveh/10 & Jveh/100
SO_2 wet scavenging rate	csca*10 & csca*20
Cloud erosion rate	dbsdtbs = 0 & 10^{-3}
Aerosol wet scavenging efficiency	rscav_ait = 0.3 & 0.7, rscav_accu = 0.7, rscav_coarse = 0.9
Coagulation kernel	coag*5

2.6.1 Nucleation rate and nucleation-mode microphysics

Binary homogeneous nucleation. UKESM1 uses a binary neutral homogeneous H_2SO_4-H_2O nucleation scheme (Vehkamäki et al., 2002) throughout the atmosphere. The upper tropospheric positive biases in N_{Total} which we see from Figure 5 could be because of a high nucleation rate. Therefore, we perform simulations where we reduce the nucleation rate by a factor of 10 and 100 to assess its influence on the large

bias in upper-tropospheric particle number concentration. These perturbations to the nucleation rate could indirectly compensate for the biases in the production rate of H_2SO_4 from SO_2 (which can affect the concentration of sulphuric acid in the atmosphere, which affects new particle formation). It should be noted that the H_2SO_4-H_2O nucleation scheme (Vehkamäki et al., 2002) is an old scheme and the parameterised nucleation rates are valid only for a limited temperature range (230 K – 305 K). A new nucleation scheme (Määttänen et al., 2018) for the H_2SO_4-H_2O system extended the validity range to lower temperatures and a wider range of environmental conditions. Global particle number concentration for both schemes were compared in that study (Määttänen et al., 2018) and the vertical profile of particle number concentration was found to be slightly higher (by ~100 particles/cm^3) at lower altitude (between 300 hPa and 800 hPa), with particle number concentrations in the upper troposphere (>300 hPa) being almost identical. This addresses the uncertainty associated with the Vehkamaki nucleation scheme for the H_2SO_4-H_2O system at low temperatures in the upper troposphere. However, this perturbation is not well-motivated by available nucleation parameterizations but is intended only as a candidate for crude tuning to compensate for model biases.

Boundary layer nucleation. We incorporated a boundary layer nucleation (BLN) scheme (Metzger et al., 2010) to account for a source of new particles in the boundary layer to address the model's boundary layer negative bias (Figure 7). Most of our measurements are over remote ocean and the scheme we use is dependent on oxidation products from organics which, in our model, originate only from terrestrial vegetation. However, these organic vapours or the nucleated particles are transported to the remote ocean and thereby affect the vertical profile. The condensation sink is also affected by BLN since the new particles that are formed can grow to larger

particles by condensation of sulphuric acid and volatile organic compounds onto their surface (Pierce et al., 2012). We perform one model simulation with boundary layer nucleation included and then one where the boundary layer nucleation rate is reduced by a factor of 10. All of the oxidation products of volatile organic compounds (VOCs) are treated similarly in the model and have been lumped into a tracer called 'Sec_org'. This could lead to biases in the BLN rate and condensational particle growth rate since in reality the oxidation products of VOCs have different volatilities which can nucleate and condense at different rates. Reducing this nucleation rate by a factor of 10 (Regayre et al., 2018; Yoshioka et al., 2019) was found to match better with observations.

New particle growth. We improved the handling of the growth of newly formed clusters in the model because the initial stage of particle growth up to about 3 nm diameter is crucial to global CCN concentrations (Gordon et al., 2017; Tröstl et al., 2016) and can affect the vertical profile of particle number concentration. Measurement of particle growth rate at diameters smaller than 3 nm is difficult for most atmospheric instrumentation. This growth of small particles is determined by competing processes where particles grow by condensation of vapour onto the particle surface and are lost by coagulation with larger pre-existing particles (Pierce and Adams, 2007). Particle growth is simulated explicitly for particle sizes larger than 3nm. However, for the sub-3nm size range, the growth is represented implicitly by defining an effective rate of production of particles at 3 nm (accounting for competing growth and loss processes). This rate is calculated using a parameterization shown in equation *(2*) (Kerminen and Kulmala, 2002).

$$J_{3nm} = J_{d_c} exp\left(\frac{CS(d_c)}{GR} \cdot {d_c}^2 \cdot \left(\frac{1}{3} - \frac{1}{d_c}\right)\right) \quad (2)$$

where J_{3nm} and J_{dc} refer to the particle production rate at 3 nm and the critical size (d_c) respectively, CS (d_c) is the coagulation sink for particles of diameter d_c onto pre-existing aerosol and GR is the growth rate of the particles. The coagulation sink for a particle of diameter d_p is $CS(d_p) = \sum_j K(d_p, d_j) \cdot N_j$, where $K(d_p, d_j)$ is the coagulation coefficient for particles of diameter d_p coagulating onto particles of diameter d_j. An assumption made to derive Eq. 2 was that the coagulation coefficient for particles was proportional to the inverse of the square of the particle diameter ($\propto d_p^{-2}$). This is not always a sufficiently good approximation and the power dependency of the coagulation coefficient can vary depending on the ambient particle size distribution which varies from one location on the planet to another (Kürten et al., 2015). For example, observations at Hyytiala in the Finnish boreal forest (Dal Maso et al., 2005) reveal that the power law dependency of the coagulation sink with particle diameter is not -2, it was in a range between -1.5 and -1.75. In a previous study (Lehtinen et al., 2007) a new analytical expression for J_{3nm} was derived as shown in equation *(3)*.

$$J_{3nm} = J_{dc} exp\left(-\gamma \cdot d_c \cdot \frac{CS(d_c)}{GR}\right) \quad (3)$$

Where $\gamma = \frac{1}{s+1}\left[\left(\frac{3}{dc}\right)^{s+1} - 1\right]$ *and* $s = \frac{log\left({}^{CS(3nm)}/_{CS(dc)}\right)}{log\left({}^{3}/_{dc}\right)}$

We have incorporated this new expression into the model, and we show (Section 2.7) that this affects the concentration of smaller particles in the atmosphere by more correctly accounting for their losses due to coagulation.

Coagulation sink. The GLOMAP coagulation scheme (Jacobson et al., 1994) includes both inter-modal (collision between particles that belong to different modes) and intra-modal (collision between particles in the same mode) coagulation. The estimation of the coagulation kernel has uncertainties in the effect of Van-der-Waals forces and charge on the particles (Nadykto and Yu, 2003). In this study we are focused only on the overall uncertainty of atmospheric processes, so we perturbed the model by scaling up the whole coagulation kernel by a factor of 5 to observe its impact on the model-observation comparison.

Condensation Sink. The two condensable species present in the model are H_2SO_4 (formed from the oxidation of SO_2) and Sec_org (formed from the oxidation of monoterpenes). The condensation sink refers to the rate at which these condensable gases condense onto aerosol particles in the atmosphere. It is equal to $2\pi \mathrm{D} \sum_j \beta_j d_j N_j$, where D is diffusion coefficient, β_j is the transition regime correction factor (Fuchs and Sutugin, 1971), d_j is the particle diameter and Nj is the particle number concentration for the jth aerosol mode. It is conceivable that the presence of too much sulphuric acid in the atmosphere results in the formation of excess new particles, which could explain the bias in N_{Total}. Therefore, having a stronger condensation sink could help reduce the bias. The model also handles the condensation of H_2SO_4 and Sec_org differently in that the sulphuric acid concentration is updated every microphysics time step (4min), while the Sec_org concentration is updated only on every chemistry time step (1hour). Since condensation in the atmosphere can happen

on very short time scales, the Sec_org concentration may need to be updated at the end of every microphysics time step as well. We perform model runs after incorporating this change to the frequency at which Sec_org is updated, and also perform simulations where we manually increase the condensation sink by a factor of 5 and 10 to see how sensitive the vertical profiles are to this perturbation (the condensation sink can also be indirectly affected by perturbations to other atmospheric processes). The motivation for increasing the condensation sink by large factors was to test the magnitude of the condensation sink required to reduce the large biases in N_{Total}. We only perturb the condensation sink directly, and not the SO_2 or particle number concentration, because perturbing the condensation sink is technically more straightforward.

2.6.2 DMS and Primary Marine Organic emissions

The DMS sea water concentration is simulated interactively by the ocean biogeochemistry component (MEDUSA) of the model (Anderson et al., 2001). This parametrisation was tuned (Sellar et al., 2019) to ensure energy balance at the top of the atmosphere. The DMS emission flux into the atmosphere is calculated using the parametrisation by Liss and Merlivat, 1986. There is significant uncertainty in the gas phase DMS emissions from the ocean with the observational derived range of the global oceanic DMS emissions being 16-28 TgS/yr (Bock et al., 2021). From past studies (McCoy et al., 2015; O'Dowd et al., 2004) we know that over marine regions, gas phase volatile organic compounds emitted from the ocean surface layer are a source of organic-enriched sea-spray aerosol. We also note that the DMS oxidation chemistry is also quite uncertain (Hoffmann et al., 2016; Veres et al., 2020) and this can lead to biases as well. Our default model version included an emission parametrization with the DMS field scaled up by a factor of 1.7 to account for

neglecting primary organic aerosol emissions in the model (Mulcahy et al., 2018). This simplified approach may not be realistic because scaling up DMS emissions will result in a larger production of SO_2 and H_2SO_4 via DMS and SO_2 oxidation. Since our goal is to reduce biases in SO_2 and particle number, we ran a simulation without the scale factor of 1.7. More recent versions of the model also include an emission parameterization to estimate the primary marine organic aerosol flux, which is significantly correlated to the chlorophyll concentration (Gantt et al., 2012). Without removing the scale factor of DMS, we tested the sensitivity of aerosol number concentration to this parameterization by running model simulations with the primary marine organic emissions switched on, and also running simulations in which the emissions are scaled up by a factor of 5.

2.6.3 Cloud pH

Cloud droplet pH is an important parameter in the model because the aqueous phase oxidation of SO_2 by O_3 (to form sulphate) (Kreidenweis et al., 2003) is very sensitive to the pH of the cloud droplet. It is assumed in the model that this reaction occurs in all clouds, but the model only tracks the sulfate produced in shallow clouds, and not in deep convective clouds, since most of the sulphate formed would be scavenged from the atmosphere by precipitation in convective clouds, but not in non- or lightly-precipitating shallow clouds. The rate of this reaction increases by a factor of 10^5 for a pH change from 3 to 6 (Seinfeld and Pandis, 2016). Droplet pH is important because the consumption of SO_2 in a cloud droplet affects the mixing ratio of gas phase SO_2 available in the atmosphere, thereby reducing the gas phase concentration of H_2SO_4 (which can form particles). The cloud pH depends on the thermodynamic and kinetic processes in a changing cloud droplet distribution, which are not explicitly simulated in our model; instead a constant cloud pH of 5 is assumed. This assumption could lead

to significant errors in regions of the planet where the pH is higher or lower than 5, owing to the regional variability in the amount of acidic and basic material present in the particles. Since we overestimate SO_2 compared to ATom observations, we performed perturbations by increasing the pH to 6 and 7 so as to lower the SO_2 and N_{Total} bias. This parameter has also been identified in previous studies as one of the most important parameters for global CCN uncertainty (Lee et al., 2013).

2.6.4 Scavenging of aerosol particles and gases

The removal of aerosol particles and gases in convective clouds is an important atmospheric process that can control the vertical profiles of N_{Total}, SO_2 and condensation sink. Convection in the model is represented using a mass flux scheme (Gregory and Rowntree, 1990) which is responsible for the vertical transport of aerosol and gases. Understanding the effect of the removal mechanism for aerosol particles and gases during their vertical transport is crucial in quantifying their vertical distribution. In the model, aerosol particles are scavenged using a convective plume scavenging scheme (Kipling et al., 2013), where scavenging coefficients for aerosol particles are assigned for each mode (denoted by the parameter 'rscav'). This convective plume scavenging scheme addresses, albeit crudely, biases that resulted from operator splitting between scavenging and convective transport and simulation of activation above cloud base, which were subsequently highlighted in other models (Yu et al., 2019). As a plume rises through the atmosphere, the change in aerosol number and mass mixing ratios is dependent on the precipitation rate, convective updraught mass flux, mass mixing ratio of ice and liquid water, and the scavenging coefficients ('rscav') assigned to each mode. The nucleation mode is not scavenged and is assigned a scavenging coefficient of 0, the Aitken, accumulation and coarse modes are assigned scavenging coefficients of 0.5, 1 and 1 respectively. We assess

the sensitivity of the model-observation comparison to perturbations in these values. These scavenging coefficients used are consistent with convective cloud models which show that the aerosol in-cloud scavenging is close to the water scavenging efficiency (less than 1) (Flossmann and Wobrock, 2010).

We also scale up the convective rain scavenging rate for all gases (denoted by the parameter 'csca') by a factor of 10 and 20. These have higher uncertainty than aerosol scavenging coefficients because gas uptake into droplets and subsequent removal depends on gas solubility, temperature, ice formation (and gas retention during freezing), and aqueous-phase chemistry (Yin et al., 2002).

2.6.5 Cloud erosion rate

The cloud erosion rate is an important tuning parameter (represented by UKESM1 parameter 'dbsdtbs') (Yoshioka et al., 2019) for the prognostic cloud fraction and prognostic condensate scheme (PC2) used in the model (Wilson et al., 2008). This parameter determines the rate at which un-resolved subgrid motions mix the clear and cloudy air, thereby removing liquid condensate, and it changes the cloud liquid fraction for shallow clouds. Changing this parameter should have an effect on SO_2 lifetime, as a result of its uptake into cloud droplets. Its effect on the fraction of cloud in each grid box will also change the amount of shortwave radiation received by Earth's surface which in turn can have feedback effects on aerosol processes. This parameter is usually tuned so that the outgoing shortwave radiation the model predicts matches observations. The default value of 'dbsdtbs' in the model is 1.5×10^{-4}. We perform two perturbation simulations with this value set to 0 and another with a value of 10^{-3}.

2.7 Results

The goal of the model one-at-a-time sensitivity tests is to understand the causes of biases in the model. Since we are interested in reducing the absolute magnitude of the biases we use the Normalised Mean Absolute Error Factor (NMAEF) (Yu et al., 2006) defined in equation *(4)* instead of NMBF to characterise the bias. This new equation allows us to calculate the percentage change in model performance as the relative change in NMAEF of a model experiment with respect to the baseline version of UKESM1 as shown in Equation *(5)*.

$$NMAEF = \begin{cases} \frac{\sum |M_i - O_i|}{\sum O_i}, & if\ \bar{M} \geq \bar{\bar{O}} \\ \frac{\sum |M_i - O_i|}{\sum M_i}, & if\ \bar{M} < \bar{\bar{O}} \end{cases} \qquad (4)$$

where M_i represents model data, O_i represents observations, $\bar{M}$ represents the model mean and $\bar{\bar{O}}$ represents the mean of the observations.

$$\textit{Percentage change in model performance} = \left(1 - \frac{NMAEF_{simulation}}{NMAEF_{UKESM\_baseline}}\right) \times 100 \qquad (5)$$

The percentage change is zero when the sensitivity test has no effect on mean model bias, positive when there is an reduction in bias, and negative when the bias increases. A model that is in agreement with observations will have an NMAEF of zero and a percentage improvement of 100%. Different simulations have varying effects on the vertical profiles at different altitudes in the troposphere and we have therefore split our analysis to study model performance with altitude. The real boundary layer height varies with latitude, but for the purposes of this study we assume it is 1 km

everywhere. Our results are similar for the boundary layer and lower troposphere, suggesting that our analysis is not sensitive to this assumed boundary layer height. In section 2.7.1 we look closely at the model's performance in the boundary layer (which we define here as altitudes below 1 km) and lower troposphere (1 km < altitude < 4 km), and in Section 2.7.2 we study the mid (4 km < altitude < 8 km) and upper troposphere (>8 km).

2.7.1 Boundary layer and lower troposphere

The performance for the different perturbation simulations in the boundary layer (altitude < 1 km) can be assessed from Figure 8. The NMAEF values for the simulations in the boundary layer are provided in *Table 2*a. The percentage change in the bias of N_{Total}, SO_2 mixing ratio, and condensation sink from each of these perturbation simulations is calculated relative to the baseline version of UKESM1 and is represented by bar plots.

Firstly, we look at the model performance with respect to N_{Total} in the altitude range 0-1 km where the model is biased low (Figure 8a). The baseline version of the model produces boundary layer N_{Total} values that are negatively biased (NMAEF = 2.21). To reduce the bias in particle number concentration near the surface, the model perturbation simulations (denoted as 'BL_nuc' and 'BL_nuc/10') that include a boundary layer nucleation mechanism show the best improvement in performance. 'BL_nuc' refers to the simulation that includes the Metzger boundary layer nucleation mechanism (Metzger et al 2010), and 'BL_nuc/10' refers to a simulation with the same nucleation mechanism but with the nucleation rate reduced by a factor of 10. Including this nucleation mechanism substantially improves model performance by 63% (NMAEF = 0.78) for 'BL_nuc' and 68% (NMAEF = 0.72) for 'BL_nuc/10'. This is an indication that the negative model bias in the boundary layer (Figure 5)

could be explained by a missing boundary layer nucleation mechanism in the model, even though this mechanism depends on terrestrial emissions of shortlived organic compounds (typically not found in large concentrations over marine regions). A nucleation mechanism other than the Metzger mechanism (Metzger et al., 2010) which could be a scheme controlled by chemical species found in the marine boundary layer like methane sulfonic acid (MSA) (Pham et al., 2005), iodine (Cuevas et al., 2018) or ammonia (Dunne et al., 2016) could help reduce model biases even more, but is not the focus of this work. All the other perturbation simulations either have no significant effect or decrease N_{Total} model performance in the boundary layer. The perturbation simulations that stand out as performing the poorest in the boundary layer are when we increase the pH (denoted by 'pH = 6' (NMAEF = 2.75) and 'pH = 7' (NMAEF = 2.94)), condensation sink (denoted by 'condsink*5' (NMAEF = 2.58) and 'condsink*10' (NMAEF = 2.89)) and scavenging of SO_2 ('csca*10' (NMAEF = 2.55) and 'csca*20' (NMAEF = 2.61)). These perturbations show (Figure 8a) an approximate decrease of 25% in N_{Total} model performance.

Secondly, we look at the parameters that significantly improve the ability of the model to reproduce SO_2 mixing ratios in the boundary layer (Figure 8b) where the model is biased high (NMAEF = 2.09). Figure 8b shows that perturbations to cloud pH, DMS emissions (denoted as 'seadms=1.0'), convective rain scavenging rate (denoted by 'csca*10' and 'csca*20') and the cloud erosion rate (denoted by 'dbsdtbs=0') all improve model performance. The DMS emission perturbation, where we removed the artificial scaling factor of 1.7 that was used to compensate for the lack of primary marine organics, was also found to improve the model performance by 36% (NMAEF = 1.34). Increases in cloud pH from the default value of 5 to 6 or 7 (denoted in the figure as 'pH=6' and 'pH=7') improve the model by 34% (NMAEF = 1.39) and 48%

(NMAEF = 1.09) respectively. In the atmosphere, a lower cloud pH is typically associated with polluted environments where particles are sulphate-rich, and higher cloud pH is associated with marine regions where particles are larger and contain carbonates from sea spray (Gurciullo and Pandis, 1997). Therefore, perturbations to cloud pH by increasing it to 6 or 7 are plausible explanations for the improved model skill since the observations are primarily over the remote ocean. Increasing the pH increases the rate of the reaction $SO_2 + O_3 \rightarrow SO_4^{2-}$ in a cloud droplet, thereby resulting in a larger consumption of aqueous SO_2. This drives more SO_2 from the gas phase to the aqueous phase, thereby reducing the gas phase SO_2 model bias. Increasing the pH can also compensate for the oxidation of SO_2 with O_3 on sea salt particles which is shown to be significant atmospheric process in marine regions (Korhonen et al., 2008). Furthermore, when the cloud erosion rate was set to zero (denoted by 'dbsdtbs_0'), it resulted in a model improvement of 25% (NMAEF = 1.56). A high value for dbsdtbs will cause more mixing of clear and dry air into clouds, thereby reducing the cloud liquid water content, cloud amount, and auto conversion of cloud droplets to raindrops. A low value of this parameter results in an increased lifetime for aerosol and precursor gases like SO_2.

Thirdly, we look at the parameters that most affect the model performance with respect to the prediction of the condensation sink (Figure 8c). The condensation sink in the boundary layer for the baseline version of the model has an NMAEF of 0.82. Simulations where we perturbed the boundary layer nucleation rate ('BL_nuc' and 'BL_nuc/10') and the primary marine organic emissions ('primmoc*5') showed a 15% (NMAEF = 0.69), 10% (NMAEF = 0.73) and 25% (NMAEF = 0.61) improvement in bias. This could be because the boundary layer is lacking particles and including a new source of particles via boundary layer nucleation and emissions

reduces the negative bias in the boundary layer (Figure 8c). The simulations where we increase the condensation sink by a factor of 5 and 10 show larger biases (NMAEF = 2.46 and 5.5 respectively). These perturbations are somewhat unrealistic, because the baseline version already agrees well (within a factor of 2) with observations, but they are useful as tests of the sensitivity of new particle formation in the model to the condensation sink.

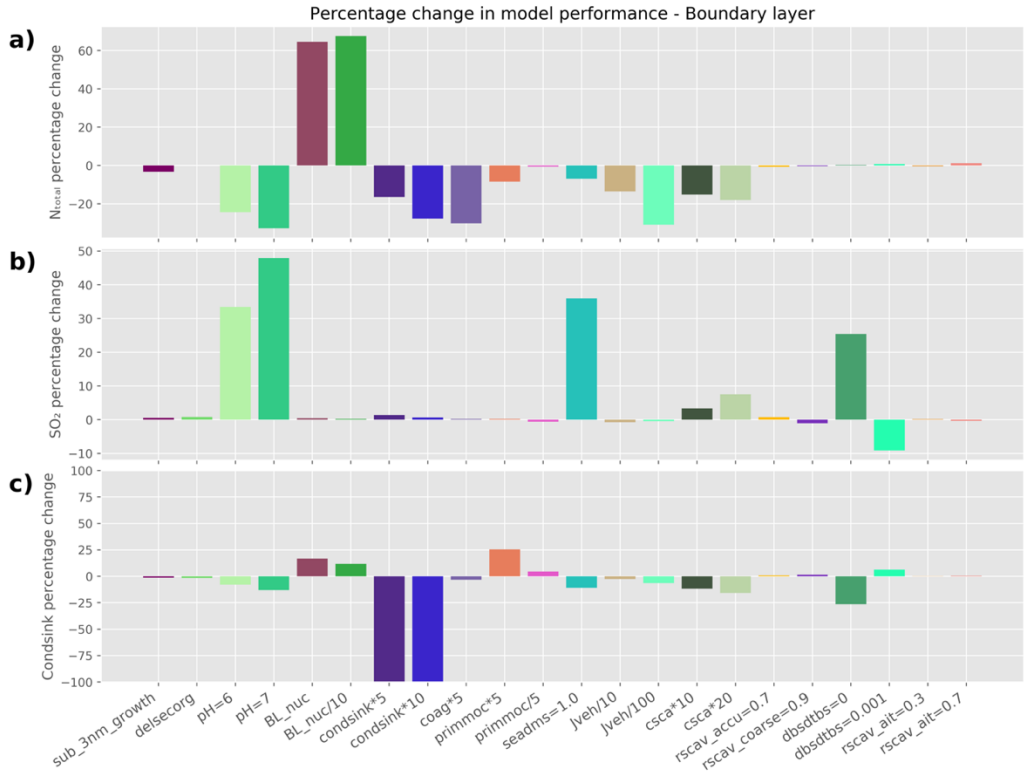

Figure 8: Percentage change in model performance for different perturbation simulations in the boundary layer (altitude < 1 km) with respect to, a) N_{Total}, b) SO_2, and c) condensation sink

The atmospheric processes that improve the skill of the model in the lower troposphere (between 1 km and 4 km) (Appendix A Figure A7) (NMAEF values are shown in Appendix A, Table A2) are the same as the boundary layer with very slight differences in the magnitude of the percentage change in model performance.

2.7.2 Mid and Upper Troposphere

The model sensitivities in the upper troposphere are shown in Figure 9. Firstly, we assess N_{Total} model performance for all the model simulations (Figure 9a). We observe that perturbations to several atmospheric processes help improve the model performance. Perturbations to the condensation sink, nucleation rate, sub 3nm growth, DMS emissions, gas scavenging rate, cloud erosion rate and cloud pH are found to have a significant effect on model performance. The range of parameter sensitivities is more diverse than in the boundary layer and the magnitudes are larger.

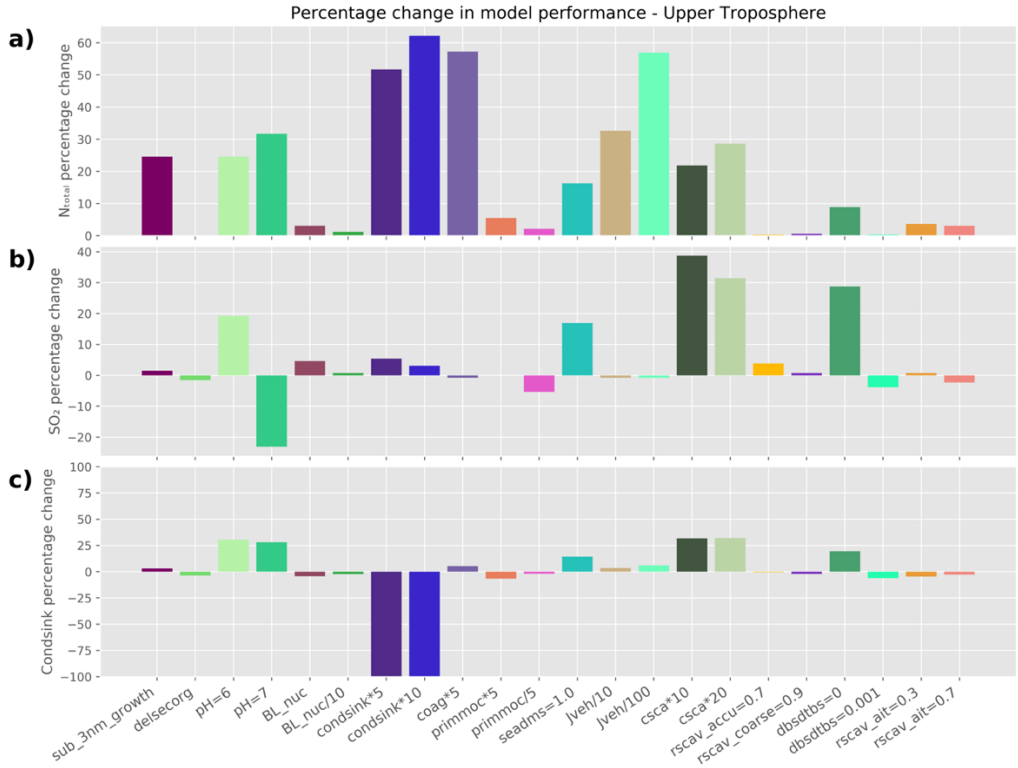

Figure 9: Percentage change in model performance for different perturbation simulations in the Upper Troposphere (>8 km) with respect to, a) N_{Total} , b) SO_2 , and c) condensation sink

First, we look at the model's performance with respect to N_{Total}. The baseline simulation produces N_{Total} values that are biased high (NMAEF = 3.25) in the upper

troposphere (*Table 2*b). The most improvement in model performance with respect to N_{Total} (Figure 9a) was for the model simulations where we directly perturbed the condensation sink. These model runs were denoted as 'condsink*5' and 'condsink*10' and shows an improvement in performance by 51% (NMAEF = 1.57) and 62% (NMAEF= 1.23) respectively (*Table 2*b). This improvement in performance is because increasing the condensation sink will increase the rate at which H_2SO_4 is removed from the atmosphere via condensation onto particles. Therefore, increasing the condensation sink can help reduce the H_2SO_4 concentration and thus reduce the N_{Total} bias. However, as noted earlier, directly scaling the condensation sink by factors of 5 and 10 in this way is unrealistic, as the model's condensation sink is within a factor of 2 of observations (Figure 8)

Perturbations to nucleation rate where we reduced nucleation rate by a factor of 10 and 100 (denoted as 'Jveh/10' and 'Jveh/100') also improved the model by 32% (NMAEF = 2.19) and 56% (NMAEF = 1.4) respectively. This improvement in model performance by reducing nucleation rate is an indication that the source of the biases in N_{Total} are mainly from small particles formed via nucleation. Model runs where we increase the convective gas scavenging rate (denoted as 'csca*10' and 'csca*20') by a factor of 10 and 20 results in a 21% (NMAEF = 2.54) and 28% (NMAEF = 2.32) improvement respectively. This scavenging rate simply scavenges the SO_2 from the atmosphere at a higher rate, which leaves less SO_2 to form H_2SO_4 via oxidation and therefore decreases N_{Total}. The cloud pH perturbation simulations show a 25% (NMAEF= 2.45) and 31% (NMAEF = 2.22) improvement for 'pH=6' and 'pH=7' respectively. Increasing cloud pH would increase the oxidation rate of SO_2 by ozone in cloud droplets (to form sulphate) thereby causing a reduction in the concentration of gaseous H_2SO_4. Incorporating the dependency of the coagulation sink on particle

diameter (by using the (Lehtinen et al., 2007) parameterization denoted as 'sub_3nm_growth') reduces the positive bias in the model and improves the model by 24% (NMAEF = 2.45). This is because in the new expression (Lehtinen et al 2007) the coagulation sink for sub-3nm particles is greater than the previous assumption (Kerminen & Kulmula 2002).

Second, we analyse the model sensitivity and performance with respect to SO_2 (Figure 9b and *Table 2*). The baseline simulation produces SO_2 mixing ratios that are biased high (NMAEF = 1.3). The simulations that have the strongest effect on the biases are the perturbations to the DMS emissions ('seadms = 1.0'), cloud pH ('pH=6') and SO_2 scavenging rate ('csca*10' and 'csca*20'), they improve the model by 17% (NMAEF = 1.08) , 19% (NMAEF = 1.05), 38% (NMAEF = 0.80) and 31% (NMAEF = 0.89) respectively (*Table 2*). The large SO_2 over-prediction by the model in the tropical upper-troposphere (NMAEF = 1.3) is corrected by the perturbations where the SO_2 in the atmosphere is removed by scavenging ('csca*10' and 'csca*20'), by reduction in DMS emissions ('seadms=1.0') or by reduction in the SO_2 mixing ratio as a result of increasing the cloud droplet pH. However, the simulation with cloud pH set to 7 results in too much SO_2 being removed by lower level clouds, leaving less available SO_2 to be convected to the upper troposphere causing a large negative bias (NMAEF = 1.6).

Third, we look at the model performance with respect to the condensation sink (Figure 9c) where the model is biased with NMAEF = 0.61. The perturbations; cloud pH ('pH =6' and 'pH=7'), convective gas scavenging rate ('csca*10' and 'csca*20'), cloud erosion rate ('dbsdtbs=0') and DMS emissions ('seadms =1.0') all improve model performance by 15-30%. Increasing the pH of a cloud drop enhances SO_2 aqueous phase chemistry in low level clouds to form sulphate, which partitions sulfur to the

aqueous phase and increases wet removal, leaving less SO_2 to be convected upward to higher altitudes. This also results in a reduction in the concentration of larger particles being transported by convection to higher altitudes, thereby reducing the condensation sink to match better with observations. Similarly, reduction in cloud erosion rate will result in greater uptake of SO_2 on cloud droplets to form sulphate, thereby increasing aerosol mass and increasing the amount of scavenged larger particles. The other perturbations, where we indirectly influenced the SO_2 mixing ratio in the atmosphere by reducing the DMS emissions and SO_2 scavenging, also reduce the positive bias in the model condensation sink by reducing the SO_2 available to form sulphate.

The atmospheric processes that are of significance to model performance with respect to N_{Total} and condensation sink in the mid troposphere are similar to the upper troposphere, with decreases in the magnitude of model performance (Figure A8, Appendix) relative to the upper troposphere. This indicates that the atmospheric processes that have been identified are of more importance at higher altitudes. However, for the model performance with respect to SO_2 in the mid troposphere shows more similarity with the lower troposphere (Figure A7, Appendix).

2.8 Model performance: A three-way comparison

2.8.1 Effect of perturbations on multiple variables

The main reason for analysing N_{Total}, SO_2 and condensation sink model performance simultaneously is to make sure that performing one-at-a-time sensitivity tests to assess model performance leads to a consistent result. Improving only one of these quantities in comparison with observations can lead to a misleading impression that overall model performance has improved. Analysing N_{Total}, SO_2 and condensation sink simultaneously helps reduce the probability of getting the right answer for the wrong

reasons. We find that different atmospheric processes affect the vertical profile of N_{Total}, SO_2 and condensation sink to varying degrees.

Firstly, we analyse the boundary layer (<1 km) and lower troposphere (1-4 km). In section 2.7.1 we identified the atmospheric processes that are important for the boundary layer and how they affected model performance with respect to N_{Total}, SO_2 and condensation sink independently. Here we look at which simulations perform the best when comparing these variables simultaneously. *Table 2* shows the NMAEF in the boundary layer and upper troposphere for all of the simulations. The NMAEF values for the baseline simulation are highlighted in yellow, the green boxes represent NMAEF values for the simulations that have the same or lower biases than the baseline simulation, and the orange boxes represent those simulations that have higher biases than the baseline simulation. The results show that the model simulations where we perturbed the cloud pH, DMS emissions, convective gas scavenging rate and cloud erosion rate all significantly reduce biases with respect to SO_2 but make the model perform worse with respect to N_{Total} and the condensation sink. In *Table 2*, the blue dotted boxes highlight the simulations for which the biases with respect to N_{Total}, SO_2 and condensation sink are less than or equal to the baseline simulation. The only model simulation that improved N_{Total}, SO_2 and condensation skill simultaneously was when we included boundary layer nucleation ('BL_nuc' and 'BL_nuc/10'). Including a boundary layer nucleation scheme adds a new source of particles which helps reduce the negative bias the model shows in the boundary layer.

Table 2: Normalised mean absolute error factor (NMAEF) with respect to N_{Total}, SO_2 and condensation sink for different model simulations. NMAEF values for the baseline simulation are highlighted in yellow. NMAEF values that are less than or equal to the baseline simulation are highlighted in green. NMAEF values that are greater than the baseline simulation are highlighted in orange. The plus (+) and minus (-) sign next to each NMAEF value indicates whether the bias is positive or negative. The dotted blue box indicates the model simulation for which NMAEF values for N_{Total}, SO_2 and condensation sink are less than the baseline simulation simultaneously; a) boundary layer (below 1km) and b) upper troposphere (>8km)

a)

NMAEF for model simulations in the Boundary layer			
Model perturbation	N_{Total}	SO_2	Condensation sink
Baseline	2.21(-)	2.09(+)	0.82(-)
sub_3nm_growth	2.28(-)	2.08(+)	0.83(-)
delsecorg	2.21(-)	2.07(+)	0.84(-)
pH=6	2.75(-)	1.39(+)	0.89(-)
pH=7	2.94(-)	1.09(+)	0.93(-)
BL_nuc	0.78(+)	2.08(+)	0.69(-)
BL_nuc/10	0.72(-)	2.09(+)	0.73(-)
condsink*5	2.58(-)	2.06(+)	2.46(+)
condsink*10	2.82(-)	2.08(+)	5.55(+)
coag*5	2.88(-)	2.09(+)	0.85(-)
primmoc*5	2.40(-)	2.09(+)	0.61(-)
primmoc	2.22(-)	2.10(+)	0.79(-)
seadms=1.0	2.36(-)	1.34(+)	0.91(-)
Jveh/10	2.51(-)	2.11(+)	0.85(-)
Jveh/100	2.89(-)	2.10(+)	0.88(-)
csca*10	2.55(-)	2.02(+)	0.92(-)
csca*20	2.61(-)	1.93(+)	0.95(-)
rscav_accu=0.7	2.23(-)	2.07(+)	0.82(-)
rscav_coarse=0.9	2.22(-)	2.11(+)	0.81(-)
dbsdtbs=0	2.21(-)	1.56(+)	1.04(-)
dbsdtbs=0.001	2.19(-)	2.28(+)	0.77(-)
rscav_ait=0.3	2.22(-)	2.09(+)	0.82(-)
rscav_ait=0.7	2.19(-)	2.10(+)	0.82(-)

b)

NMAEF for model simulations in the upper troposphere			
Model perturbation	N_{Total}	SO_2	Condensation sink
Baseline	3.25(+)	1.30(+)	0.61(+)
sub_3nm_growth	2.45(+)	1.28(+)	0.59(+)
delsecorg	3.25(+)	1.31(+)	0.63(+)
pH=6	2.45(+)	1.05(-)	0.42(+)
pH=7	2.22(+)	1.60(-)	0.44(-)
BL_nuc	3.15(+)	1.24(+)	0.63(+)
BL_nuc/10	3.21(+)	1.29(+)	0.62(+)
condsink*5	1.57(+)	1.23(+)	5.8(+)
condsink*10	1.23(+)	1.25(+)	12.1(+)
coag*5	1.39(+)	1.31(+)	0.57(+)
primmoc*5	3.07(+)	1.30(+)	0.65(+)
primmoc	3.18(+)	1.37(+)	0.62(+)
seadms=1.0	2.72(+)	1.08(+)	0.52(+)
Jveh/10	2.19(+)	1.30(+)	0.58(+)
Jveh/100	1.40(+)	1.30(+)	0.57(+)
csca*10	2.54(+)	0.80(-)	0.41(+)
csca*20	2.32(+)	0.89(-)	0.41(-)
rscav_accu=0.7	3.26(+)	1.25(+)	0.61(+)
rscav_coarse=0.9	3.26(+)	1.29(+)	0.62(+)
dbsdtbs=0	2.96(+)	0.93(-)	0.49(+)
dbsdtbs=0.001	3.24(+)	1.35(+)	0.64(+)
rscav_ait=0.3	3.19(+)	1.29(+)	0.63(+)
rscav_ait=0.7	3.27(+)	1.33(+)	0.62(+)

In the upper troposphere (*Table 2*b), several simulations improve N_{Total} model performance. The positive model bias in N_{Total} is significantly reduced by perturbations to the sub 3 nm growth, cloud pH, condensation sink, coagulation sink, primary marine organic emissions, DMS emissions, nucleation rate, and SO_2 gas scavenging rate. Direct perturbations to the condensation sink, although they improve N_{Total} model skill significantly, worsen the model performance with respect to the condensation sink (NMAEF = 12.1 for 'condsink*10' simulation). Thus, from *Table 2*b, the blue dotted boxes indicate the simulations for which the model biases for N_{Total}, SO_2 and condensation sink are less than (or equal to) the baseline version of the model simultaneously.

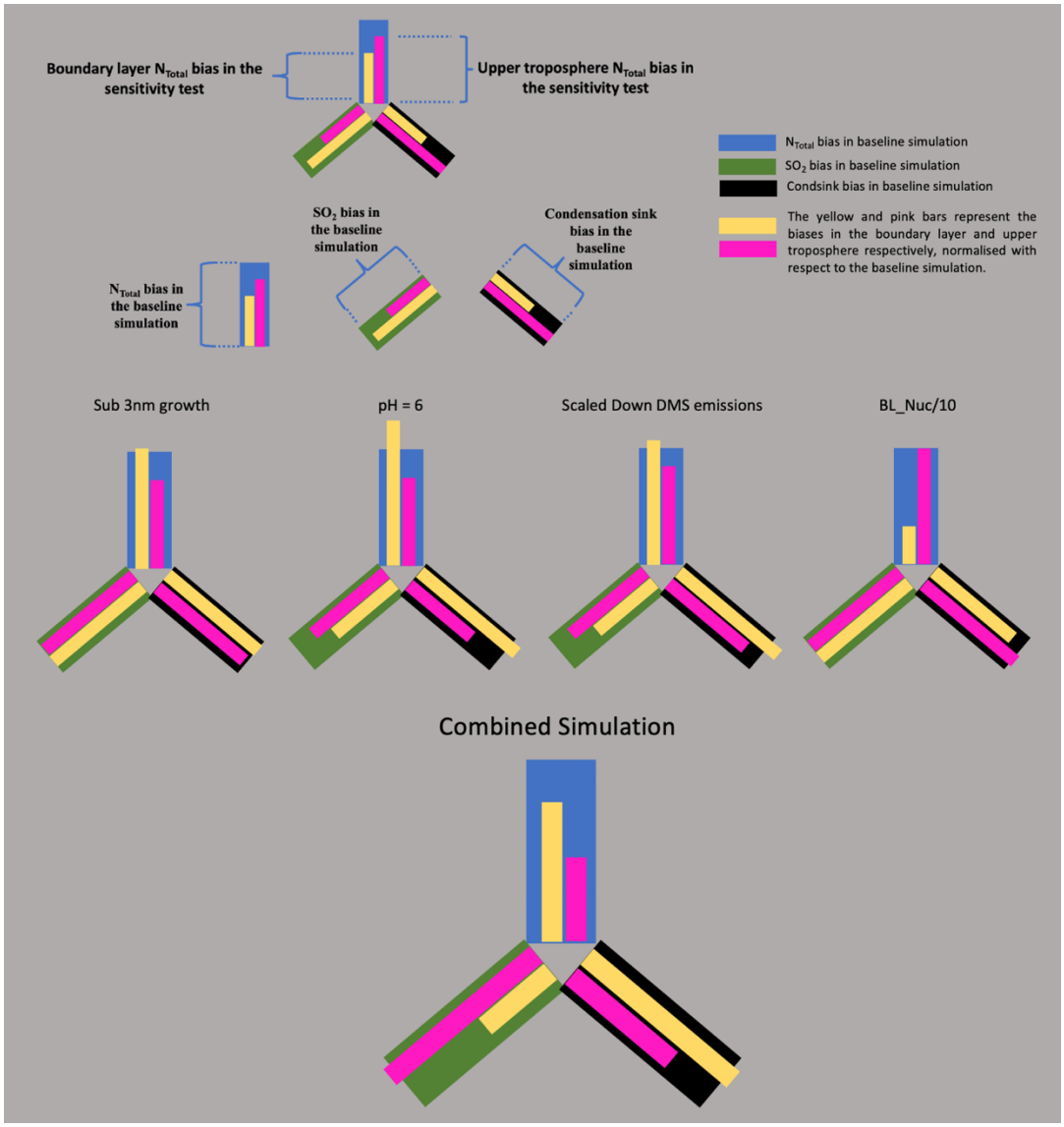

Figure 10: Diagram to represent of the N_{Total}, SO_2 and condensation sink biases (in the boundary layer and upper troposphere) for the one at time sensitivity tests: sub 3nm growth, Cloud pH = 6, scaling down DMS emissions, boundary layer nucleation/10. The blue, green and black legs of the diagram represent the N_{Total}, SO_2 and condensation sink bias respectively. The yellow and pink bars represent the biases in the boundary layer and upper troposphere normalised with respect to the baseline simulation.

We see this simultaneous reduction of biases in the mid (Table A2 appendix) and upper troposphere for simulations where we perturbed sub 3nm growth, cloud pH, DMS emissions, nucleation rate, SO_2 gas scavenging rate and cloud erosion rate. The one main difference between the simulations in the mid and upper troposphere is that the perturbation to cloud pH (pH =7) improves overall model performance in the mid-

troposphere but not in the upper troposphere. At pH = 7 the model in the upper troposphere also shows a larger SO_2 bias (NMAEF = 1.6) than the baseline (NMAEF = 1.3).

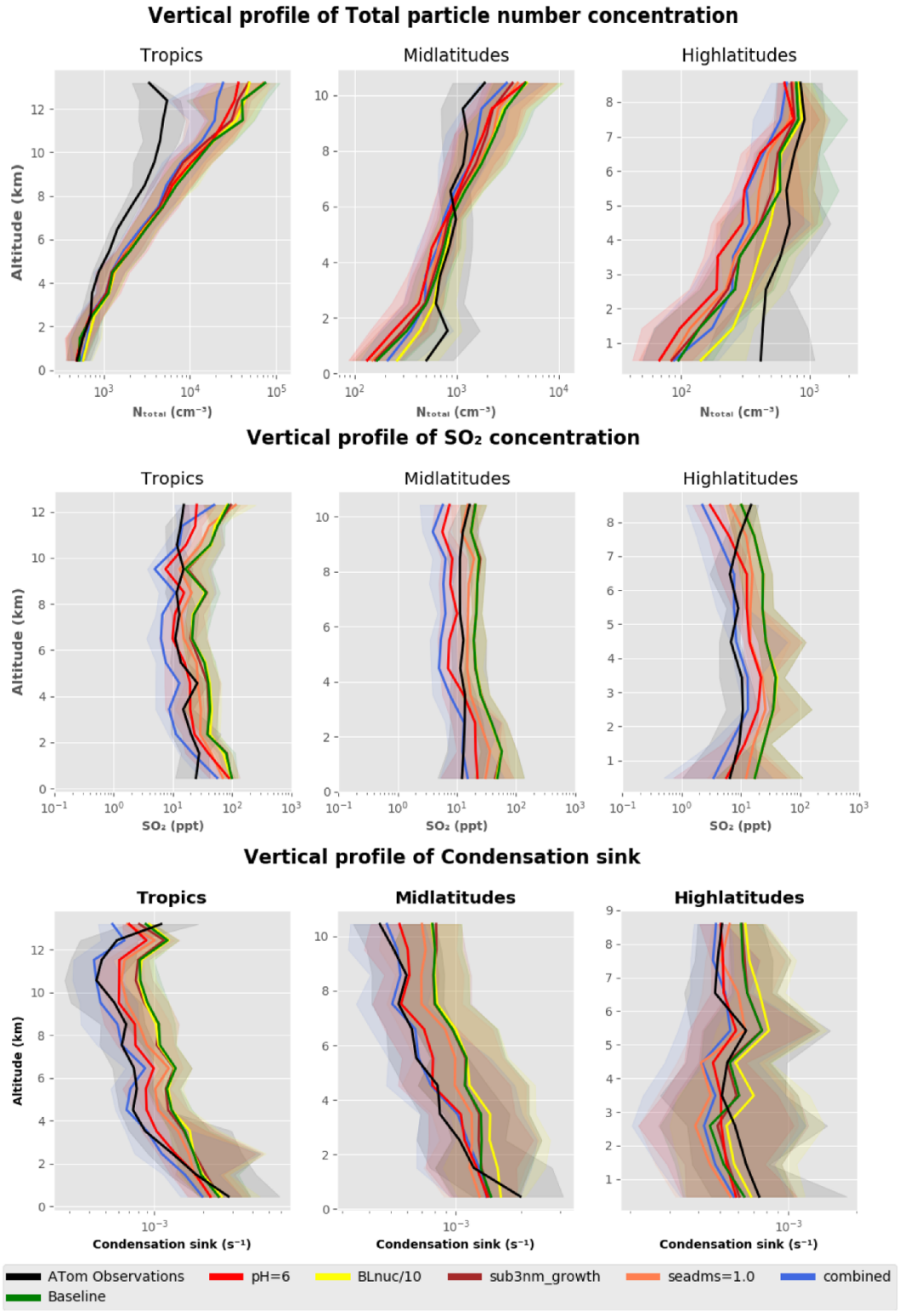

Figure 11: The vertical profile of a) N_{Total}, b) SO_2 and c) condensation sink for different model experiments that were found to have the most influence on model performance. The vertical profiles of observation data, the baseline simulation and perturbation simulations of cloud pH, boundary later nucleation, sub-3 nm growth, scaled-down DMS emissions, and the combined simulation are shown and categorised into three regions of the earth: the tropics (25^oN-25^oS), midlatitudes (25^oN-60^0N and 25^oS-60^oS), and high latitudes (60^oN-90^oN and 60^oS-90^oS).

We show the combined model bias for a select few sensitivity tests in the boundary layer and upper troposphere using a bar diagram (Figure 10). In this presentation, the blue, green and black bars represent the normalised NMAEF in N_{Total}, SO_2 and condensation sink for the baseline simulation. The yellow and pink bars represent the corresponding biases in the boundary layer and upper troposphere for any given sensitivity test (normalised with respect to the baseline simulation). If the length of the blue, green or black bars is greater than the length of the corresponding yellow and pink bar, then the bias in the sensitivity test is less than the baseline simulation. The vertical profiles for the simulations used in Figure 10 are shown in Figure 11. Simulations where we perturbed sub-3 nm growth, pH = 6, DMS scaling, and boundary layer nucleation/10 showed a reduction in biases and in some cases increased biases negligibly. The boundary layer nucleation simulation (BL_nuc/10) reduces biases in the boundary layer N_{Total} by ~67% without affecting the upper tropospheric N_{Total} bias. This simulation does not have any effect on the SO_2 mixing ratio but does reduce the condensation sink bias in the boundary layer by ~11% and shows a negligible change in bias (~2%) in the upper troposphere. Changing the pH to 6 causes a slight degradation in the model's N_{Total} and condensation sink (increase in bias by ~24% and ~8%) in the boundary layer and improved the SO_2 by 33%. However, in the upper troposphere perturbations to pH has a positive effect on model performance against observations. The 'sub_3nm_growth' simulation improves the

upper tropospheric N_{Total} bias by ~24% without significantly affecting other parameters. Removing the scaling factor for DMS emission helps improve the upper tropospheric N_{Total}, SO_2, and condensation sink bias by 16%, 17% and 14% respectively. It also reduces the boundary layer SO_2 bias by 35% and shows a small increase of 6% and 10% in the N_{Total} and condensation sink bias respectively. Thus, we have identified the perturbation simulations; 'BL_nuc/10', 'pH = 6', 'Seadms = 1.0' and 'sub_3nm_growth' as the simulations that help reduce model biases in most cases across N_{Total}, SO_2 and condensation in the boundary layer and upper troposphere. These perturbations are well-motivated in that they improve the physical basis of the model and can be looked at more closely when developing future versions of UKESM1.

2.8.2 Effect of combined perturbations on multiple variables

We performed one simulation incorporating the 4 perturbations (BL_nuc/10, pH = 6, 'Seadms = 1.0' and 'sub_3nm_growth') discussed in section 2.8.1 simultaneously (bottom row in Figure 10) to assess model performance. For N_{Total}, the model's boundary layer and upper tropospheric performance is improved (NMAEF reduced by 24% and 54% respectively). The positive SO_2 bias improves by 54% in the boundary layer but showed a slight degradation of 10% in the upper troposphere. The positive condensation sink bias shows a negligible increase of 4% in the boundary layer and a 29% decrease in the upper troposphere. From Figure 11, the SO_2 profile for the combined simulation shows better agreement with observations in the tropics and high latitudes and shows a small negative bias in the midlatitude free troposphere. The condensation sink profile of the combined simulation does show a much better agreement with the observations in tropics, midlatitudes and high latitudes. The combined simulation also shows a substantial reduction in the upper tropospheric

N_{Total} bias in the tropics and midlatitudes but the large negative bias in the high latitudes remains, and at high altitudes in the high latitude regions, it is exacerbated. In the boundary layer, the combined simulation shows a small improvement in the midlatitudes but otherwise performs similar to the baseline simulation. The interhemispheric differences in the vertical profile of the combined simulation and baseline simulation are shown in the Appendix (Figure A9). Overall, the combined simulation performs better than the baseline simulation in both hemispheres, with a couple of notable exceptions. The combined simulation underpredicts observations of N_{Total} in the southern high latitude upper troposphere and of SO_2 concentration in the northern high latitude upper troposphere by up to a factor of 2 more than the baseline simulation. We speculate that a marine nucleation mechanism or regional changes in cloud pH that are not simulated in the model currently could be the reason for these interhemispheric biases.

In the tropical free troposphere, the fact that the SO_2 and condensation sink for the combined simulation agree very well with observations and N_{Total} is still overpredicted suggests a missing loss process for nucleation mode particles in the upper troposphere, or a bias in the downward transport of these particles to lower altitudes. The biases in N_{Total} in the high-latitude and mid-latitude boundary layer for the combined simulation could be because of a missing source of small particles from a marine nucleation mechanism which is not included in the model, for example involving iodine or methane sulfonic acid (Baccarini et al., 2018; Hodshire et al., 2019). Even though simulations with the Metzger boundary layer nucleation scheme (Metzger et al., 2010) helped reduce this bias, this nucleation scheme is primarily dependent on the concentration of organic vapors from terrestrial sources, which are low over marine regions. The biases in the boundary layer high latitudes could also be due to

uncertainties associated with the sea spray parametrisation in the model (Regayre et al., 2020).

To summarise, our new combined simulation performs significantly better than the baseline model we started with for all three variables, N_{Total}, SO_2 and condensation sink. However, we were still unable to reproduce observations of N_{Total} in the tropical free troposphere, the mid-latitude boundary layer, and the high latitudes with the well-motivated adjustments we applied. Clearly structural errors in the model remain, possibly associated with the way that aerosols and trace gases are incorporated in the convection parametrisation (Prein et al., 2015) or other atmospheric processes: this study motivates future model developments to address the biases and indicates where the developments should be focused.

2.9 Discussion and Conclusions

We have evaluated the vertical profile of N_{Total}, SO_2 and condensation sink from UKESM1 against ATom aircraft measurements. The model captured the trends in the vertical profiles. Quantitatively, the model reproduced the vertical profile of condensation sink moderately well but shows higher biases in the N_{Total} and SO_2 vertical profile. We performed model simulations to help understand which atmospheric processes influence the model skill and thereby help match the model's prediction of N_{Total}, SO_2, and condensation sink simultaneously with observations. We found that different atmospheric processes have a varying impact on model skill with altitude.

In the boundary layer and lower troposphere, the model showed negative biases in N_{Total} (up to a factor of 3) and positive biases in SO_2 (up to a factor of 6) with moderate positive/negative model biases in the condensation sink (within a factor of 2). We

found that simulations with boundary layer nucleation included were the only simulations that reduced the biases in N_{Total} and condensation sink in the boundary layer simultaneously with negligible changes to the SO_2 mixing ratio.

In the middle and upper troposphere, the largest biases were again observed in N_{Total} (positive biases up to a factor of 15) and SO_2 (positive biases up to a factor of 6), with the model's condensation sink showing modest positive/ negative biases (within a factor of 2). However, in contrast to lower altitudes, we found that adjustment of several atmospheric processes improved overall model performance. From our one-at-a-time sensitivity tests we found that simulations with perturbations to the sub-3 nm growth, cloud pH, DMS emissions, nucleation rate, gas scavenging rate and cloud erosion rate all help reduce model biases in N_{Total}, SO_2, and condensation sink simultaneously at higher altitudes.

Simulations where we increased the condensation sink by a factor of 10 or reduced the nucleation rate by a factor of 100 also substantially improved the model's N_{Total} profile in the tropical upper troposphere. However, while useful to understand the sensitivity, artificial adjustment of the condensation sink is unrealistic because the model shows only a factor of 2 bias compared to observations. Substantial reduction of the nucleation rate was also explored as this is the main source of particles in the cold upper troposphere. However, the default nucleation rate (Vehkamäki et al., 2002) has been shown to be reasonably accurate or even underestimated for a given sulphuric acid concentration, temperature and humidity (Määttänen et al., 2018). If the effective nucleation rate in the model is indeed too high by a factor of 100, then this may instead suggest a structural deficiency in the way nucleation is implemented in the model, which we discuss below. Any adjustment of the nucleation rate itself is

not supported by our current understanding of the rate of nucleation under upper tropospheric conditions.

Though there are differences in the importance of certain atmospheric processes over others at low and high altitudes, we have identified a few well-motivated changes that help reduce the bias in the boundary layer and upper tropospheric regions of the tropics, mid-latitudes and high latitudes. From our analysis we can suggest the following,

1. Including a boundary layer nucleation scheme helps reduce model biases at lower altitudes without causing large changes in biases in the upper troposphere.
2. Changing the value of cloud pH from 5 to 6 produces a significant improvement in model performance in the mid and upper troposphere. However, this change does result in a slight degradation of the model's N_{Total} profile at lower altitudes.
3. Improvements to the model's microphysics by updating the parameterization of nuclei growth (Kerminen and Kulmala, 2002) to include a corrected dependency of coagulation sink on particle diameter (Lehtinen et al., 2007) improves upper tropospheric model performance without significant degradation of the model at lower altitudes.
4. Removing the scaling factor for DMS emissions also helps reduce the positive biases in SO_2 both in the boundary layer and upper troposphere. This simulation does however increase the biases in N_{Total} and condensation sink in the boundary layer.

We performed a simulation with these four perturbations included simultaneously and found the model's performance in the boundary layer and upper troposphere improved simultaneously. The combined simulation's SO_2 and condensation sink profiles agree very well with observations and perform much better than the baseline simulation.

However, the N_{Total} profile for the combined simulation in the tropics and high-latitudes, while performing better than the baseline simulation, still has significant biases when compared to observations. The fact that this adjusted simulation reduces the N_{Total} bias, but does not completely eliminate it, will help us identify the possible deficiencies of the model in future work. The absence of a scavenging mechanism for nucleation mode particles (for example on cirrus clouds) or uncertainties in the downward transport of particles could explain the reason for the N_{Total} positive bias in the upper troposphere-tropics. The negative bias in the boundary layer N_{Total} could be explained by uncertainties associated with the sea spray parametrisation or the absence of a nucleation scheme involving gaseous precursors found in the marine environment. Thus, in this work, we have identified several atmospheric processes and parameters in UKESM1 that are key to the skilful simulation of SO_2 mixing ratio, condensation sink and N_{Total} simultaneously, although we reached a limit in how much the N_{Total} can be improved upon with the current set of simulations. These perturbations shed light on the influence of different atmospheric processes on aerosol number concentration and motivate further development of parameterizations in the model. Our work will also help inform future perturbed parameter ensemble studies designed to analyse and constrain the effect of a combination of parameters on model skill.

Chapter 3 - Climatic effect of New particle formation

The contents of this chapter are going to be submitted as a Brief Communication to Nature Geoscience

3.1 Abstract

For over 20 years, nucleation of new aerosol particles has been recognised as an important source of atmospheric aerosol in many environments. Here we show that nucleation also plays a fundamental role in Earth's climate. Climate model simulations show that nucleation causes a planetary cooling of 2.45 Wm^{-2}, which exceeds the global warming effect of all atmospheric methane. The globally pervasive background of nucleated aerosol strongly damps the climatic effect of large changes in natural and anthropogenic aerosol emissions.

3.2 Introduction

New particle formation (NPF), or Nucleation, is an atmospheric process whereby gas molecules collide and form molecular clusters that subsequently grow to form aerosol particles. These aerosol particles can impact the global energy balance by scattering and absorbing solar radiation (aerosol-radiation interaction, ARI) and also change the microphysical properties of clouds (aerosol-cloud interaction, ACI) (Albrecht, 1989; Twomey, 1977). Nucleation is a key atmospheric process that regulates global aerosol concentration and has been observed in various environments across the earth

(Kerminen et al., 2018b). Our molecular-level understanding of nucleation has evolved significantly over the last decade, with recent research highlighting the roles played by ions, organic compounds, nitric acid, iodic acid, ammonia and amines (He et al., 2021; Pierce, 2017; Wang et al., 2020) in NPF. Modelling studies in the past have highlighted the contribution of nucleation to aerosol number concentration (Kazil et al., 2010; Spracklen et al., 2006). Nucleation is found to be responsible for approximately half of the cloud-forming particles globally in the present day and about two-thirds of the cloud-forming particles in the pre-industrial environment (Gordon et al., 2017).

In this work, we explore the role played by nucleation in regulating various aspects of climate using a climate model. To quantify its role we use a global climate model, the UK Earth System Model (UKESM1) (Mulcahy et al., 2020). We compare simulations of a planet with and without nucleation to assess the impact nucleation would have on the radiation balance, aerosol forcing, aerosol concentration, black carbon, cloud droplet number concentration, liquid water path and cloud fraction. We also look at the role played by nucleation in the dampening of cloud responses when fire emissions are perturbed.

3.3 Model Setup

The model used in this work is a modified version of the United Kingdom Earth system Model version 1 (UKESM1) (Mulcahy et al., 2020; Sellar et al., 2019) in its atmosphere-only configuration (with fixed sea surface temperatures). The model version used in this study has prescribed biogenic emissions rather than it being calculated interactively. The DMS emission flux is also scaled by a factor of 1.7 to account for a missing primary marine organic (PMO) source from oceans (this scaling factor is absent in the original version of UKESM1 with PMO aerosol incorporated

into the model). The latest HadGEM3 global coupled (GC) climate configuration of the UK Met office was used to develop UKESM1. HadGEM3 consists of the core physical dynamical processes of the atmosphere, land, ocean and sea ice systems (Ridley et al., 2018; Storkey et al., 2018; Walters et al., 2017). The UK's contribution to the Coupled Model Intercomparison Project Phase 6 (CMIP 6) (Eyring et al., 2015) is comprised of model simulations from the HadGEM3 and UKESM1 models.

Atmospheric composition is simulated with the chemistry-aerosol component of UKESM1 which is the UK Chemistry and Aerosol model (UKCA) (Morgenstern et al., 2009; O'Connor et al., 2014; Archibald et al., 2020). The aerosol scheme within UKCA is referred to as the Global Model of Aerosol Processes, GLOMAP-mode, (Mann et al., 2010; Mulcahy et al., 2020). It uses a two-moment modal approach and simulates multicomponent global aerosol which includes sulphate, black carbon, organic matter and sea salt. GLOMAP-mode includes aerosol microphysical processes of new particle formation, condensation, coagulation, wet scavenging, dry deposition and cloud processing. The aerosol particle size distribution is 5 log-normal modes with their size ranges shown in Table A1 (Appendix A). UKCA is coupled to other modules in UKESM1 to handle tracer transport by convection, advection and boundary layer mixing. Originally in GLOMAP-mode, sulphate and secondary organic formation was driven by prescribed oxidant fields (Mann et al., 2010). However, in this study the UKCA chemistry and aerosol modules are fully coupled (Mulcahy et al., 2020), with the prognostic oxidant concentrations calculated online by the UKCA chemistry scheme.

The model can be run in different configurations (Walters et al., 2017), in this work we use the N96L85 configuration which is 1.875^{o} x 1.25^{o} longitude-latitude,

corresponding to a horizontal resolution of approximately 135km. The model has 85 vertical levels up to an altitude of 85 km from the Earth's surface, with 50 levels between 0 and 18km, and 35 levels between 18 and 85 km. We run the model in a nudged configuration for the year 2014, in which model's wind fields are relaxed towards fields from the ERA–interim reanalysis fields (Dee et al., 2011; Telford et al., 2008) for the year 2014. A relaxation time constant of 6 hours is chosen (equal to the temporal resolution of the reanalysis fields), and the nudging is applied between model levels 17 and 80.

Binary nucleation involving sulphuric acid and water molecules, is the only nucleation mechanism that the model simulates in its default configuration. For the purposes of this study, we incorporate two nucleation mechanisms that involve highly oxygenated organic compounds (HOMs) as well. HOMs are similar to sulphuric acid in that they have a low vapor pressure and can nucleate to form new particles by themselves (ion induced pure-biogenic nucleation)(Kirkby et al., 2016) or in the presence of sulphuric acid (Metzger nucleation scheme)(Metzger et al., 2010). We run a baseline simulation of UKESM1 with H_2SO_4-H_2O, ion induced pure biogenic, and H_2SO_4-HOM nucleation schemes is run for the year 2014, with present day emissions. The same simulation with all the nucleation schemes turned off is run to simulate a planet without nucleation. A corresponding baseline (Nucleation-ON) and Nucleation-OFF simulation are also carried out for a pre-industrial environment by using pre-industrial anthropogenic emissions. To study the influence of nucleation on the radiative effect of primary aerosol emissions in a pristine environment, a simulation with nucleation ON and OFF, with double the fire emissions was carried out.

In this work we used this model to perform the following simulations,

1. Baseline present day simulation (Nucleation ON).
2. Baseline pre-industrial simulation (Nucleation ON).
3. A present-day simulation with Nucleation OFF.
4. A pre-industrial simulation with Nucleation OFF.
5. A pre-industrial simulation with Nucleation ON, and double the fire emissions
6. A pre-industrial simulation with Nucleation OFF, and double the fire emissions

We have analysed the results from these simulations in the next section.

3.4 Results and Discussion

Using UKESM1 we simulate a planet without nucleation and compare it against a baseline simulation. The baseline simulation is a global model simulation of UKESM1 which has a detailed representation of different atmospheric processes in the earth system as described in section 3.3. The Earth without nucleation has significant differences in the aerosol number concentration, black carbon load, CDNC, LWP, cloud fraction and the radiation balance, when compared to the baseline simulation. We explore the effects on each of them in Figure 12 and Figure 13.

In the present-day atmosphere, NPF is predominantly driven by sulphur containing compounds. Gaseous sulphur compounds like SO_2 from anthropogenic activity/natural sources and DMS from oceanic phytoplankton can get oxidised to form sulphuric acid which can condense onto pre-existing particles, growing them to larger sizes or nucleate to form new particles via NPF. The organic compounds that also participate in NPF originate from vegetation in the form of monoterpenes which are oxidised to form HOMs which can nucleate with H_2SO_4 or nucleate with itself to

form particles. HOMs like H_2SO_4 have a low vapor pressure and can condense onto pre-existing aerosol particles too.

Figure 12a shows the longitudinal mean vertical profile of the ratio of the total aerosol number concentration globally (averaged over a year) on a planet without nucleation relative to the baseline simulation $\left(\frac{N_{No\_nucleation}}{N_{baseline}}\right)$. On a planet without nucleation, the upper tropospheric particle number concentrations would be reduced to 0.01% of that of a planet with nucleation (Figure 12a). Over most of the ocean regions at the surface, particle number concentrations would be 75% lower, and more than 90% lower in pristine regions like the Southern Ocean away from primary particle sources (Figure 12b). Over most land regions where there are strong sources of primary particles from anthropogenic and natural emissions, particle concentrations without nucleation would be 50-75% lower.

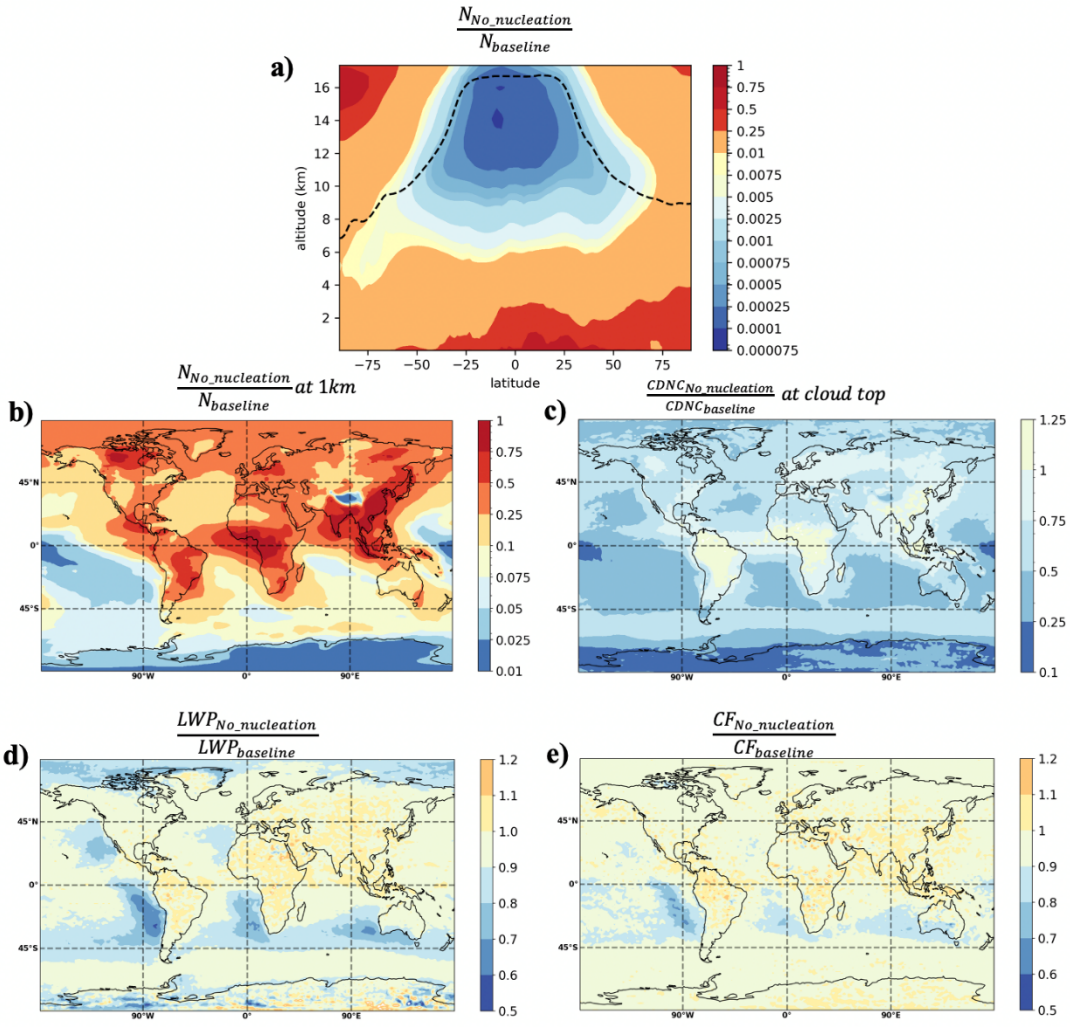

Figure 12: Global effect of nucleation on aerosol concentration, Cloud droplet number concentration, liquid water path and cloud fraction: a) Longitudinal mean vertical profile of ratio of total particle number concentration of particles on a planet without nucleation relative to the baseline present day simulation (the black dashed line represents the tropopause height), b) Spatial map of the factor change in aerosol number concentration above ground level, c) Factor change in cloud droplet number concentration at cloud top, d) Factor change in liquid water path, e) Factor change in Cloud fraction

Nucleation also regulates the cloud droplet number concentration in the atmosphere. Figure 12c shows the factor change in the cloud droplet number $\left(\frac{CDNC_{No\_nucleation}}{CDNC_{baseline}}\right)$ at cloud top. We estimate that the Earth's atmosphere without nucleation would have 33% lower cloud droplet number concentration. Droplet number concentrations would be around 75% lower over most of the Pacific, Atlantic and Indian Oceans

(Figure 12c). Concentrations over the Southern Ocean below 45°S would be only around 50% lower because higher emissions of sea spray aerosol dominates aerosol concentrations in this region. In contrast to the decreases in cloud droplet concentration, cloud droplet concentrations would be 25% higher in parts of South America and Western Africa. This is because, in the absence of nucleation, there will be more available condensable vapor like H_2SO_4 in the atmosphere which grows smaller aerosol particles to larger sizes. Aerosol particles in the size range between 100nm and 500nm (aerosol accumulation mode) experience 1.8 times increase in the condensation flux of H_2SO_4 onto their surface, globally, with around a 5 times increase over most of South America where the increase in cloud droplets is pre-dominantly observed (Appendix B, Figure B1a and B1b).

The changes in CDNC would strongly influence cloud bulk properties like liquid water path (LWP) and cloud fraction (CF) via rapid adjustments. Figure 12d and Figure 12e shows the factor change in Liquid water path $\left(\frac{LWP_{No\_nucleation}}{LWP_{baseline}}\right)$ and cloud fraction $\left(\frac{CF_{No\_nucleation}}{CF_{baseline}}\right)$ on a planet without NPF relative to the baseline simulation. In stratiform clouds globally, we estimate that liquid water path would be 8% lower and cloud fraction 3% lower without nucleation. The changes in liquid water path and cloud fraction are most pronounced over oceanic regions than land regions (Figure 12d and Figure 12e). Over regions of persistent stratocumulus cloud on the western coasts of North America, South America, Africa and Australia liquid water path would be 25-50% lower. Decreases in cloud fraction are largest (~30%) over the stratus-to-cumulus transition regions further away from the coast (Christensen et al., 2020). Aerosols have been shown to enhance the lifetime of clouds in this transition region (Christensen et al., 2020). The lack of aerosol in an NPF-free environment

drives a more pronounced reduction in cloud fraction in this region. With that said a complete understanding of the aerosol influence on cloud morphology in the stratus-to-cumulus transition zone is still an open question.

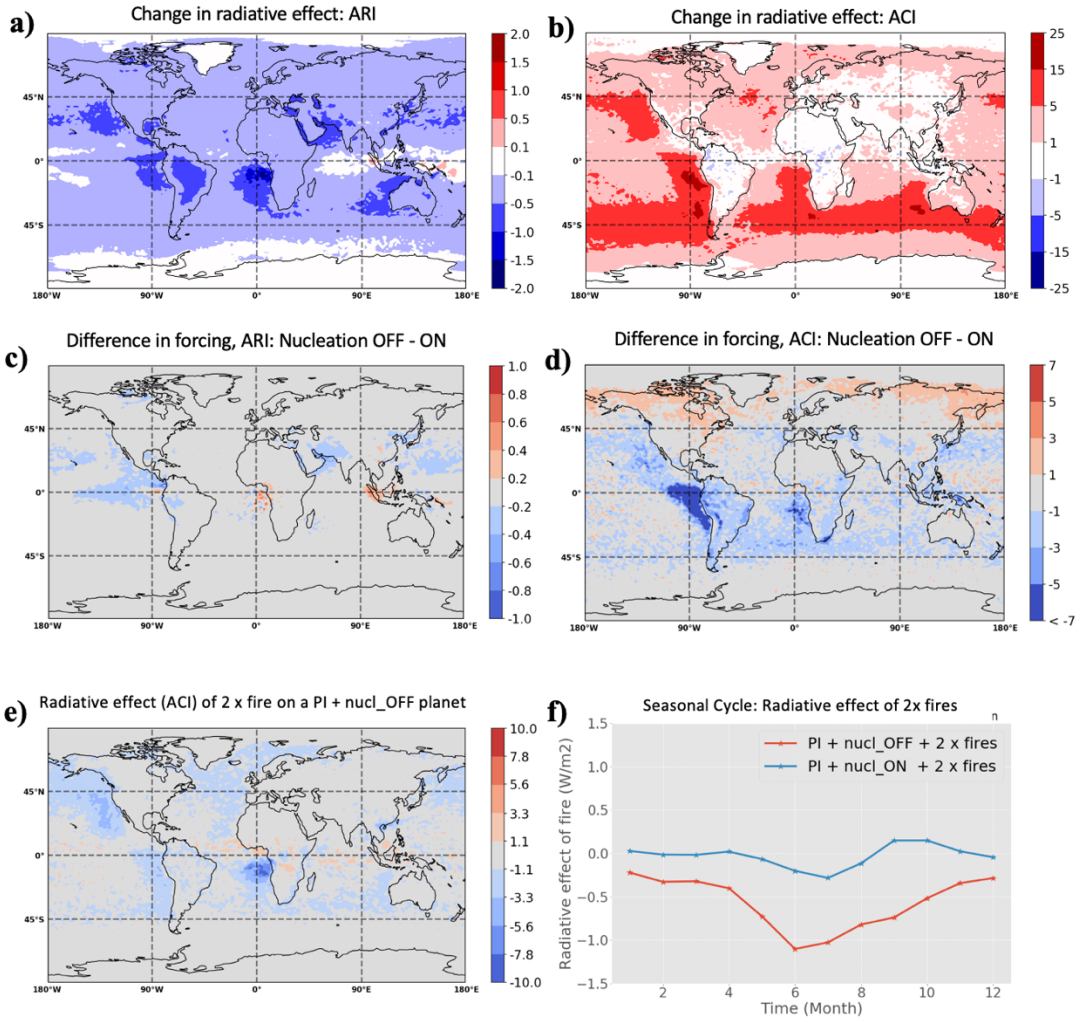

Figure 13: Role played by nucleation in the radiation balance, aerosol forcing and its buffering effect on fire emissions: a) Change in the ARI component of the radiative effect in the absence of nucleation, b) Change in the ACI component of the radiative effect in the absence of nucleation, c) Change in the ARI component of the aerosol forcing between a planet without and with nucleation, d) Change in the ACI component of the aerosol forcing between a planet without and with nucleation, e) The ACI component of the radiative effect of doubling fire emissions on a pre-industrial without nucleation switched off (nucl_OFF), f) Seasonal cycle of the radiative effect (ACI) of doubling fire emissions on a pre-industrial planet with (PI+nucl_ON+2 x fires) and without nucleation (PI+nucl_OFF+2 x fires).

As a result of these large changes in aerosols and clouds, Earth's atmosphere without nucleation would have a very different energy budget. We estimate the net top of

atmosphere radiative flux by subtracting the outgoing shortwave and longwave radiation on a planet without nucleation from the baseline simulation. We then isolate the differences in the net radiative flux into its ARI and ACI components by using the methodology described in Ghan et al 2013. The net radiative effect of nucleation at the top of the atmosphere in our model is 2.45 W m^{-2}, which is comprised of 2.74 W m^{-2} from aerosol-cloud interaction (i.e., planetary warming in a world without nucleation) and -0.25 W m^{-2} from aerosol-radiation interactions (planetary cooling) (Figure 13a and Figure 13b). Based on current estimates of Earth's climate sensitivity (Sherwood et al., 2020), the total radiative effect of nucleation translates to global mean temperatures which would be about 2^0C higher. This total radiative effect of nucleation is approximately 94% of the radiative effect of solar radiation scattering and absorption by all atmospheric aerosol (Schmidt et al., 2010). It is also 1.75 times the greenhouse effect of all atmospheric methane, 1.4 times that of nitrous oxide and about 10% of the effect of carbon dioxide (Schmidt et al., 2010). The decreases in liquid water path and cloud fraction drives the warming effect (ACI radiative effect) as seen from Figure 13b, with the stratocumulus regions near South America experiencing up to 25W/m^2 in warming. In contrast, the ARI radiative effect (Figure 13a) shows a moderate cooling effect which occurs due to primary aerosol particles which are more exposed to sunlight and scatter more solar radiation in an atmosphere with lesser cloud cover. We estimate an increase as high as 8% in the single scattering albedo (SSA) (Appendix B, Figure B2a), up to an 80% increase in the scattering coefficient (Appendix B, Figure B2b) and 4% decrease in the annual black carbon load (Appendix B, Figure B2c) which all contributes to the cooling radiative effect. The absence of clouds as indicated by the strong ACI response, leads to the primary aerosol particles that would have otherwise been present below clouds, to scatter solar

radiation. The decrease in the black carbon load is caused by ageing due to more available condensable vapor which would otherwise participate in nucleation.

In addition to altering the Earth's radiative energy balance, the aerosol particles generated by nucleation strongly damps the climatic response to changes in primary aerosol emissions. This damping occurs because clouds become increasingly insensitive to changes in aerosol as concentrations increase (Carslaw et al., 2013). Without nucleation the background aerosol concentration is much lower, therefore the aerosol radiative forcing caused by changes in anthropogenic aerosol emissions over the industrial period is -1.34 W m^{-2} compared to -0.89 W m^{-2} in the standard model (a 50% increase). The change in aerosol forcing (Figure 13d) between a simulation without and with nucleation varies regionally between -7 W m^{-2} and +3W m^{-2}, with the negative values over oceanic regions of South America and Africa, and the positive values over the boreal forest regions in the northern hemisphere. Cloud responses in the pristine pre-industrial atmosphere are more sensitive to changes in aerosol concentration, than the present day. Therefore, the absence of nucleation leads to stronger negative aerosol forcing globally. In contrast, the positive change in aerosol forcing over the boreal forests is due to a larger fraction of aerosol particles in the present-day relative to the pre-industrial with nucleation on than off. The present day has a higher H_2SO_4 concentration relative to the pre-industrial environment due to anthropogenic activity. H_2SO_4 molecules nucleates with organic species (Metzger et al., 2010) emitted from this region and is responsible for more particles in this region in the present day. This nucleation mechanism is not prominent in the pre-industrial environment due to a lower H_2SO_4 concentration.

The effect of large increases in primary aerosol emissions is also buffered by nucleation. For example, we estimate that a typical factor of two inter-annual variability in natural fires in the pre-industrial atmosphere (Ward et al., 2016) would cause a global mean radiative effect of only -0.03 W m^{-2}, but in an atmosphere without nucleation the radiative effect rises nearly 20-fold to -0.56 W m^{-2}, with up to -12 W m^{-2} near the African west coast (Figure 13e). During the months of June-August (Figure 13f), when fire emissions are at their peak globally, NPF reduces the radiative effect of doubling fires by a factor of ~5.

3.5 Conclusions

Thus, in this chapter, we illustrate the role played by nucleation in the climate system. We illustrate the contributions of nucleation to the global aerosol number concentration, cloud responses and radiation balance. We estimate that the radiative effect of nucleation exceeds the global warming effect of methane. Nucleation is also found to play a role in dampening the climatic effect of primary aerosol.

Only about ten years ago nucleation was not understood well enough to include in global climate models and the key aerosol-cloud-radiation processes were parameterized to capture observed atmospheric behaviour. Due to nucleation's effect in dampening the radiative effect of primary aerosol, models that don't represent nucleation accurately will be more sensitive to the uncertainties associated with primary aerosol emissions. After including nucleation in the model, we can appreciate the vital role it plays in our climate system.

Chapter 4 - Importance of isoprene gas phase and aqueous phase chemistry

4.1 Abstract

Using the UK earth system model (UKESM1), we highlight the global impact of secondary organic aerosol (SOA) generated from isoprene. The SOA generated from isoprene contributes to 62% of the global SOA budget, where 42% is attributed to isoprene gas phase chemistry and 20% to the isoprene aqueous phase chemistry. SOA generated from isoprene in the aqueous phase has strong regional radiative effects of up to -0.5W m^{-2} over parts of South America. The current version of UKESM1 doesn't have a theoretical representation for an isoprene forming SOA mechanism, and has only SOA generated from monoterpenes which is scaled up by a factor of 2. Comparing a simulation with isoprene SOA and a baseline UKESM1 simulation, we estimate a change in radiative effect globally of -0.11W m^{-2} and we find significant regional contributions to the radiative effect of up to -2 W m^{-2} over parts of South America.

4.2 Introduction

Biogenic volatile organic compounds (BVOCs) in the atmosphere, such as monoterpenes and isoprene, are by-products of photosynthesis and are emitted from vegetation (Guenther, 1995). These BVOCs are then oxidised in the atmosphere to form low volatility products that can nucleate and grow aerosol particles via condensation on their surface, forming secondary organic aerosol (SOA) (Jimenez et al., 2009). Monoterpene and isoprene oxidation products have been observed in the laboratory (Kroll et al., 2005, 2006) and in ambient aerosol measurements (Claeys et al., 2004), which contributes to the organic aerosol mass. Organic aerosol (OA)

dominates the fine aerosol mass across the earth, but the climatic effects of biogenic SOA are not well understood. Organic aerosol is around 20-50% of the total sub-micrometer aerosol mass (Jimenez et al., 2009), with around 90% of it being SOA. Atmospheric SOA can scatter and absorb solar radiation, and also alter the microphysical properties of clouds, thus affecting the earth's radiation balance (Albrecht, 1989; Bellouin et al., 2020; Scott et al., 2014; Twomey, 1977). The annual mean estimate of the ARI (Aerosol radiation interactions) component of the radiative effect of SOA is estimated to be between -0.01W/m^2 and -0.29 W/m^2 (Goto et al., 2008; O'Donnell et al., 2011), but regional effects can be high as -1 W/m^2 over tropical forest regions, and between -0.37 W/m^2 and -0.74 W/m^2 over boreal regions (Lihavainen et al., 2009; Rap et al., 2013).

SOA formation in climate models is typically represented as a simple flux parameterization, whereby the secondary organic compounds are formed directly from BVOCs via a reaction with a fixed yield, without characterizing the intermediates of the chemical reaction. In climate models typically a choice between an accurate computationally demanding parametrization and model performance needs to be balanced. It has been shown that models perform similarly with both simple and complex SOA mechanisms (Pai et al., 2020) and that added complexity may not be constrainable using atmospheric measurements (Sengupta et al., 2021). Despite different SOA mechanisms, climate models are able to simulate the concentration of OA in the boundary layer with reasonable accuracy, but are subject to higher uncertainties at higher altitudes between 1km and 6km where most of the clouds are present (Hodzic et al., 2020b). Our currently limited understanding of formation, removal and ageing of organic compounds in the atmosphere results in large uncertainties in the global OA budget, spatial distribution of OA (Organic

aerosol) and its impact on the earth's radiation balance (Hodzic et al., 2020b; Tsigaridis et al., 2014). The uncertainties in the global SOA burden are large, and it spans the range between 12 Tg/yr to 450 Tg/yr (Hodzic et al., 2016). There is an increasing motivation to reduce these uncertainties since in the future with efforts to reduce SO_2 emissions and sulphate aerosol, OA will become the dominant fraction of the submicron anthropogenic aerosol mass, globally.

In this chapter we examine the global importance of gas phase and aqueous phase isoprene. Isoprene (C_5H_8) has the highest emissions of any biogenic organic compound. Its atmospheric mixing ratio can be as high as several parts per billion by volume in the Amazon rainforest despite its high reactivity (Lee et al., 2016). Atmospheric isoprene is oxidised by the OH radical which triggers a complex peroxyradical chemistry which results in many reaction products like hydroperoxyl aldehydes (HPALD), hydroxy-hydroperoxides (ISOPOOH) and second-generation low volatility organic compounds like isoprene epoxy diol (IEPOX) (Berndt et al., 2016; Teng et al., 2017) These compounds can condense onto aerosol particles and form SOA, or dissolve and react in the aqueous phase inside cloud droplets. SOA formation from isoprene is an important pathway which is not represented in UKESM1 (UK Earth system model), instead the SOA from monoterpene is scaled up by a factor of 2 to account for the absence of isoprene SOA and SOA from AVOCs (anthropogenic VOCs) in the model. In this study we explore the importance of isoprene gas phase and a novel isoprene cloud processing mechanism (Lamkaddam et al., 2021) with a global climate model.

Our knowledge of gas-phase chemistry leading to SOA production has significantly improved over the last decade. Isoprene generates secondary organic compounds at a

fixed molar yield of 3% in the gas phase which is based on experimental studies (Kroll et al., 2005, 2006). However, SOA formed via cloud processing in the aqueous phase from isoprene (AqSOA) has not received much attention except for a few studies (Ervens, 2015; Ervens et al., 2018; Hallquist et al., 2009). Laboratory experiments have shown major SOA components like organic acids being formed in the aqueous phase (Hallquist et al., 2009; Herrmann et al., 2015). SOA production via in-cloud processing modulates the atmospheric OA concentration. However the reaction mechanism has remained unquantifiable because of experimental limitations in reproducing isoprene cloud chemistry under atmospheric conditions of a cloud droplet. Isoprene's oxidation products are water soluble (Liu et al., 2012) and its chemical reactions in cloud droplets could constitute a substantial source of SOA production in the aqueous phase (Tsui et al., 2019). In this work aqueous SOA formation from isoprene was studied experimentally under atmospherically relevant conditions, using a wetted-wall flow reactor (WFR) (Lamkaddam et al., 2021). AqSOA production rates and yields were determined and implemented into the atmosphere-only configuration of the UKESM1. Using this model, we assess the impact of SOA from gas phase and aqueous phase on global climate.

4.3 Methods

The results in this chapter were possible because of a combination of experimental and model development work. Section 4.3.1 highlights the experimental work pertaining to the novel aqueous phase isoprene cloud chemistry publication Lamkaddam et al 2021, in which I was a co-author. Section 4.3.2 focuses on the UKESM1 model development work done to incorporate the gas and aqueous phase isoprene chemistry into the model.

4.3.1 Experimental Work

The experimental work was carried out by colleagues at PSI who authored the publication Lamkaddam et al., 2021. The experiments were performed in a wetted-wall flow reactor (WFR), which consists of a quartz glass cylinder with a 6 cm internal diameter and 125 cm in length. Around 8 to 58ml of water is injected into the WFR and rotated with a rotational velocity of 15 rotations per minute, to maintain a 35 to 250 micrometer water microlayer on the wall of the WFR. Nine ultraviolet B lamps are placed around the WFR to run experiments with photochemical reactions. The experiments were carried out at a temperature of 295K and 100% relative humidity; ozone, OH, water vapor, isoprene and its oxidation products were introduced into the WFR in the presence of light and in the dark. These species then are allowed to react in the gas and aqueous phase. The properties of the chemical reaction products like yields, solubility, volatility etc, were characterized using a proton transfer reaction time-of-flight mass spectrometer (PTR-TOF-MS) and an acetate chemical ionization mass spectrometer (acetate-CIMS). The experiments were conducted at low NOx conditions with isoprene oxidation products such as isoprene epoxy diol (IEPOX) and hydroxy hydroperoxide (ISOPOOH). This experimental study simulates aqueous phase chemistry in cloud water which is unique in comparison to some past studies where highly concentrated mixtures were studied, which are characteristic of wet aerosols rather than cloud water. These past studies also accounted for molecules with only a low solubility (with the effective Henry's Law coefficient as low as 10^{-5} M atm^{-1}) (Ervens, 2015; Ervens et al., 2011), which therefore results in an inaccurate representation of the dissolved organic matter and chemistry inside a cloud droplet. Some chamber experiments (Bregonzio-Rozier et al., 2016) did try to simulate more realistic conditions using laboratory generated cloud droplets, however an accurate quantitative assessment of aqueous SOA yields was not possible because of the short

lifetimes of these droplets and high chamber wall losses. This study is the first to quantify the partitioning of organic vapours onto cloud droplets under near ambient conditions.

The dissolution of the organic compounds with low (10^3-10^5 M atm^{-1}) and high (>10^6 M atm^{-1}) effective Henry's law constants into the WFR water microfilm is assessed in this study, to estimate the organic aqueous phase fraction. Under atmospheric conditions the partitioning of the organic compounds into the gas and aqueous phase happens at quasi-equilibrium which is represented by the following equation (Ervens et al., 2011),

$$f_{aq} = \frac{(LWC)H_A^{eff}RT}{1+(LWC)H_A^{eff}RT} = \frac{{}^{LWC}/_{C^*_{aq}}}{1+{}^{LWC}/_{C^*_{aq}}} \quad \text{…. (6)}$$

Where f_{aq} is the equilibrium fraction in the aqueous phase, C^*_{aq} is the saturation vapor concentration over water, LWC is the liquid water content , R is the ideal gas constant, T is the temperature and H^{eff}_A is the effective Henry's law constant.

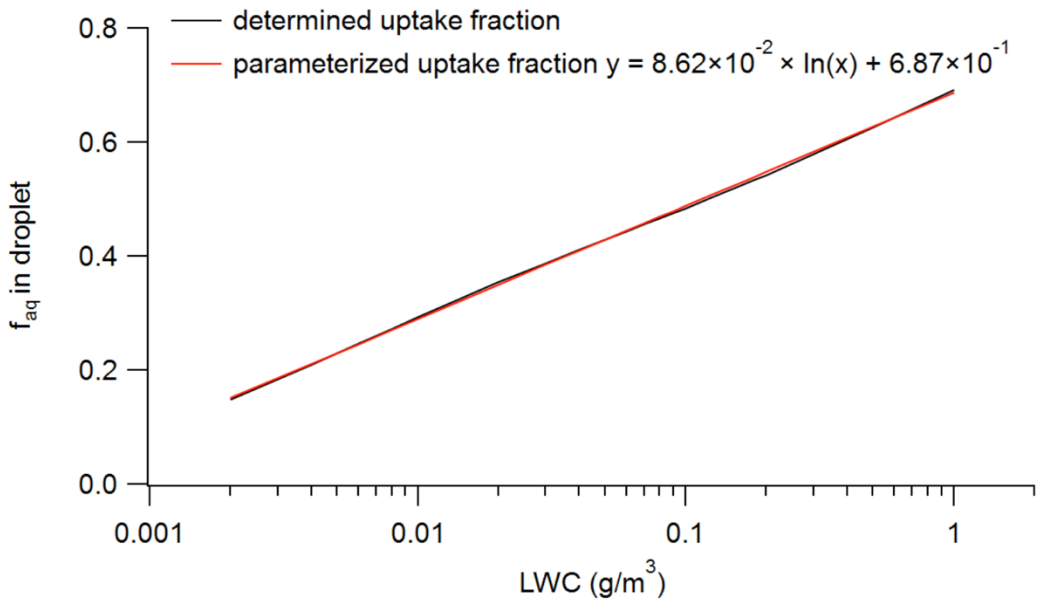

Figure 14: Aqueous phase fraction parametrised as a function of LWC, with the aqueous phase fraction on the Y-axis and LWC on the X-axis. This image was taken from (Lamkaddam et al., 2021)

From past studies as detailed in Ervens et al 2011, the LWC used in experiments and laboratory studies varied over several orders of magnitude. Experiments simulating bulk solution represent a LWC of 10^6 g m^{-3} and those simulating cloud droplets have a LWC between ~ 0.1 to 1g m^{-3}. From equation 6 we can see that the LWC will have a significant effect on the aqueous phase uptake of the gas. Using the experimental results, the fraction of organic compounds that partition onto a cloud droplet was estimated using Equation 6. A parametrization (f_{aq}= 8.62×10^{-2} × ln(LWC) + 6.87×10^{-1}) to represent the relationship between the equilibrium aqueous fraction as a function of LWC (ranges between 0.001 g m^{-3} and 1g m^{-3}) is shown in Figure 14**.** We use this to inform our model development work to incorporate the SOA production mechanism from isoprene aqueous phase chemistry.

4.3.2 Modelling description

The model in its default configuration produces SOA only via monoterpene oxidation by OH, NO_3 and O_3 with a molar yield of 13% and is scaled up by a factor of 2 to account for other sources of SOA (Mann et al., 2010; Mulcahy et al., 2020). All the oxidation products from monoterpene are lumped into one tracer "sec_org" in the model, which is done to reduce model complexity. In a new simulation we remove this scaling factor of 2 and include isoprene SOA formation mechanisms via gas and aqueous phase chemistry. The isoprene emission files were obtained from the CMIP6 inventory. We assume the gas phase oxidation of isoprene with the OH radical to form condensable organic vapors (represented as the tracer "sec_org" in the model) occurs at a 3% molar yield. The main product from isoprene gas phase oxidation is ISOPOOH. We use this as a proxy for the organics from isoprene that interacts in the aqueous phase with the OH radical. The uptake of ISOPOOH onto cloud droplets occurs via the parametrization from Figure 14. ISOPOOH and OH react to form SOA with a reaction rate constant of $(3.8\pm1.9)\times10^{8}\ M^{-1}s^{-1}$ (Ervens, 2018).

Table 3: Description of the simulations used in the study, where simulation 1 describes the baseline version of UKESM which has only Monoterpene SOA, which is scaled up by a factor of 2. Simulation 2 doesn't have a monoterpene SOA scaling factor and has incorporated a gas phase isoprene SOA production mechanism. Simulation 3 is the same as simulation 2 but with an additional isoprene aqueous phase SOA production mechanism present.

S.no	SOA scaling factor	Monoterpene gas phase SOA	Isoprene gas phase SOA	Isoprene aqueous phase SOA
Simulation 1	2	yes	No	No
Simulation 2	1	yes	yes	No
Simulation 3	1	yes	yes	yes

Three simulations were carried out for the analysis in this chapter, which are described in Table 3. Simulation 1 is the baseline version of UKESM1 which has only SOA production mechanisms from monoterpene (scaled up by a factor of 2) and none from isoprene. In simulation 2 we remove the monoterpene SOA scaling factor and incorporate a gas phase isoprene SOA formation mechanism, with simulation 3 having an additional isoprene aqueous phase SOA formation mechanism as well.

The results of these simulation are detailed in section 4.4 below.

4.4 Results

In this section we use the above simulations to analyse the importance of isoprene to the climate system. We divide the results into 3 subsections.

1. Section 4.4.1: We look at isoprene emissions globally in comparison to monoterpene and motivate the need for including SOA production from isoprene into the model.
2. Section 4.4.2: We quantify the importance of isoprene aqueous phase chemistry and describe my contributions to the study Lamkaddam et al., 2021
3. Section 4.4.3: We incorporate both a gas phase and aqueous phase isoprene SOA and compare it with the default version of UKESM1 which has no isoprene SOA (but has a SOA yield scaling factor of 2).

4.4.1 Monoterpene and isoprene emissions

Annual emissions of isoprene is ~6.3 times higher than monoterpenes (Sindelarova et al., 2014). Figure 15a shows the ratio of the annual mean emission flux of isoprene

and monoterpene, estimated using the CMIP6 emission files. Isoprene is more abundant than monoterpenes in most regions across the earth. The boreal forest regions in the NH emit up to 5 times more isoprene than monoterpenes. Parts of Australia, South America and Africa have isoprene emissions which are a factor of 50 higher than that of monoterpenes. This regional variability in the isoprene/monoterpene ratio emphasises the need to have isoprene SOA formation mechanisms in the model.

The seasonal cycle (Figure 15b) of the emission ratio shows a higher proportion of isoprene to monoterpene in the SH. Isoprene emissions are up to a factor of 6 and 9 higher than monoterpene emissions in the NH and SH respectively. The highest isoprene emission has been shown to be from drought deciduous woodlands and tropical rainforests, rather than boreal forests (Guenther et al 1995). The seasonal variation in emissions from tropical rainforests is mainly driven by changes in temperature, with the highest isoprene emission occurring during the hottest months. Emissions from deciduous forests however are driven by changes in foliar density which peak right after the rainy season (Guenther et al 1995). Therefore, the SH seasonal cycle (Figure 15b) is driven by large tropical forest ecosystems, with the temperate and boreal forests regions dominating emissions in the NH.

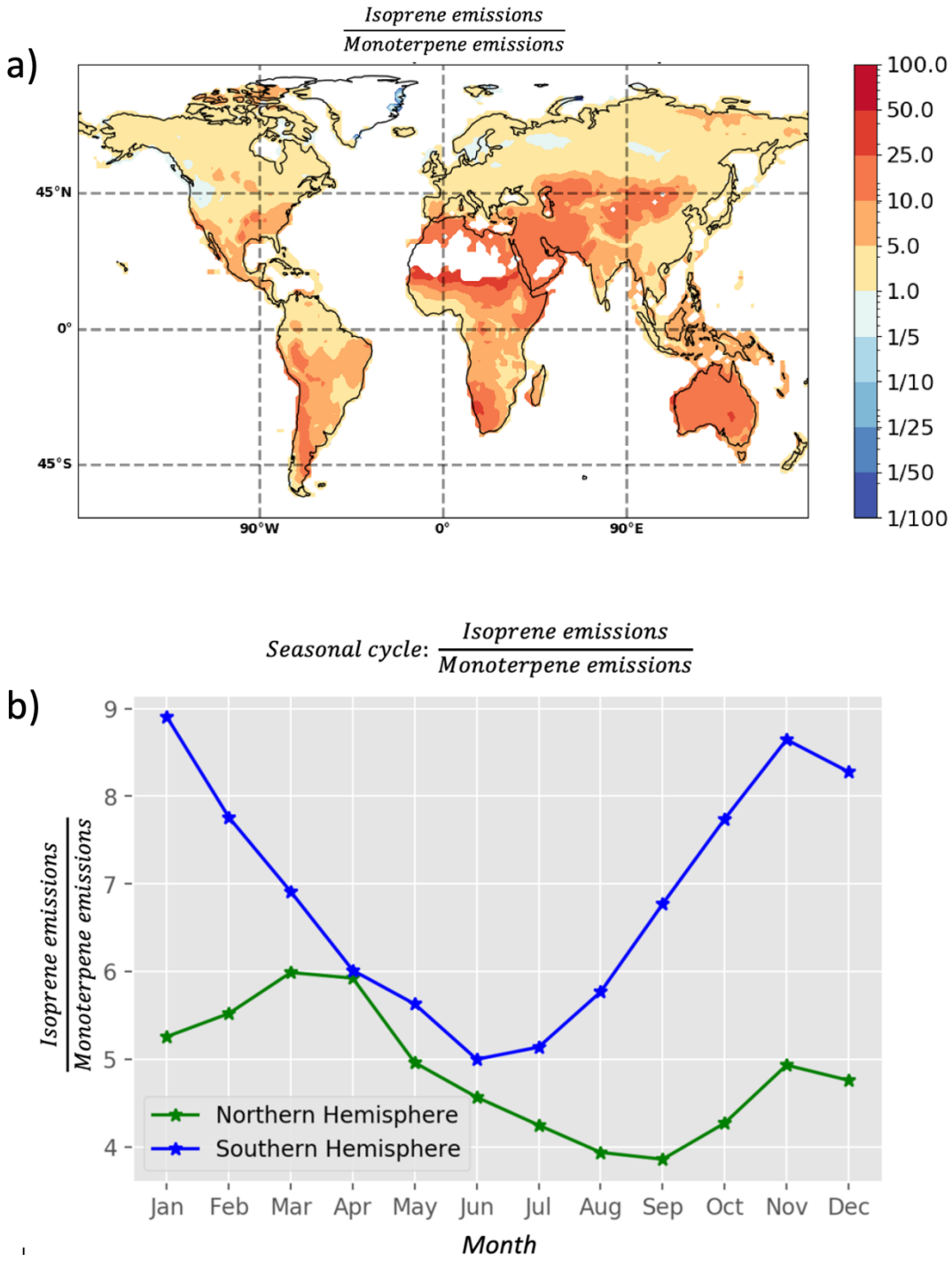

Figure 15: a) Spatial map of the ratio between the annual mean isoprene and monoterpene emission flux obtained from the CMIP6 emission files, b) Seasonal cycle of the ratio between isoprene and monoterpene emissions globally.

These differences highlight a need to have a better representation of organics in UKESM1 by including isoprene SOA because of the impact it can have on the global SOA budget, SOA seasonal cycle, and its radiative impacts.

4.4.2 Effect of Isoprene aqueous phase chemistry

The novel aqueous isoprene chemistry discussed in Lamkaddam et al 2021, which was briefly summarised in section 4.3.1, was implemented into UKESM1. We compare a simulation with isoprene aqueous phase SOA (simulation 3) and one without it (simulation 2) to isolate the global impact of isoprene aqueous phase chemistry.

Figure 16 shows the longitudinal vertical profile of SOA production rate (aqSOA) from aqueous phase chemistry of isoprene oxidation products. The aqSOA, which is dependent on the LWC which decreases with altitude which leads to less AqSOA from isoprene at high altitudes. Therefore, SOA from isoprene oxidation at altitudes higher than 10km is negligible. We simulate up to 50 $\mu g/m^3$ annual mean SOA concentration at around 2km. There is more aqSOA in the SH than the NH owed to high isoprene concentration in the SH (Figure 16). Globally we estimate the aqSOA contributes ~6.9 Tg of SOA annually, which is 20% of the global biogenic SOA budget per year.

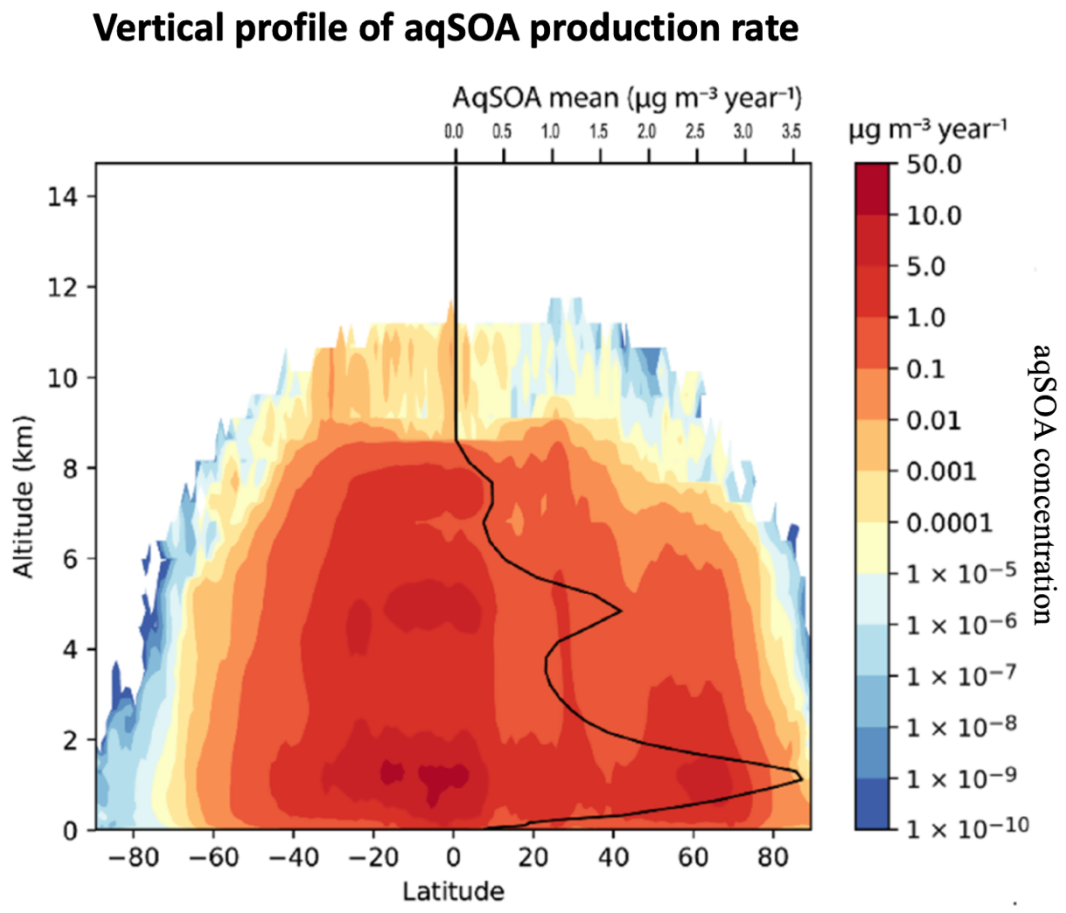

Figure 16: Longitudinal mean vertical profile of the annual SOA production rate from isoprene aqueous phase chemistry.

Figure 17 illustrates the SOA formation rate via the different chemical pathways: monoterpene gas phase (t_{gas}SOA), isoprene gas phase (i_{gas}SOA) and isoprene aqueous phase (aqSOA) varies regionally, as shown in the pie charts. The total SOA production from the model globally is ~34.9 Tg/yr where t_{gas}SOA, i_{gas}SOA and aqSOA are 13.09 Tg/yr, 14.89 Tg/yr and 6.89 Tg/yr respectively. Figure 17 also illustrates the percentage change in the SOA formation rate after incorporating aqueous phase isoprene chemistry in the model. The percentage increase in the SOA production rate is between 20-40% over most of the continental regions in the SH. Coastal regions of the South America and Australia shows the highest increase (~90%) in SOA owing to the transport of isoprene and formation of SOA over ocean.

From the pie charts in Figure 17, we can see that globally isoprene contributes to ~63% of the total SOA budget. Western Europe and Eurasia are the only regions with the SOA from monoterpene exceeds that of isoprene, with monoterpene contributing ~60% and ~51% of the SOA budget respectively in these regions. Over every other continent the SOA budget from isoprene is higher than monoterpenes, with the isoprene contribution to SOA being the highest over Australia (~76%).

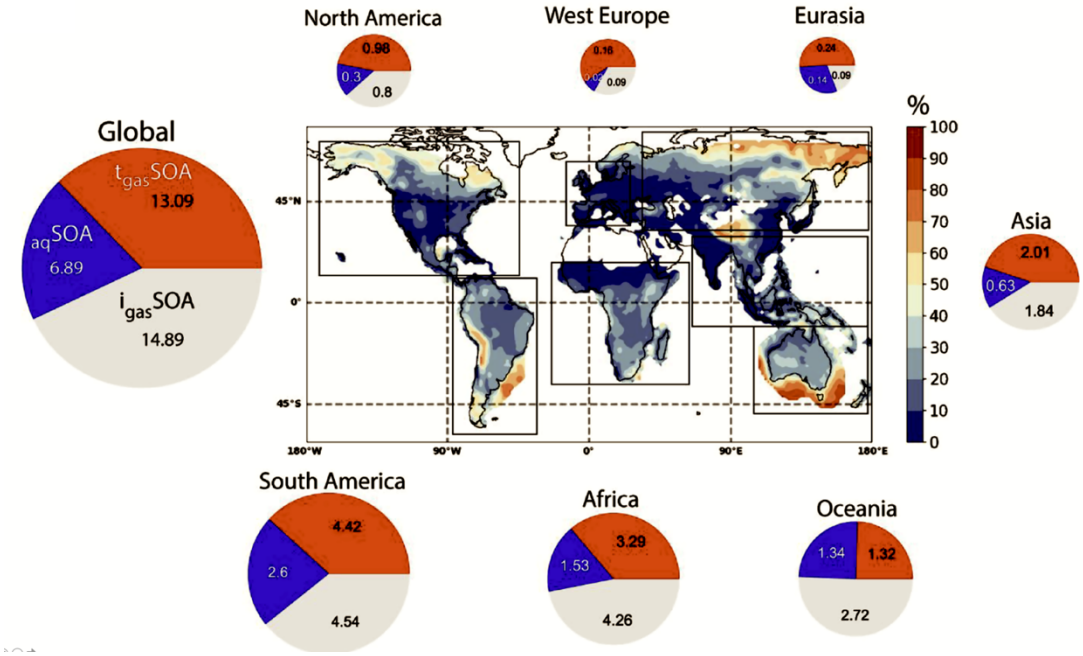

Figure 17: Percentage change in the SOA formation rate after incorporating isoprene aqueous phase chemistry (i.e., percentage change between simulation 3 and simulation 2). The pie charts represent the total SOA formed globally and across continental regions (Tg/yr) via the three different SOA formation pathways: monoterpene gas phase chemistry (t_{gas}SOA), isoprene gas phase chemistry (i_{gas}SOA) and isoprene aqueous phase chemistry (aqSOA). The regions with SOA formation rates less than 1Tg/yr have been masked (white parts of the map) (image taken from lamkkadam et al 2021)

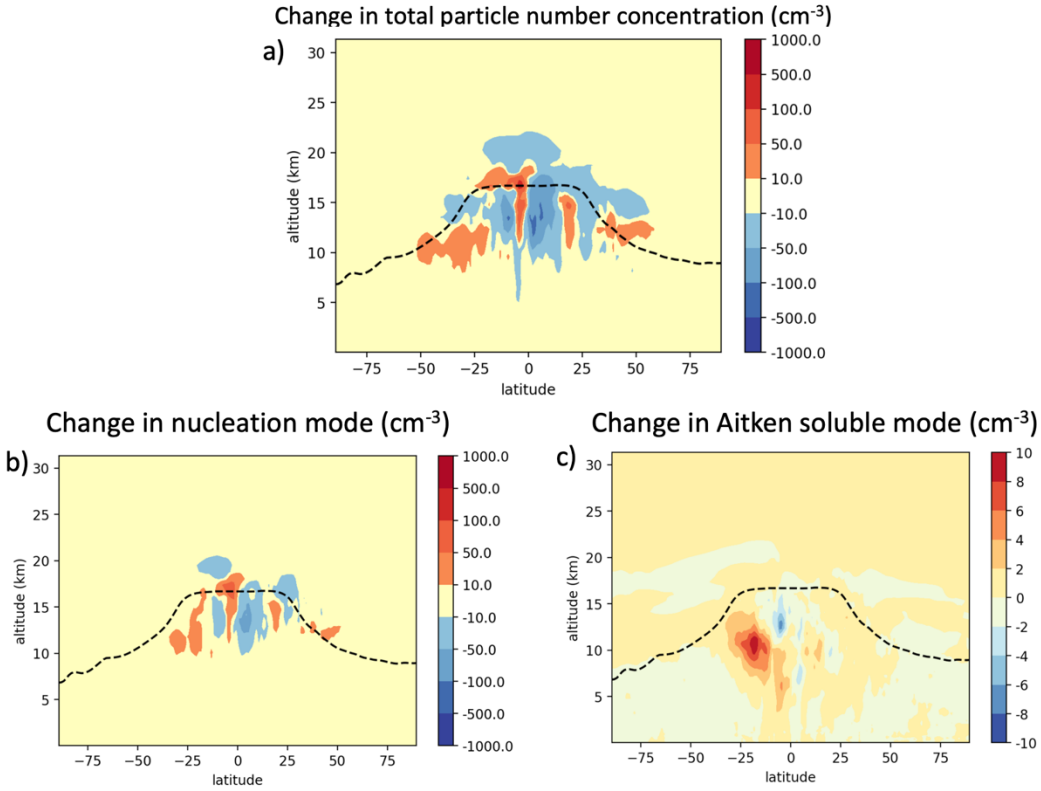

Figure 18: Change in the aerosol number concentration between simulation 3 (monoterpene SOA + isoprene gas phase SOA + isoprene aqueous phase SOA) and simulation 2 (monoterpene SOA + isoprene gas phase SOA).

The longitudinal mean vertical profile of the change in the aerosol number concentration between a simulation with isoprene aqueous phase chemistry (simulation 3) and one without it (simulation 2) is shown in Figure 18. Figure 18a shows a reduction in total aerosol number at high altitudes with a decrease of up to 500 particles/cm^3 in the upper troposphere. To better understand the size of the particles contributing to the change in aerosol number, we also looked at individual aerosol modes (Figure 18a and Figure 18b). The decrease in mainly in the nucleation mode concentration, with a small increase in the Aitken mode concentration at 10km altitude. A reduction in the aerosol number is driven by an increase in condensation sink at lower levels of the atmosphere due to increased aqueous phase isoprene SOA

production (Figure 16) which adds to the mass of the aerosol particles. These particles consume the existing condensable vapor which decreases the concentration of available vapor for nucleation.

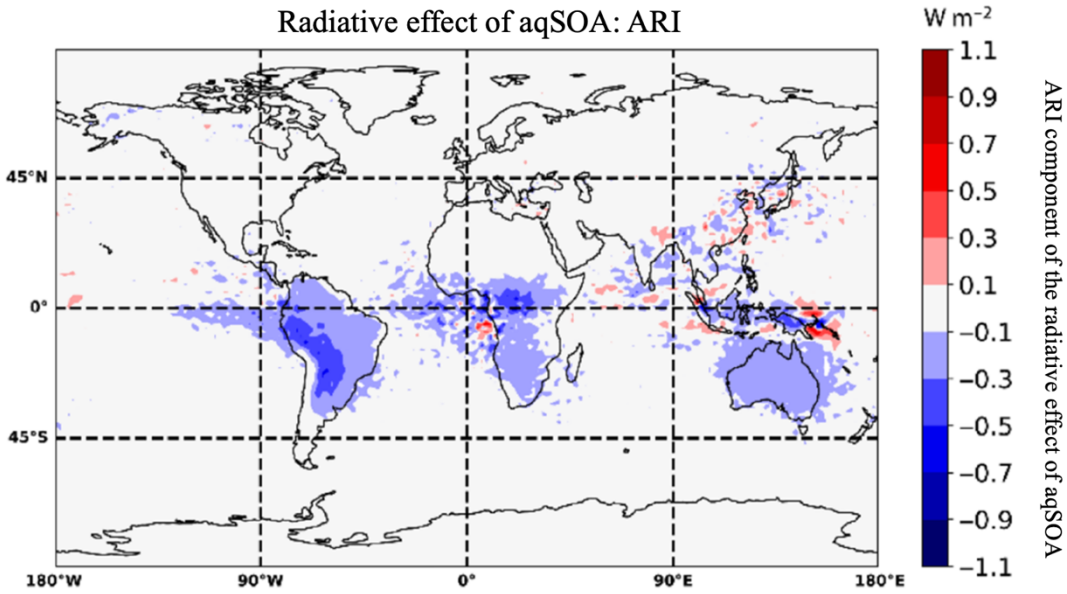

Figure 19: Radiative effect of aqueous phase isoprene chemistry (Change in the ARI component of the radiative effect between simulation 3 and 2)

We also explore how the earth's radiation balance is affected by the inclusion of the isoprene aqueous phase chemistry. We found that it had a small effect on the ACI (Aerosol cloud interactions) component of the radiative effect, we see small changes in the accumulation mode aerosol concentrations but not significant enough to alter ACI in a meaningful way. However, we found that it had a stronger impact on the ARI component. Figure 19 shows the change in the ARI component of the radiative effect between simulation 3 and 2, which isolates the impact of the isoprene aqueous phase chemistry on the radiation balance. The direct radiative effect of aqSOA is as negative as -0.5W/m^2 over South America and Africa, and -0.3W/m^2 over Australia.

Thus, we can see that isoprene aqueous phase chemistry contributes significantly to the SOA budget and radiative effect.

4.4.3 Comparison of a simulation with isoprene gas and aqueous SOA vs the baseline UKESM1

In this section, we compare simulation 3 (monoterpene SOA+ isoprene gas phase SOA + isoprene aqueous phase SOA + no monoterpene scaling factor) against simulation 1 (the default UKESM1 simulation which has monoterpene SOA scaled up by a factor of 2 and no isoprene SOA). The goal of this section is determine whether incorporating isoprene SOA into the model is important and to justify whether or not there is a pressing need to incorporate it into the model. In the following subsections we highlight the differences in aerosol number concentration, SOA budget and the radiative effects of the simulation with isoprene SOA (simulation 3) and the baseline UKESM1 simulation (simulation 1).

4.4.3.1 Change in Aerosol number concentration

The longitudinal mean vertical profile of the change in aerosol number concentration between simulation 3 and simulation 1 is shown in Figure 20. Figure 20a shows a substantial reduction in the total aerosol number concentration at higher altitudes. We estimate a reduction in the total particle number concentration in the upper troposphere by up to 1000 particles/cm^3 (STP), with a small increase in concentration between 18 km and 20 km. To identify the size of the particles contributing to the change in number concentration seen in Figure 20a, we look at Figure 20b, Figure 20Figure 20d which shows the change in nucleation mode, Aitken soluble mode and accumulation mode. A reduction in the aerosol number concentration is driven by an increase in the condensation sink (i.e accumulation mode) at lower levels in the atmosphere. In the model we also incorporated the dissolution of OH radical onto

cloud droplets for the aqSOA formation mechanism. This results in the reduction of gas phase OH concentration which leads to an increased lifetime of SO_2 which is about 5 to 10% higher at 20km in simulation 3 compared to simulation 1 (Figure 21). Thus, the SO_2 is getting convected to higher levels in the atmosphere where it gets oxidised forming new particles at around 20km.

There is however a small increase in Aitken mode in the upper troposphere and accumulation mode particles in the boundary layer, which is due to longer lifetime of gas phase isoprene SOA and an increase in aerosol mass via isoprene cloud chemistry respectively.

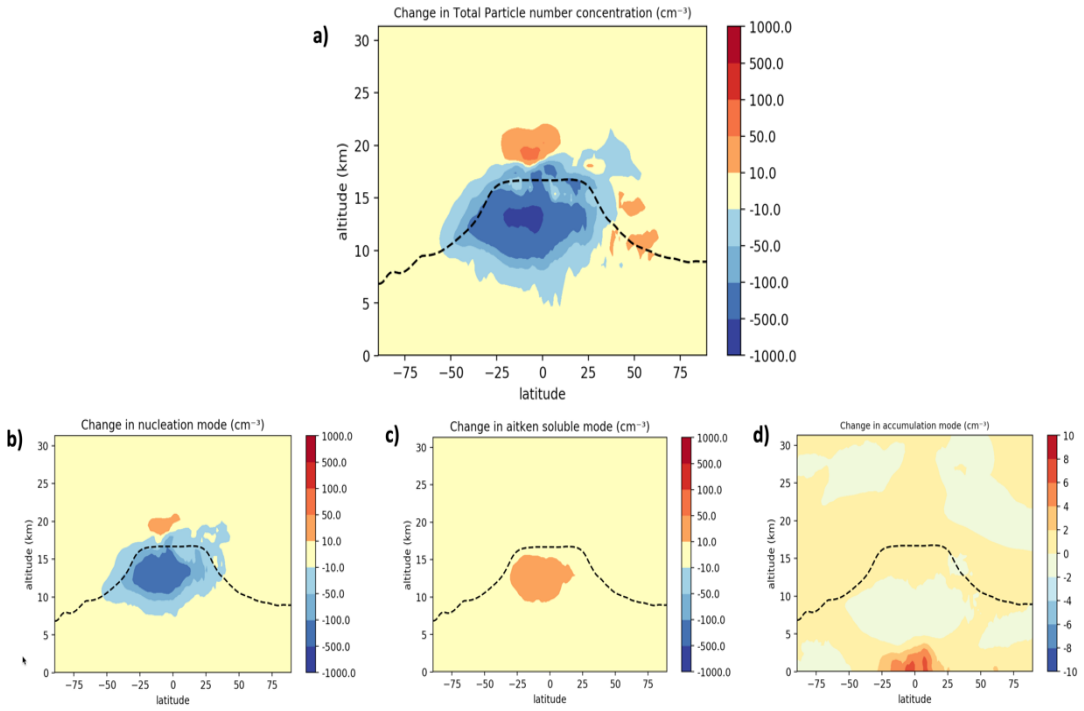

Figure 20: Comparison between simulation 3 (with isoprene & monoterpene SOA with a SOA yield scaling factor of 1) and simulation 1 (only monoterpene SOA which is scaled up by a factor of 2): Change in a) total particle number concentration, b) nucleation mode number concentration, c) Aitken mode number concentration and d) accumulation mode number concentration.

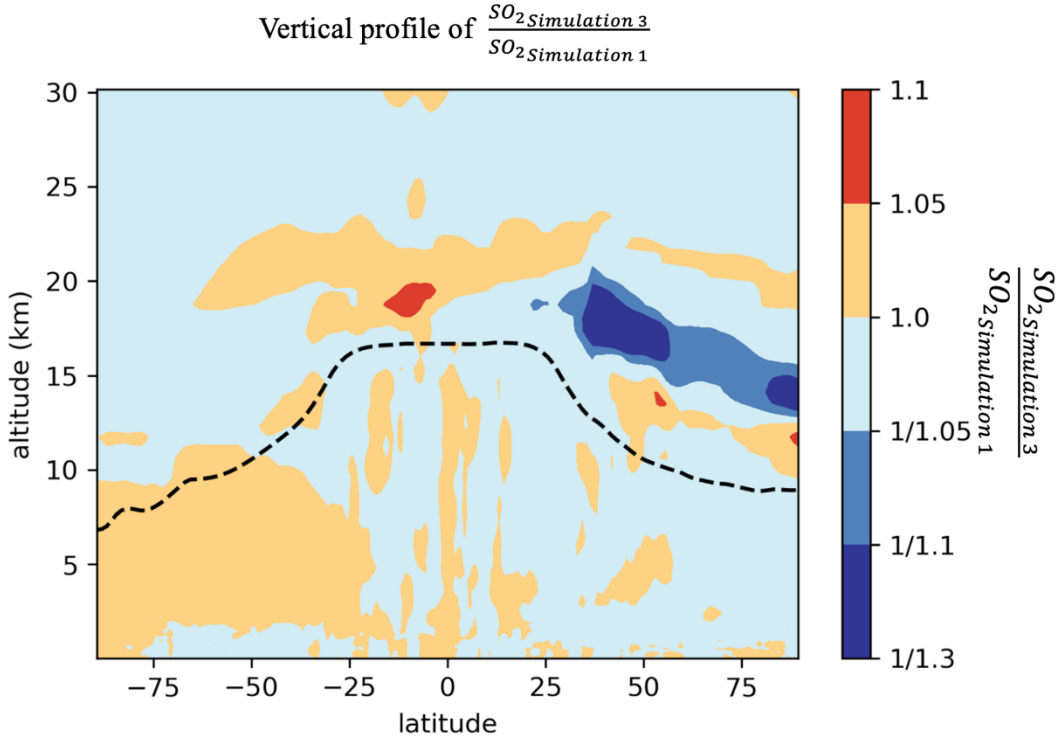

Figure 21: Longitudinal mean vertical profile of the ratio of the SO_2 concentration between simulation 3 and simulation 1.

4.4.3.2 Effect on the global SOA budget and radiative effect

The longitudinal mean vertical profile of the change in SOA formation rate between a simulation 3 and simulation 1 is shown in Figure 22. The SOA formation rate is the highest (~1 Tg/yr) at lower altitudes (<2km) between 25N and 25S, with the higher SOA formation rates skewed to the SH owing to more isoprene emissions in the SH relative to the NH. We also see a local maximum in the SOA formation rate at higher altitudes (~12km), owed to the longer lifetime and abundance of isoprene. In the model, monoterpene is consumed by OH, O_3 and NO_3 in the default simulation (simulation 1). However, isoprene is consumed only by OH in the gas and aqueous phase, which results in a longer lifetime than monoterpenes. Given the abundance of isoprene combined with stronger convection in the tropics, isoprene reacts with OH

in gas phase at higher altitudes which leads to a local maxima in the SOA formation rate at an altitude of ~12km.

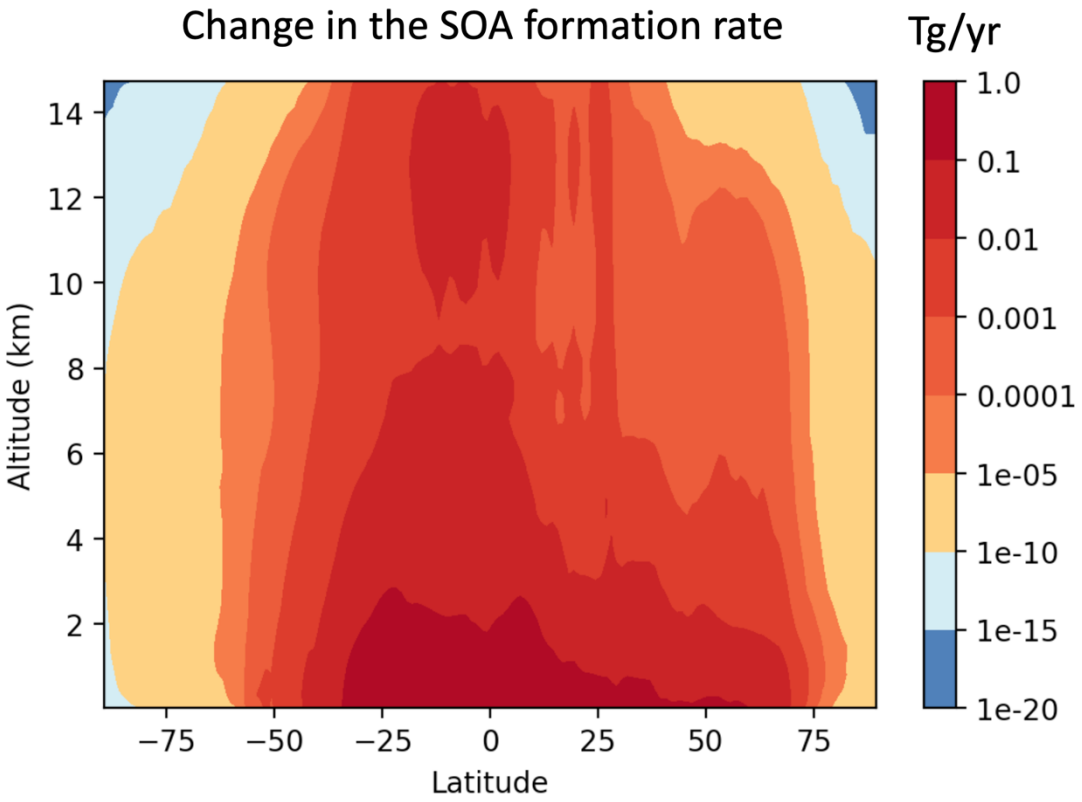

Figure 22: The longitudinal mean vertical profile of the change in SOA formation rate between a simulation with isoprene & monoterpene SOA with a SOA yield scaling factor of 1 (simulation 3) and a simulation with only monoterpene SOA scaled up by a factor of 2(simulation 1).

The changes in aerosol concentration (Figure 20) and SOA budget (Figure 22) influence the net solar radiation at the top of the atmosphere. Figure 23 shows the spatial map of the ARI and ACI components of the change in the radiative effect between the simulation with isoprene producing SOA (simulation 3) and the baseline simulation (simulation 1).

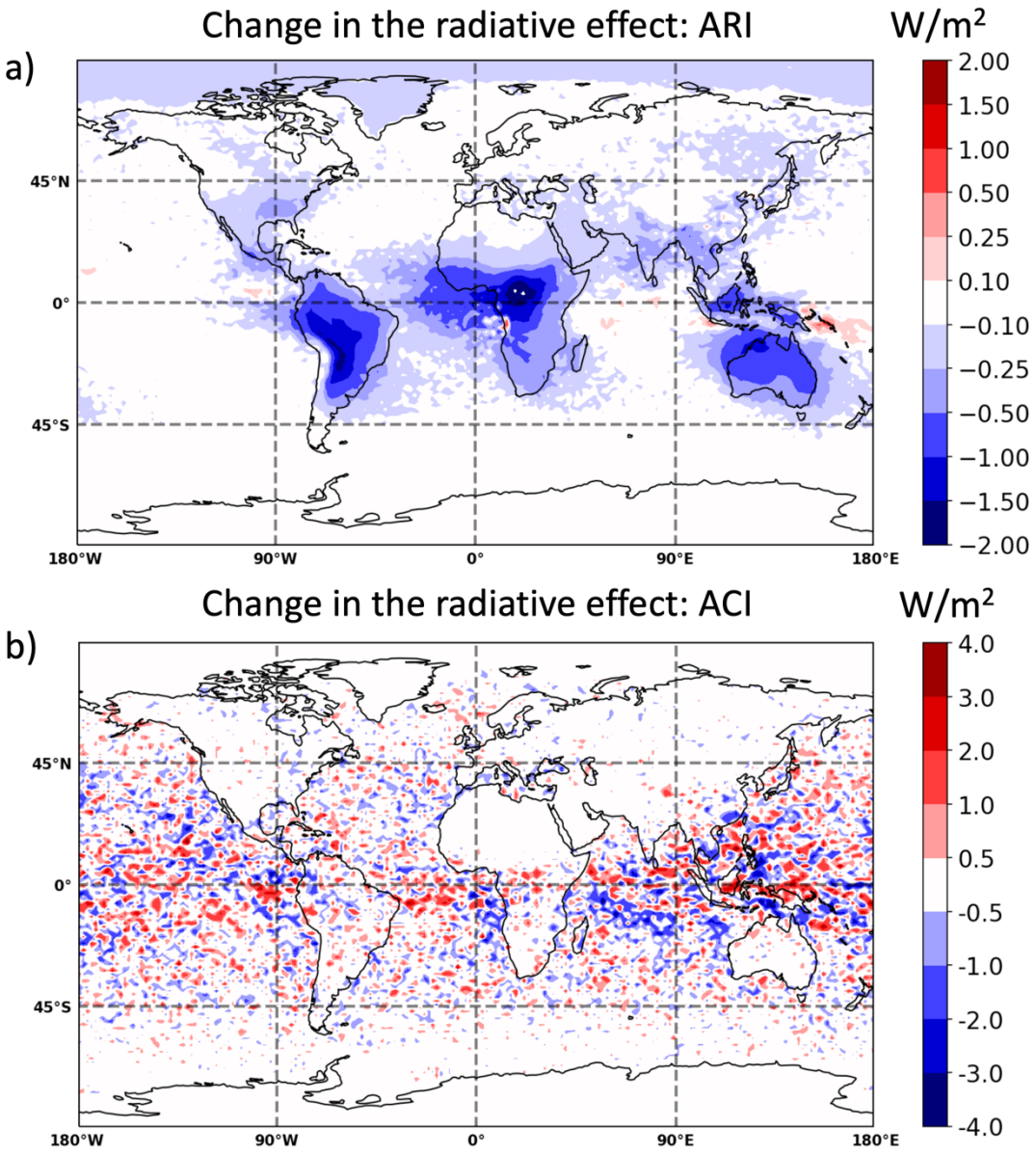

Figure 23: Change in the radiative effect (W m^{-2}) between simulation 3 and simulation 1: a) ARI component of the radiative effect, b) ACI component of the radiative effect

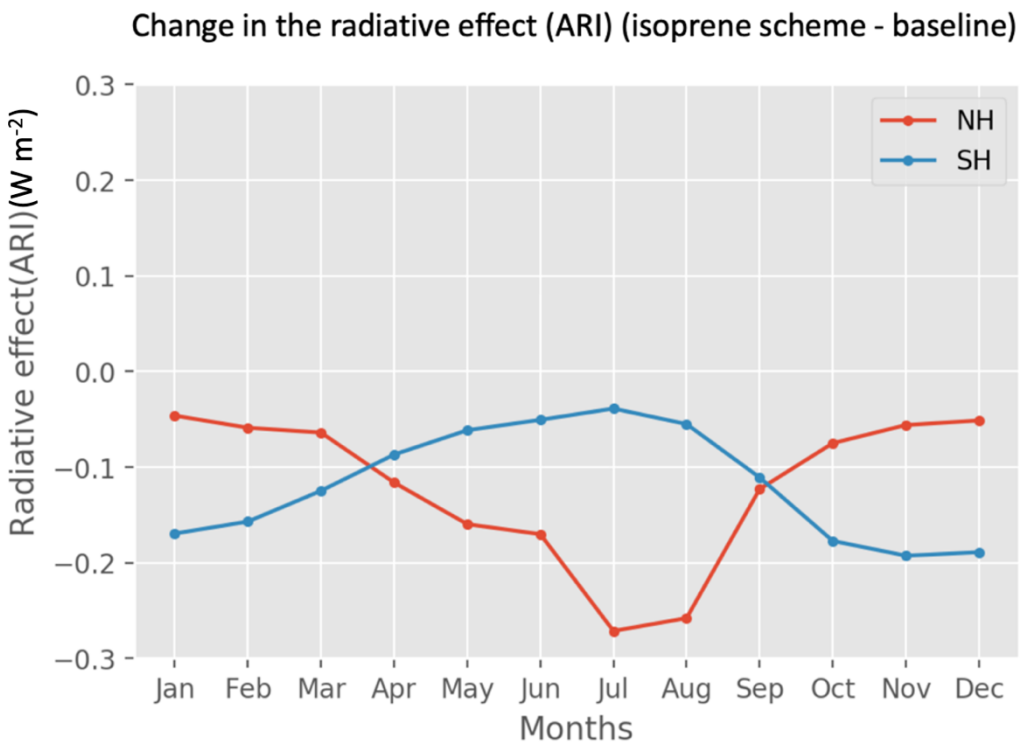

Figure 24: Seasonal cycle of the ARI component of the change in the radiative effect between a simulation with isoprene & monoterpene SOA with a SOA yield scaling factor of 1 (simulation 3) and one with only monoterpene SOA scaled up by a factor of 2 (simulation 1)

The annual mean change in the global radiative effect is estimated to be -0.11 W/m^2. Regional changes in ARI are much stronger with up to -2 W/m^2 over South America, Africa and Australia which correspond to regions with the highest isoprene/monoterpene ratio (Figure 15a). There is also a radiative effect in the Arctic of approximately -0.25 W/m^2. However, the changes in the ACI component of the radiative effect (Figure 23b) are minimal. To better understand this, we also plotted the changes in CCN and CDNC (Appendix C, Figure C1). Figure C1a shows the ratio between the CDNC in simulation 3 and simulation 1, and Figure C1b shows the ratio between the CCN (at 2% supersaturation) in simulation 3 and simulation 1. The CCN concentration in simulation 3 in most regions has minimal changes when compared

to simulation 1, with the percentage increase in CCN being as high as 15% over parts of Australia. This translates to around a 5% increase in CDNC over parts of Australia and minimal changes across the world (Figure C1a). The small increase in CDNC explains the minimal response in the ACI component (Figure 23b) of the radiative effect.

The seasonal cycle of the ARI component of the change in the radiative effect between simulation 3 and the baseline simulation (simulation 1) is shown in Figure 24. A substantial radiative effect of -0.28 W/m^2 and -0.2 W/m^2 during the NH and SH-summertime is simulated. Thus, the inclusion of SOA from isoprene in the model has strong radiative effects both globally and regionally.

4.5 Conclusions

Given the uncertainties associated with SOA in climate models, we incorporate a gas phase and an aqueous phase SOA production mechanism (Lamkaddam et al., 2021) from isoprene in UKESM1 and assess its regional and global effects. After the inclusion of the isoprene SOA production mechanism in the aqueous phase in the model, we find that it contributes to about 20% of the global SOA budget. The radiative effect of aqSOA varies regionally and contributes to about -0.5W/m^2 and -0.3W/m^2 over parts of South America and Africa respectively. AqSOA is predominant at lower altitudes with its concentration reaching 50 $\mu g/m^3$ at 2km altitude. Thus, isoprene cloud chemistry is an important atmospheric process, that has spatially varied radiative impact and significant contribution to the SOA budget.

We also compared a simulation with isoprene gas and aqueous phase SOA generation against the baseline UKESM1 simulation with no isoprene SOA. We find a substantial decrease of 1000 particles/cm^3 in the upper-tropospheric aerosol number concentration in a simulation with isoprene SOA included, relative to the baseline. We also see an increase in the SOA formation rate as high as 1 Tg/yr in the lower troposphere and 0.1 Tg/yr in the upper troposphere respectively. Isoprene SOA contributes to around -0.11 W/m^2 to the earth's radiation budget globally, with regional effects of up to -2.0 W/m^2 over South America, Africa, and Australia.

Thus, we find that isoprene SOA has a strong effect on the radiation budget and aerosol concentrations, which highlights the need to incorporate these mechanisms in UKESM1.

Chapter 5 : Conclusions

5.1 Summary

The cooling effect aerosols have on global climate (IPCC, 2021) makes it an exciting avenue of research which is the focus of this thesis. Since pre-industrial times greenhouse gases contribute about 1^0C to 2^0C of warming and aerosols (both primary and secondary) contribute to a 0^0C to 0.8^0C cooling. In this thesis we study the impact of secondary aerosol particles formed from gas-to-particle conversion ('nucleation') of gaseous precursors and condensation of gaseous precursors onto pre-existing aerosol, on the climate system.

Past studies (Ekman et al., 2012; Gordon et al., 2017; Merikanto et al., 2009; Scott et al., 2014; Watson-Parris et al., 2019) have gone a long way in improving our understanding of secondary aerosol and atmospheric processes leading to their formation. Research work in the past using UKESM1 have evaluated aerosol processes (Mulcahy et al., 2018) and the vertically averaged aerosol number concentration (Mulcahy et al., 2020) against observations. In this thesis, we build on past work by using UKESM1 to improve our understanding and representation of atmospheric processes involving secondary aerosol. The scientific work done in chapter 2, we explore the role of various atmospheric processes in controlling the vertical profile of atmospheric aerosol. We identified areas for improvement in UKESM with the representation of nucleation and organic compounds controlling aerosol growth, being two of them. We examined the impact of nucleation (in Chapter 3) on cloud responses and the radiation balance by simulating a planet without

nucleation. These simulations highlight the importance of representing nucleation accurately in UKESM1 and other climate models as well, given its majority contribution to the secondary aerosol budget across the earth. We then examined the climatic impact of organic compounds and their oxidation products in chapter 4, with a specific focus on isoprene. Isoprene chemistry in the gas and aqueous phase can contribute to the secondary aerosol budget, and both these atmospheric processes are not represented in UKESM1. The research work in Chapter 2 helped drive the research in chapters 3 and 4, and together these three chapters improve our understanding of secondary aerosol and informs future scientific/model development work in UKESM1. We describe some of the main results from these chapters in the following paragraphs in this section.

In Chapter 2, the UK Earth system model was used to better understand the vertical profiles of three interdependent atmospheric variables: total aerosol number concentration, sulphur dioxide and condensation sink. We used high temporal resolution model data and compared it against aircraft measurements from the ATom campaign. The model's biases were quantified, and we found that the condensation sink predicted by the model was within a factor of 2 of observations. However, the model showed significant biases in aerosol number concentration and sulphur dioxide. We performed a series of model sensitivity tests to identify atmospheric processes that have the strongest influence on overall model performance.

We found that boundary layer nucleation, sub 3nm particle growth, pH of cloud droplets and DMS emissions are key atmospheric parameters/processes that help reduce model biases. A simulation including all these modifications to the default version of UKESM1 has a much better sulphur dioxide and condensation sink profile,

which agrees very well with observations. However, the aerosol number concentration profile still showed large deviations especially in the upper troposphere-tropics (bias is a factor of ~4). The biases in aerosol number concentration could not be reduced further with the parameters used in this study and we suspect that there could be a structural issue with how nucleation or gas/particle transport or aerosol scavenging is handled in the model. This requires further investigation and is not addressed in this thesis.

In Chapter 3, we studied the role of nucleation in the climate system. We estimate that without nucleation the upper tropospheric aerosol number concentration would be reduced to 0.01% of its value. A planet without nucleation would have 33% lower cloud droplet concentration, 8% reduction in liquid water path and 3% reduction in cloud fraction. These changes to aerosol concentration and cloud properties are estimated to cause a net planetary cooling of 2.45W m^{-2}, which exceeds the global warming effect of all atmospheric methane. We also find that nucleation can dampen cloud responses of primary aerosol emissions in pristine environments. On a pre-industrial planet, turning on nucleation reduced the radiative effect of doubling fire emissions by a factor of 20.

In Chapter 4, we examined the role isoprene plays in producing secondary organic aerosol (SOA) and assessed its global impact. We estimate that isoprene contributes to 62% of the global SOA budget, with 20% attributed to isoprene aqueous phase chemistry and 42% to isoprene gas phase chemistry. We incorporate a novel isoprene aqueous phase chemistry mechanism from a recent study (Lamkaddam et al., 2021) into UKESM1. We find that AqSOA contributes a substantial regional radiative effect of about -0.5W m^{-2} and -0.3W m^{-2} over parts of South America and Africa

respectively. AqSOA is predominant at lower altitudes with its concentration reaching 50 μg/m^3 at 2 km altitude. The default version of UKESM1 does not have a mechanism for the production of SOA from gas and aqueous phase isoprene chemistry, instead the SOA yield from monoterpenes is scaled up a factor of 2 to account for the absence of isoprene SOA in the model. We compare a simulation with gas and aqueous phase isoprene SOA mechanisms incorporated into UKESM1, against the default UKESM1 simulation with no isoprene SOA (but has a monoterpene SOA scaled up by a factor of 2). Gas and aqueous isoprene SOA simulation accounts for -0.11 W/m^2 to the earth's radiation budget globally, with regional effects of up to -2.0 W/m^2 over South America, Africa, and Australia.

This thesis sheds light on the role of secondary aerosol and microphysical processes that lead to their formation, in the climate system. There still remains open questions that could be explored further, discussed in the next section.

5.2 Future Work

The research work in this thesis improves our understanding of secondary aerosol and microphysical processes in the atmosphere. However, there are certain open questions/ideas that were not addressed as part of this thesis.

In Chapter 2: Constraints on global aerosol number concentration, sulphur dioxide and condensation sink in UKESM1 using ATom measurements

- We evaluated the impact of various atmospheric processes on model biases, and this was done via one at a time sensitivity tests. By trial and error, we

identified the best combination of parameter perturbations that best improves the model's performance. We overlooked the interaction between different parameters, and this can be best explored in a perturbed parameter ensemble study in the future.

- We overlooked the impact of our analysis on the radiative effect and aerosol forcing. Certain combinations of parameter perturbations could be discarded because they result in unrealistic aerosol forcing estimates.
- Through our suggested improvements to the model, we were able to reduce model biases in SO_2 and condensation sink, however model biases in total aerosol number concentration still persists. The biases in total aerosol number concentration could not be reduced further with the parameters used in this study and there could be a structural issue with how nucleation or gas/particle transport or aerosol scavenging is handled in the model. This requires further investigation.

In Chapter 3: Role of nucleation in the climate system

- The nucleation schemes used in this study involve H_2SO_4, H_2O, HOMs and ions. Our molecular understanding of nucleation has progressed considerably over the last decade, we know now that ammonia, nitric acid, iodic acid and amines can also participate in nucleation. It would be interesting to evaluate how the climate system responds to the inclusion of these new nucleation schemes.
- The latest version of UKESM1 will have a nitrate aerosol scheme. Perhaps implementation of nucleation mechanisms involving nitrogen containing species is within reach and would be an interesting research topic.

In Chapter 4: Role of isoprene in the production of secondary organic aerosol

- Our work highlights the importance of SOA production via isoprene, and this work can be made robust by comparing the results with observations. Vertical profiles of SOA from various atmospheric observation stations and aircraft measurements can be used to evaluate the isoprene gas phase and aqueous phase chemistry.

Chapter 6 : Supplementary

6.1 Appendix A

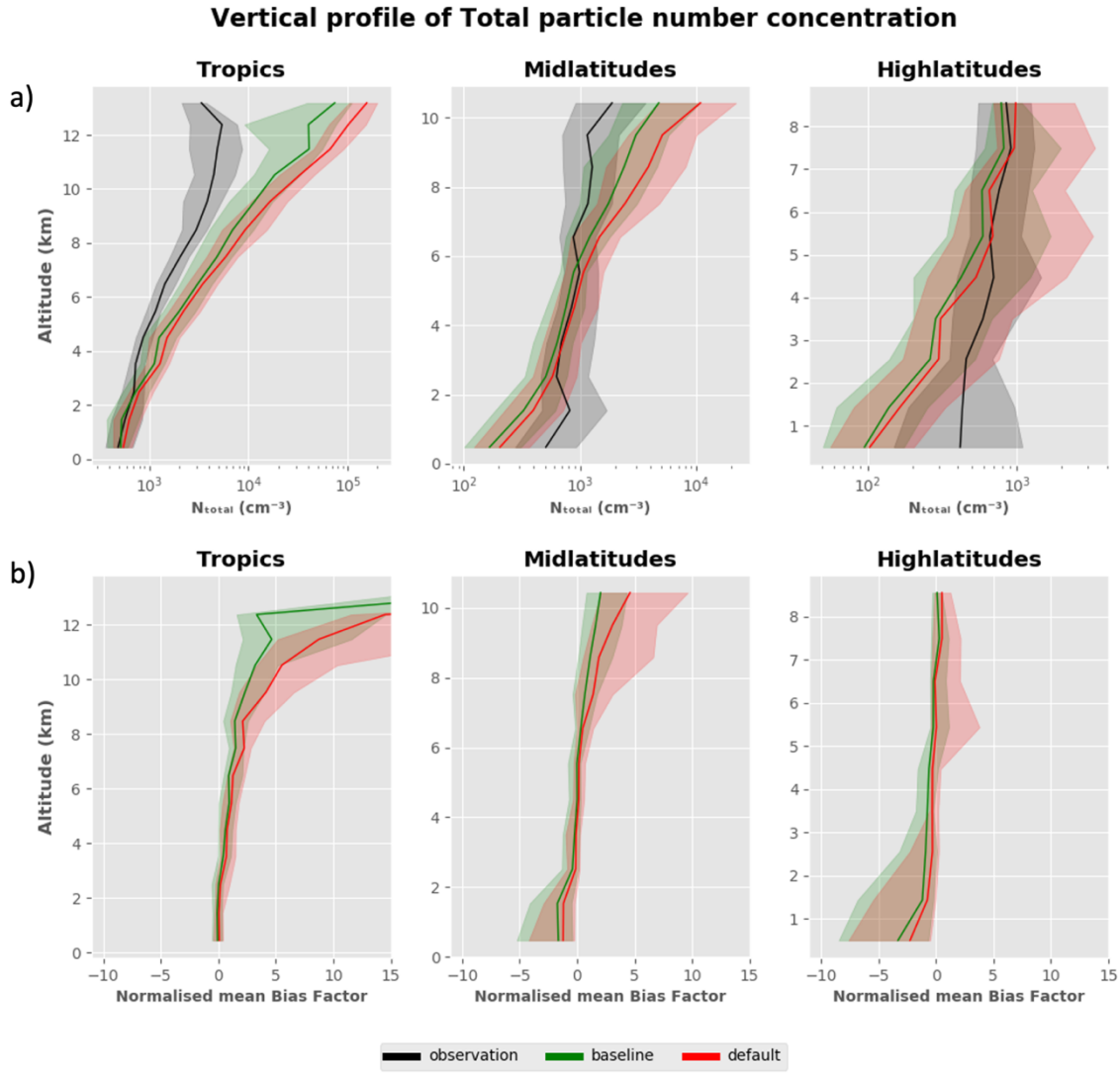

Figure A1: The vertical profile of the total particle number concentration (at standard temperature and pressure (STP)) as observed (ATom1-4) and in the simulated data from the default and baseline (bug-fixed) configurations of the UKESM, b) The vertical profile of the normalised mean bias factor (NMBF) for the two configurations of the model. The vertical profiles have been provided for the tropics (25^{o}N-25^{o}S), Midlatitudes (25^{o}N-60^{0}N and 25^{o}S-60^{o}S) and High latitudes (60^{o}N-90^{o}N and 60^{o}S-90^{o}S). In both a) and b) the bold line represents the median and the shaded region represents the corresponding interquartile range (25th and 75th percentile) in a 1km altitude bin.

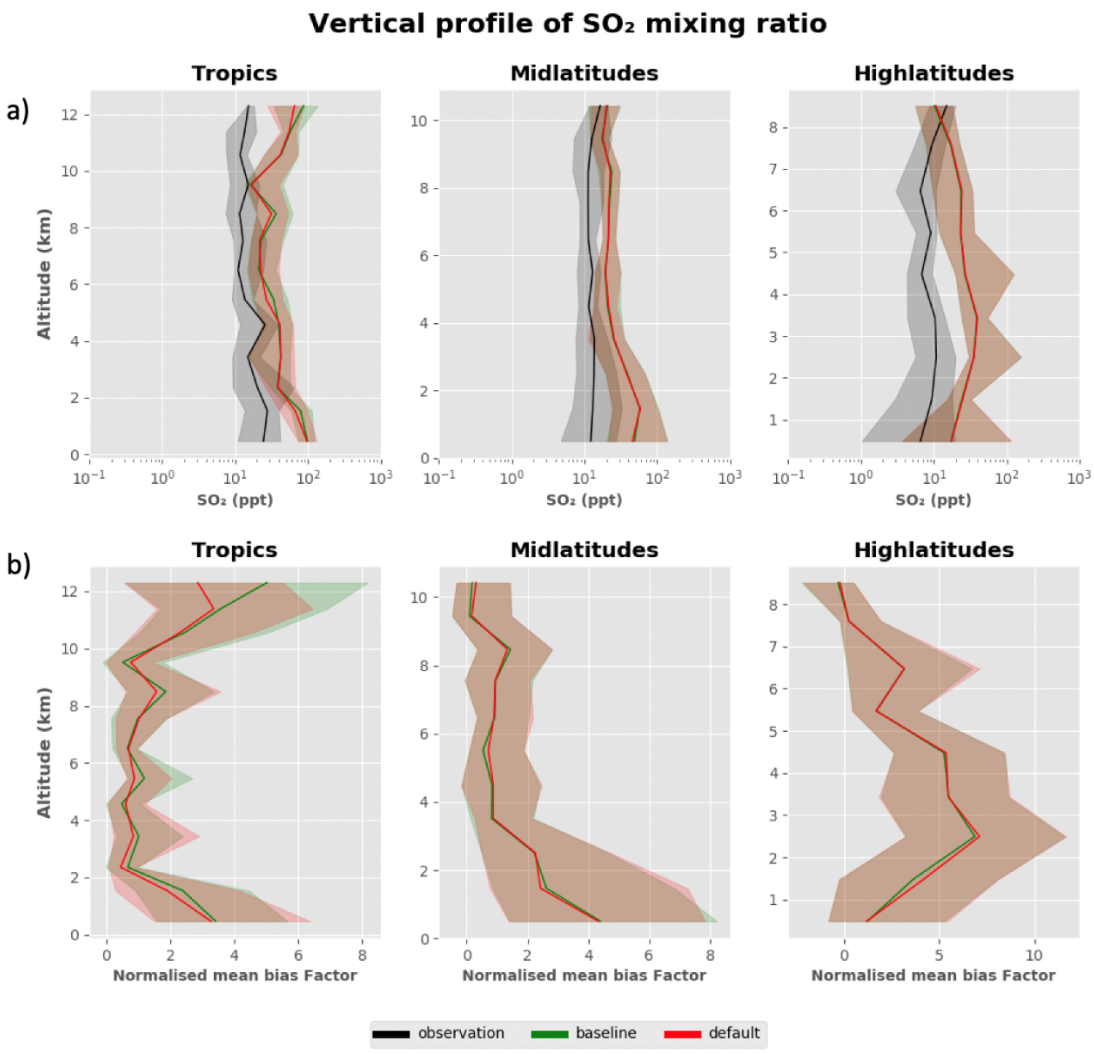

Figure A2: a) The vertical profile of the SO_2 mixing ratio as observed (ATom4 (April – May 2018)) and in the simulated data from the default and baseline configurations of the UKESM, b) The vertical profile of the Normalised Mean Bias Factor (NMBF) for the two configurations of the model. The vertical profiles have been provided for the tropics (25°N-25°S), midlatitude (25°N-60^{0}N and 25°S-60°S) and high latitudes (60°N-90°N and 60°S-90°S). In both a) and b) the bold line represents the median and the shaded region represents the corresponding interquartile range (25th and 75th percentile) in a 1km altitude bin.

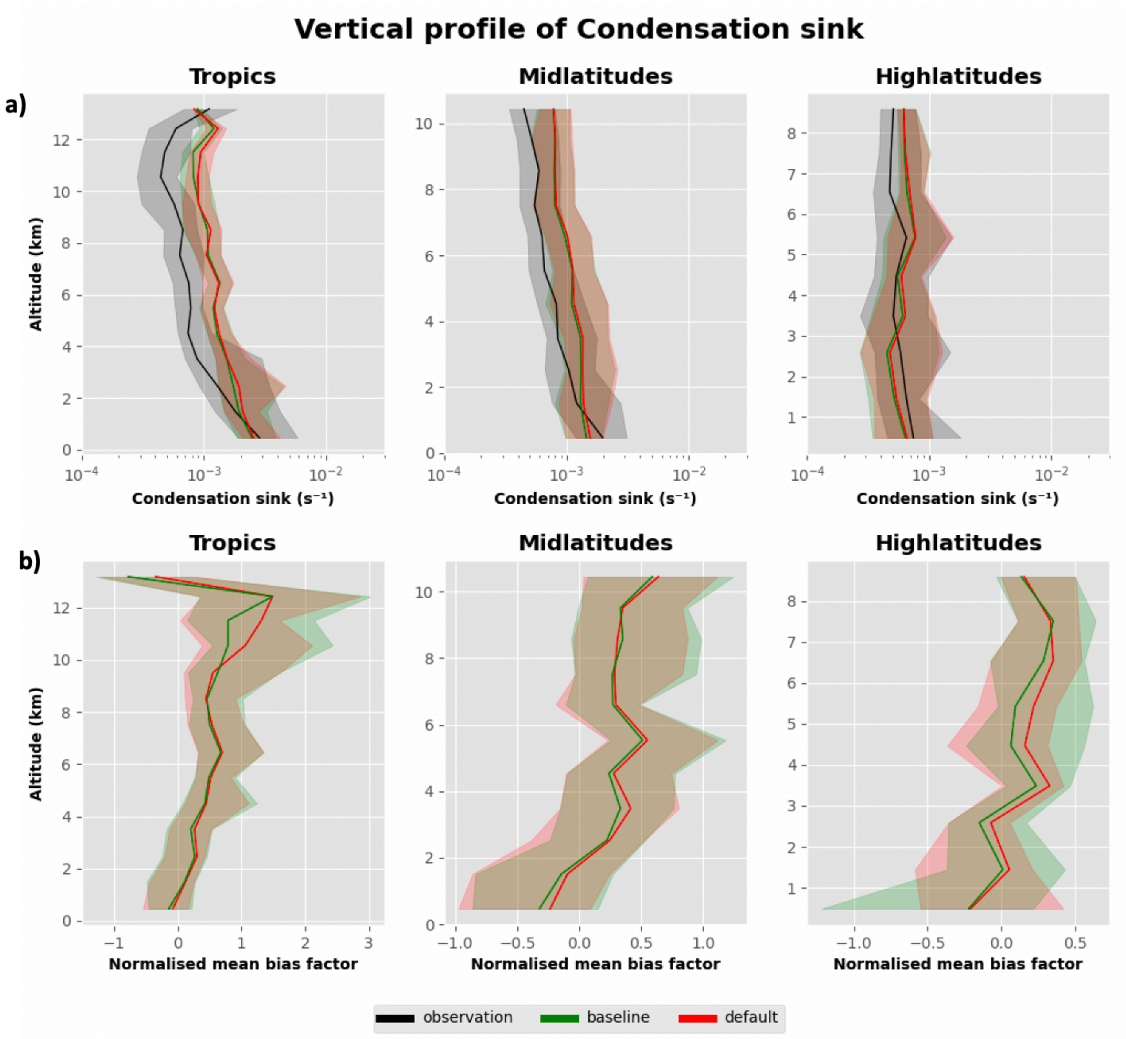

Figure A3: a) The vertical profile of the dry condensation sink in the atmosphere, as observed, and in simulated data from the default and baseline configurations of UKESM, b) The vertical profile of the Normalised Mean Bias Factor (NMBF) for the two configurations of the model. The vertical profiles have been provided for the tropics (25ºN-25ºS), Midlatitudes (25ºN-60^{0}N and 25ºS-60ºS) and High latitudes (60ºN-90ºN and 60ºS-90ºS). In both a) and b) the bold line represents the median and the shaded region represents the corresponding interquartile range (25th and 75th percentile) in a 1km altitude bin.

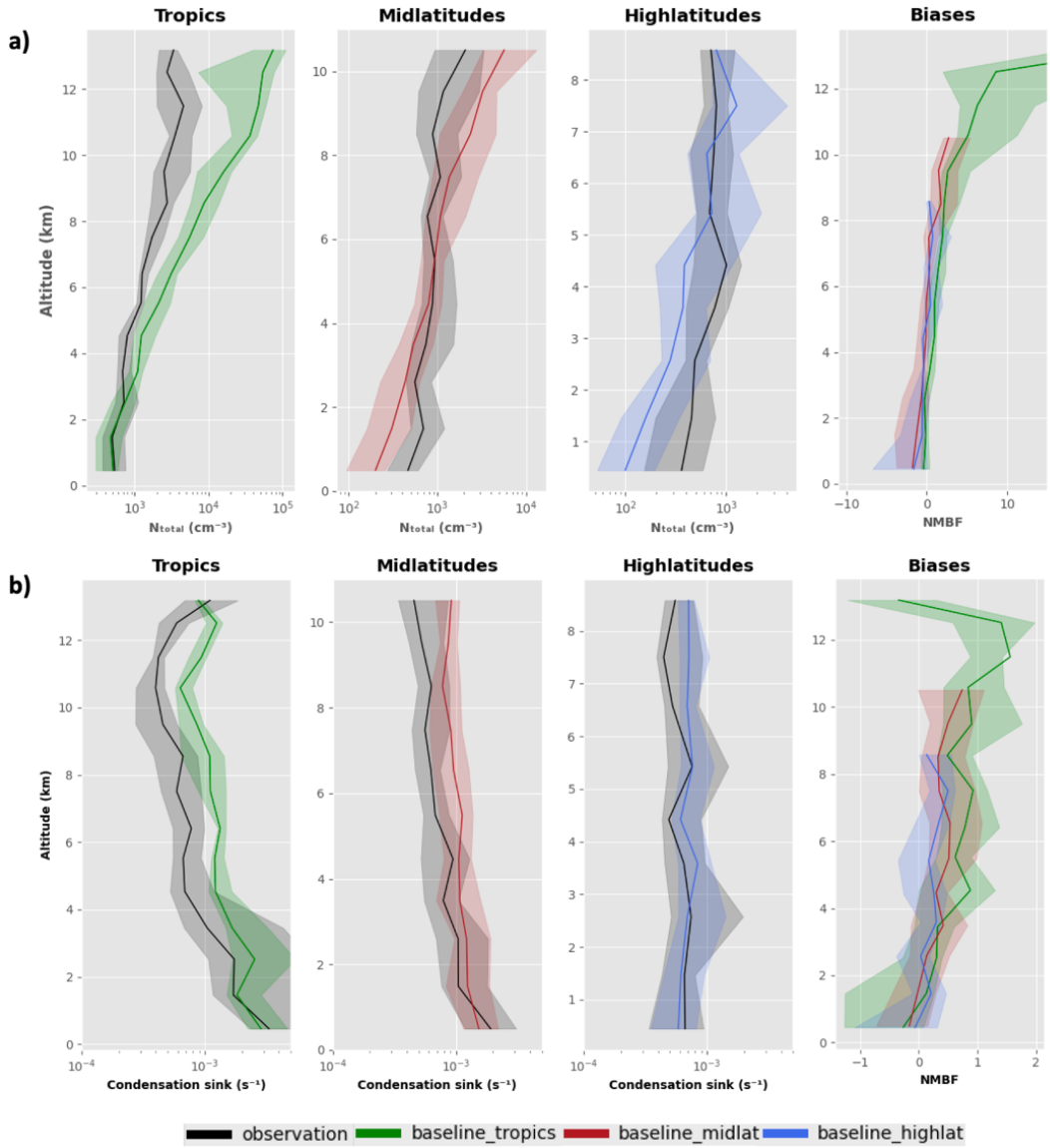

Figure A4: Vertical profiles of the baseline model and Observation a) N_{Total} and b) Condensation sink for only the ATom4 campaign. The first three columns show the vertical profile (at standard temperature and pressure (STP)) as observed and in the simulated data from the baseline (bug-fixed) configuration of UKESM in the Tropics (25°N-25°S), midlatitudes (25°N-60^{0}N and 25°S-60°S) and Highlatitudes (60°N-90°N and 60°S-90°S). The fourth column shows the NMBF of the baseline simulation in the Tropics, Midlatitudes and Highlatitudes. The bold line represents the median and the shaded region represents the corresponding interquartile range (25th and 75th percentile) in a 1km altitude bin.

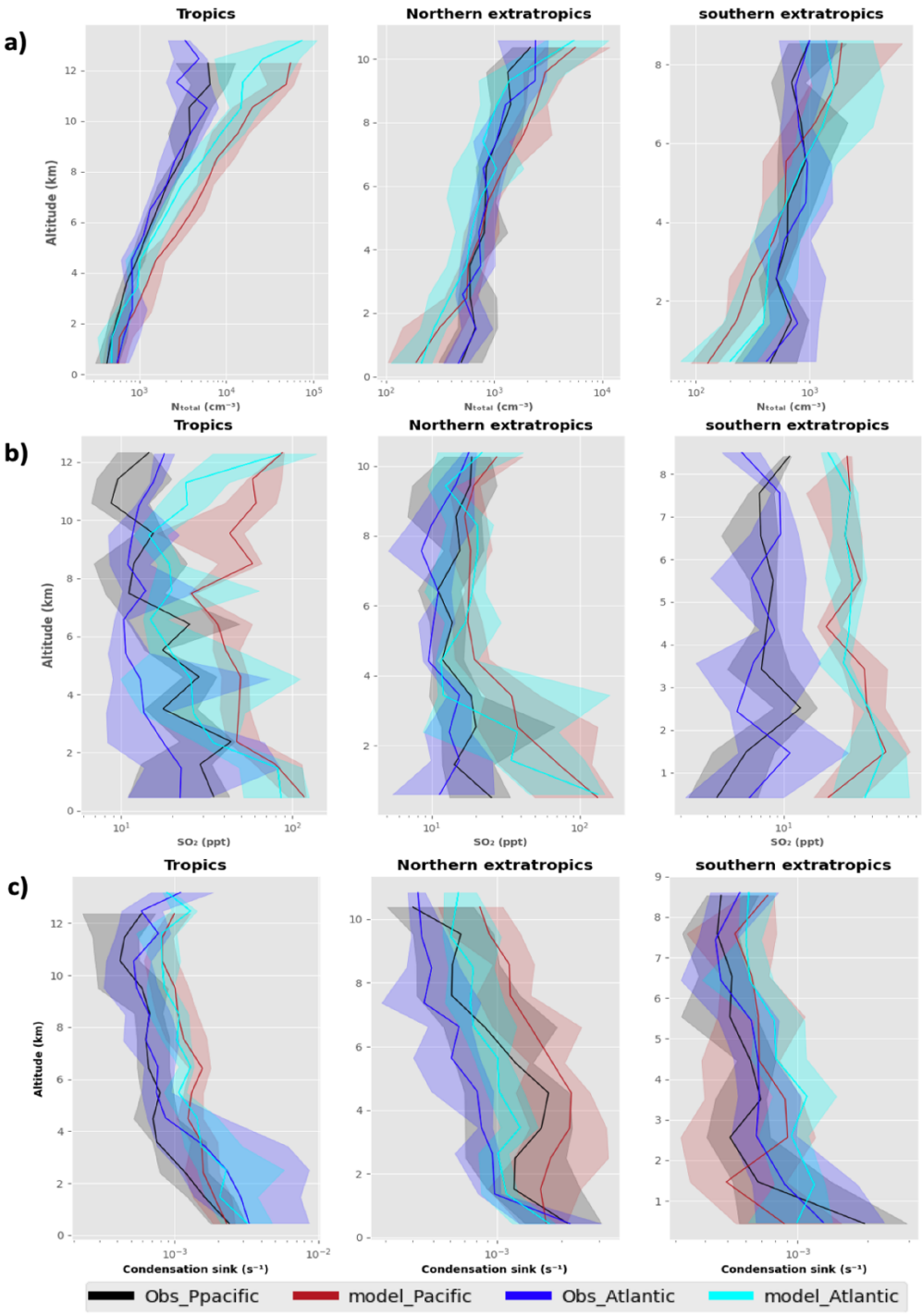

Figure A5: The vertical profiles of ATom and baseline model (Tropics, Northern extratropics (25°N-90°N) and southern extratropics (25°S-90°S)) in the Pacific and Atlantic ocean, a) N_{Total}, b) SO_2 and c) Condensation sink

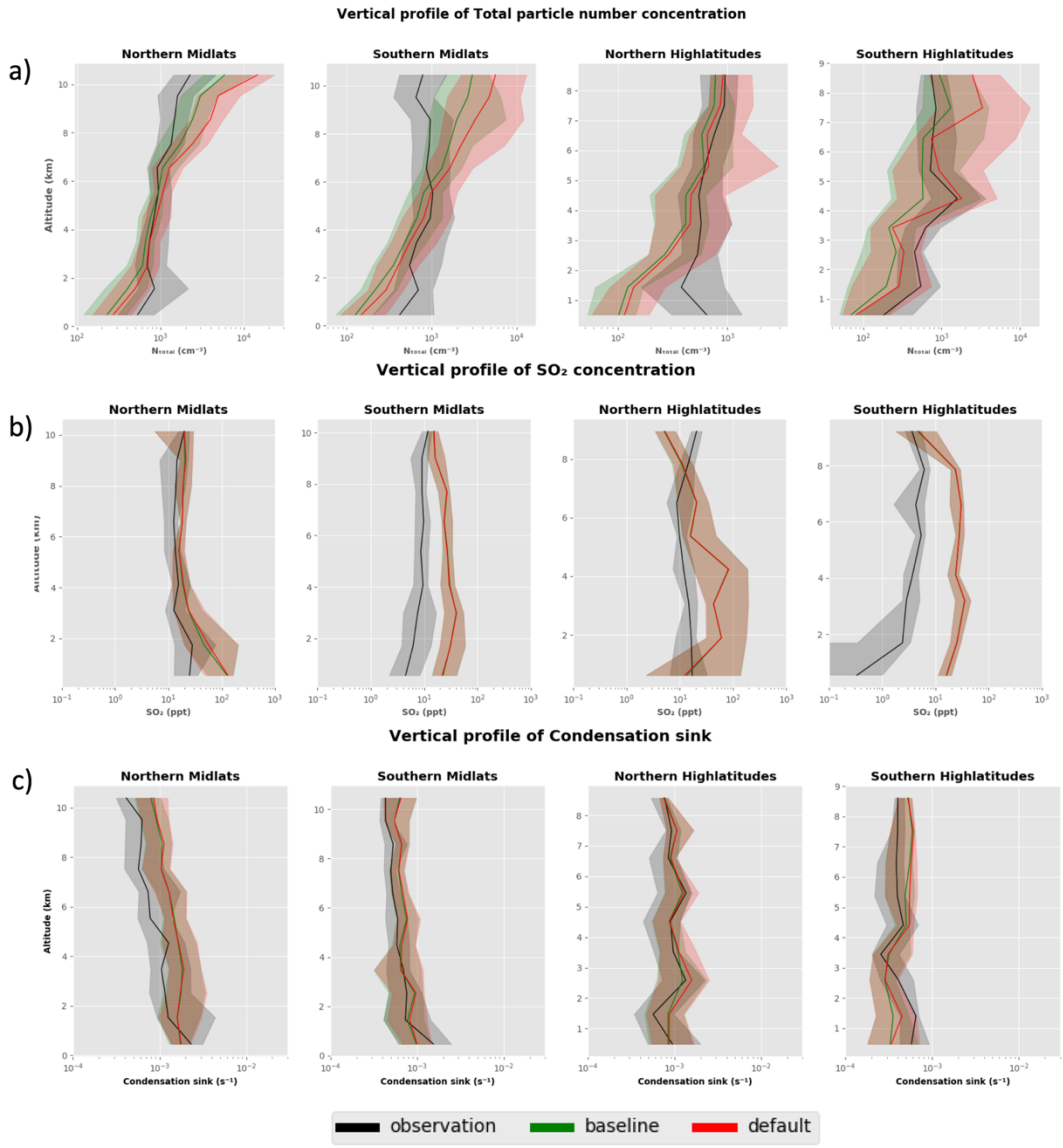

Figure A6: a) The vertical profile of the total particle number concentration, b) The vertical profile of SO_2 mixing ratio and c) The vertical profile of the condensation sink. The Vertical profiles are provided for the Northern and southern Midlatitudes (25°N-60^{0}N and 25°S-60°S) as well as the northern and southern highlatitudes (60°N-90°N and 60°S-90°S). The bold line represents the median and the shaded region represents the corresponding interquartile range (25th and 75th percentile) in a 1km altitude bin.

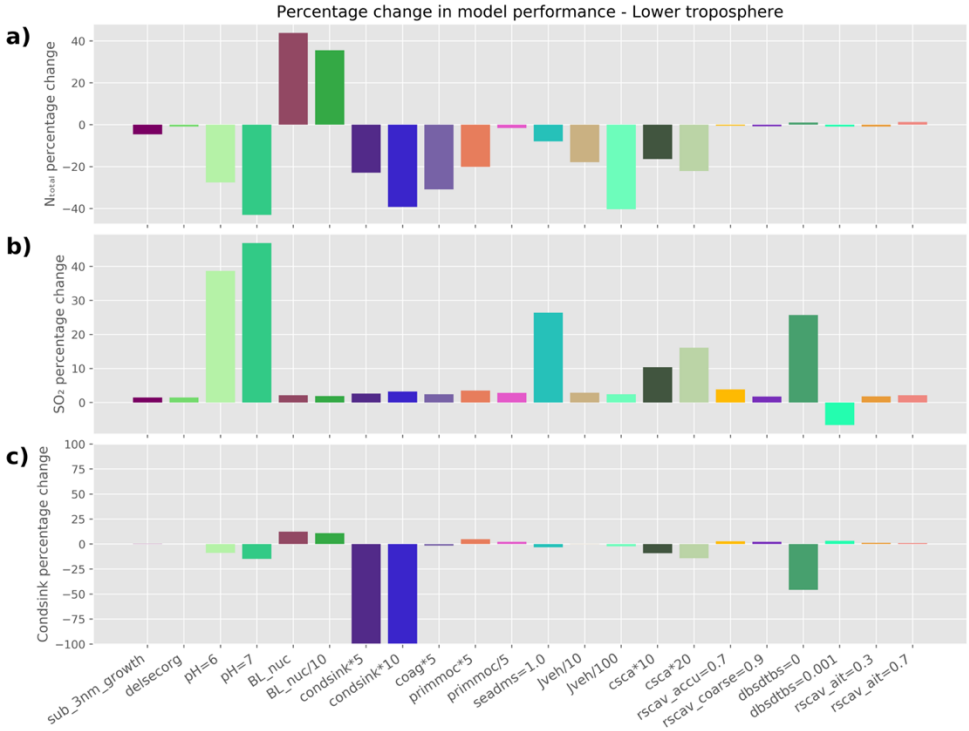

Figure A7: Percentage change in model performance for the different perturbation experiments in the Lower Troposphere (1km < altitude < 4km) with respect to, a) N_{Total}, b) SO_2, and c) condensation sink

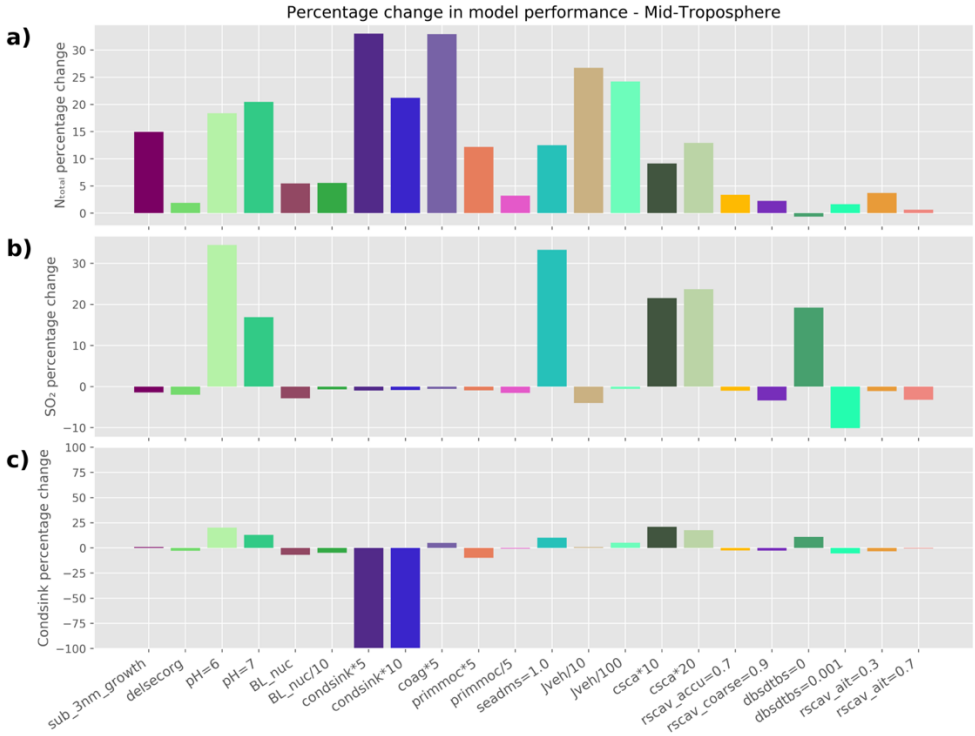

Figure A8: Percentage change in model performance for the different perturbation experiments in the Mid Troposphere (4km < altitude < 8km) with respect to, a) N_{Total}, b) SO_2, and c) condensation sink

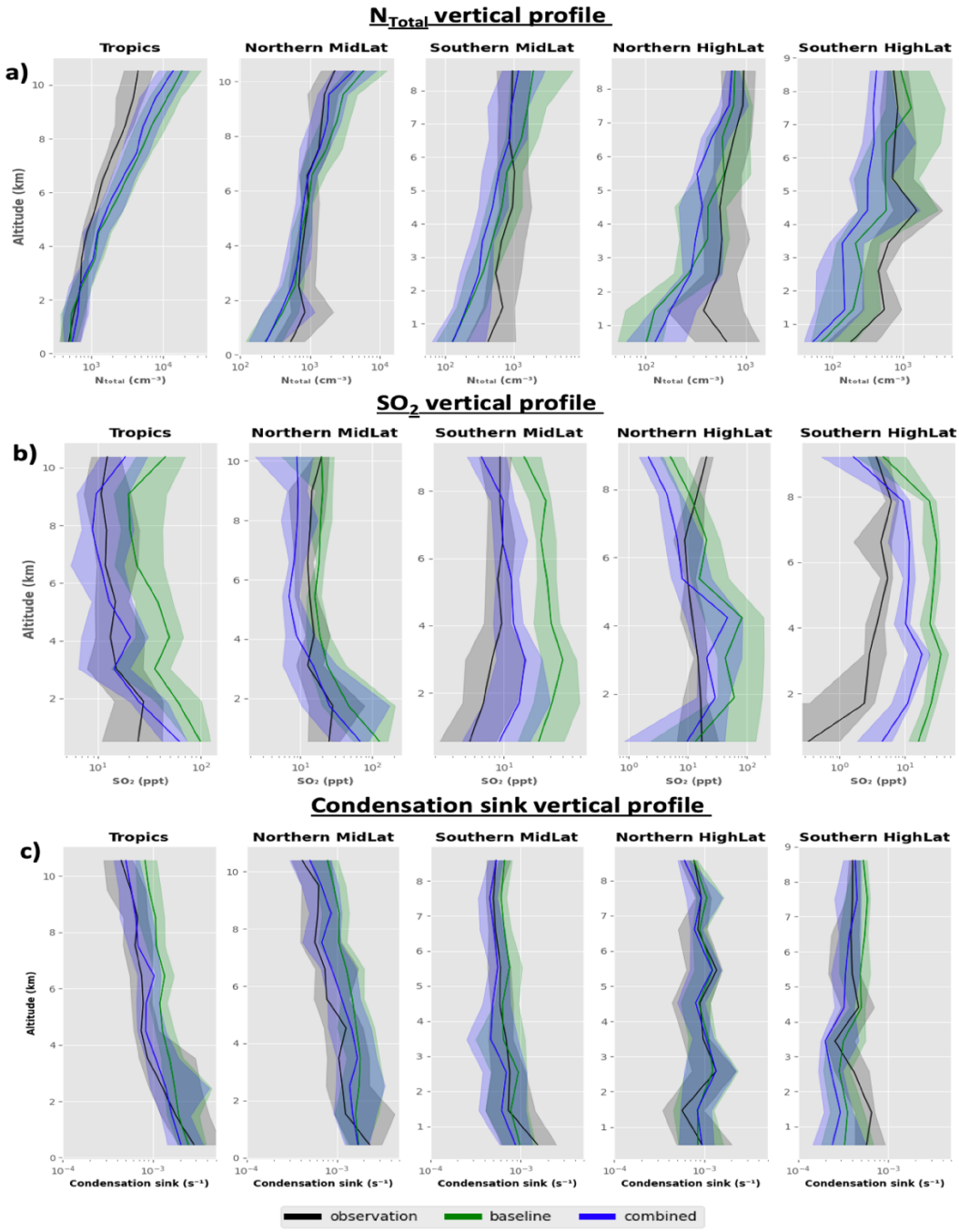

Figure A9: The Vertical profiles for the baseline simulation and the combined simulation a) N_{Total} b) SO_2 and c) Condensation sink in the tropics (25°S-25°N), northern Mid (25°N-60°N) and High-latitudes (60°N-90°N), and southern mid (25°S–60°S) and High latitudes (60S-90S)

Table A1: The different aerosol size modes in UKESM along with their size ranges, mode standard deviation and aerosol species in each mode. The species are organic matter (OM), sulphate (SO_4), BC (black carbon) and sea salt. Dust is treated separately as described in the text.

Aerosol Mode	Geometric mean diameter $\bar{d}$(nm)	Mode standard deviation	Species
Nucleation Soluble	$\bar{d}$ < 10 nm	1.59	OM, SO_4
Aitken Soluble	10 nm < $\bar{d}$ < 100 nm	1.59	OM, SO_4, BC
Accumulation Soluble	100 nm < $\bar{d}$ < 500 nm	1.40	OM, SO_4, BC, Sea salt
Coarse Soluble	500 nm < $\bar{d}$ < 10000 nm	2.00	OM, SO_4, BC, Sea salt
Aitken Insoluble	10 nm < $\bar{d}$ < 100 nm	1.59	OM, BC

Table A2: Normalised mean absolute error factor (NMAEF) wSith respect to N_{Total}, SO_2 and condensation sink for different model simulations. NMAEF values for the baseline simulation is highlighted in yellow. NMAEF values that are less than (or equal to) the baseline simulation are highlighted in green. NMAEF values that are greater than the baseline simulation are highlighted in orange. The plus (+) and minus (-) sign next to each NMAEF value indicates whether the bias is positive or negative. The dotted blue box indicates the model simulation for which NMAEF values for N_{Total}, SO_2 and condensation sink are less than (or equal to) the baseline simulation simultaneously; a) lower troposphere (between 1km and 4km) and b) mid troposphere (between 4km and 8km)

a)

NMAEF for model simulations in the lower troposphere			
Model perturbation	N_{Total}	SO_2	Condensation sink
Baseline	1.21(+)	2.13(+)	0.71(-)
sub_3nm_growth	1.27(+)	2.10(+)	0.71(-)
delsecorg	1.23(+)	2.10(+)	0.71(-)
pH=6	1.55(+)	1.31(+)	0.78(-)
pH=7	1.74(+)	1.13(+)	0.82(-)
BL_nuc	0.68(+)	2.09(+)	0.63(-)
BL_nuc/10	0.78(+)	2.09(+)	0.64(-)
condsink*5	1.49(-)	2.08(+)	3.18(+)
condsink*10	1.69(-)	2.06(+)	7.01(+)
coag*5	1.59(-)	2.08(+)	0.73(-)
primmoc*5	1.46(+)	2.06(+)	0.68(-)
primmoc	1.23(+)	2.07(+)	0.70(-)
seadms=1.0	1.31(+)	1.57(+)	0.74(-)
Jveh/10	1.43(+)	2.07(+)	0.72(-)
Jveh/100	1.70(-)	2.08(+)	0.73(-)
csca*10	1.41(+)	1.91(+)	0.78(-)
csca*20	1.48(+)	1.79(+)	0.82(-)
rscav_accu=0.7	1.22(+)	2.05(+)	0.70(-)
rscav_coarse=0.9	1.22(+)	2.09(+)	0.70(-)
dbsdtbs=0	1.20(+)	1.58(+)	1.04(-)
dbsdtbs=0.001	1.23(+)	2.27(+)	0.69(-)
rscav_ait=0.3	1.23(+)	2.09(+)	0.71(-)
rscav_ait=0.7	1.20(+)	2.08(+)	0.72(-)

b)

NMAEF for model simulations in the mid troposphere			
Model perturbation	N_{Total}	SO_2	Condensation sink
Baseline	1.15(+)	1.27(+)	0.58(+)
sub_3nm_growth	0.97(+)	1.27(+)	0.57(+)
delsecorg	1.12(+)	1.29(+)	0.59(+)
pH=6	0.93(+)	0.83(+)	0.46(-)
pH=7	0.91(+)	1.05(-)	0.50(-)
BL_nuc	1.08(+)	1.30(+)	0.62(+)
BL_nuc/10	1.08(+)	1.27(+)	0.61(+)
condsink*5	0.77(-)	1.28(+)	5.08(+)
condsink*10	0.90(-)	1.28(+)	10.76(+)
coag*5	0.77(-)	1.28(+)	0.55(+)
primmoc*5	1.00(+)	1.28(+)	0.63(+)
primmoc	1.11(+)	1.28(+)	0.58(+)
seadms=1.0	1.00(+)	0.84(+)	0.52(+)
Jveh/10	0.84(+)	1.32(+)	0.57(+)
Jveh/100	0.87(-)	1.27(+)	0.55(+)
csca*10	1.04(+)	0.99(+)	0.46(-)
csca*20	1.00(+)	0.97(+)	0.48(-)
rscav_accu=0.7	1.11(+)	1.28(+)	0.59(+)
rscav_coarse=0.9	1.12(+)	1.31(+)	0.59(+)
dbsdtbs=0	1.15(+)	1.02(+)	0.51(-)
dbsdtbs=0.001	1.13(+)	1.39(+)	0.61(+)
rscav_ait=0.3	1.10(+)	1.28(+)	0.60(+)
rscav_ait=0.7	1.14(+)	1.31(+)	0.58(+)

6.2 Appendix B

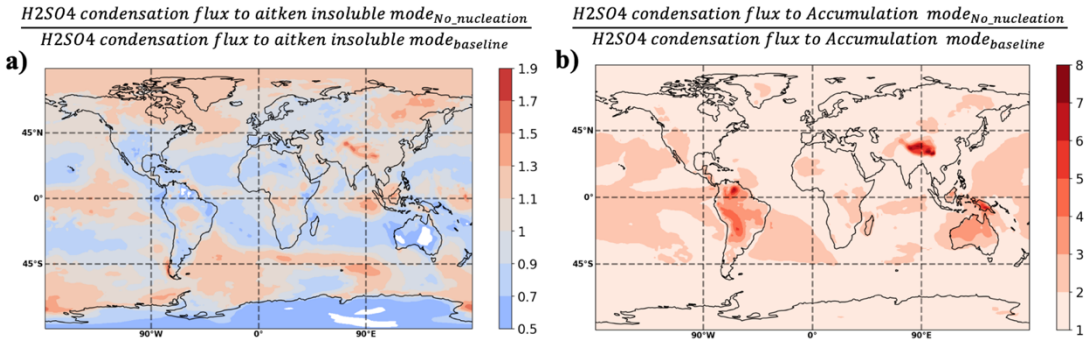

Figure B1: a) Ratio of the condensation flux of H_2SO_4 vapor onto the Aitken insoluble mode (10nm to 100nm) on a planet without nucleation and the baseline simulation b) Ratio of the condensation flux of H_2SO_4 vapor onto the accumulation aerosol mode (100nm to 500nm) on a planet without nucleation and the baseline simulation

---

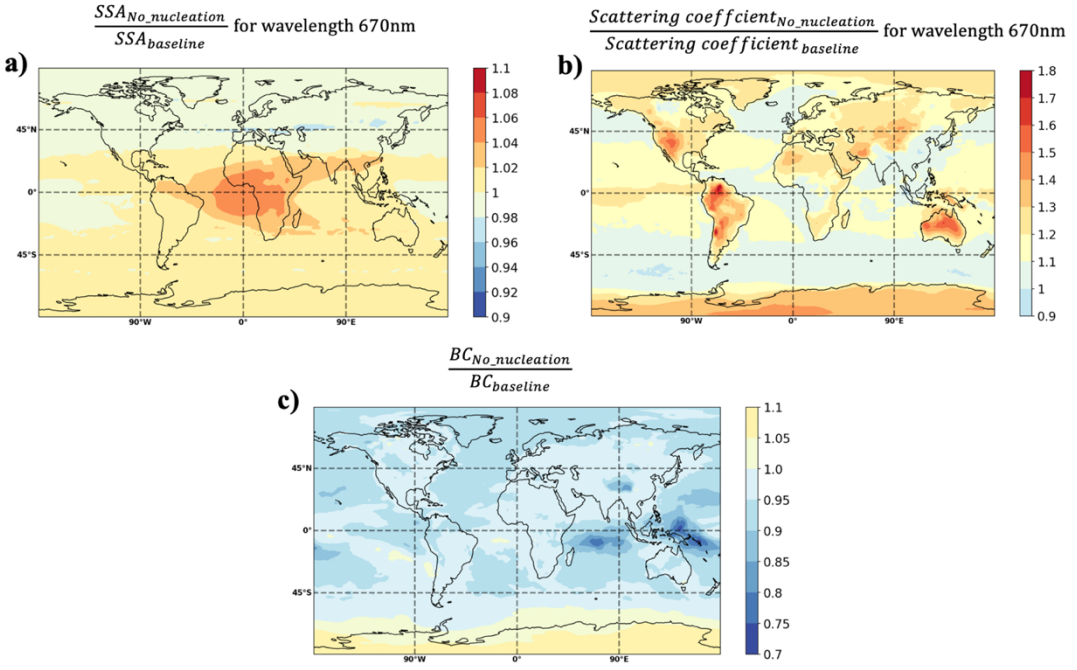

Figure B2: Ratio of the a) single scattering albedo, b) scattering coefficient and c) black carbon load on a planet without nucleation ('No_nucleation') relative to a planet with nucleation ('baseline')

6.3 Appendix C

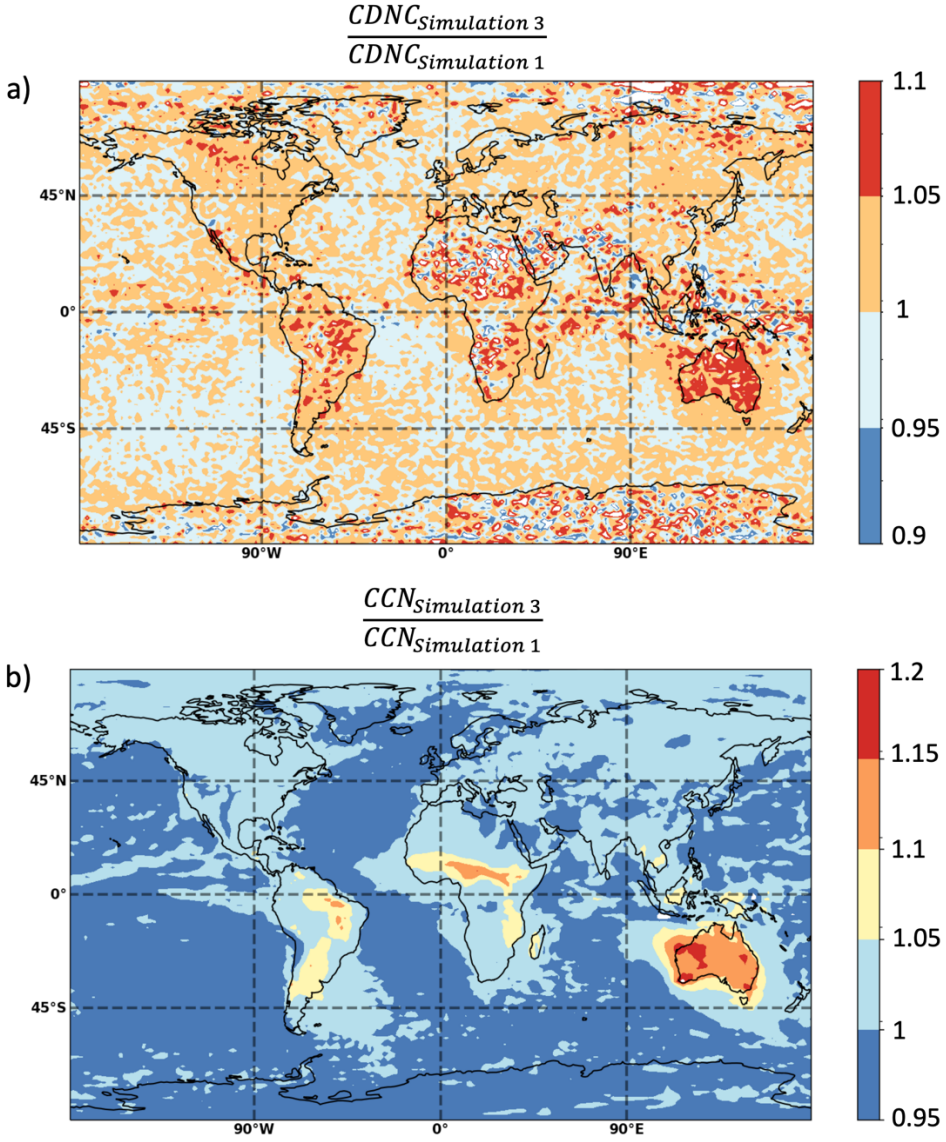

Figure C1: Comparison between the a) CDNC and b) CCN in simulation 3 and simulation 1

Chapter 7 : References

Ackerman, A. S., Toon, O. B., Stevens, D. E., Heymsfield, A. J., Ramanathan, V. and Welton, E. J.: Reduction of tropical cloudiness by soot, Science (80-.)., doi:10.1126/science.288.5468.1042, 2000.

Albrecht, B. A.: Aerosols, cloud microphysics, and fractional cloudiness, Science (80-.)., doi:10.1126/science.245.4923.1227, 1989.

Almeida, J., Schobesberger, S., Kürten, A., Ortega, I. K., Kupiainen-Määttä, O., Praplan, A. P., Adamov, A., Amorim, A., Bianchi, F., Breitenlechner, M., David, A., Dommen, J., Donahue, N. M., Downard, A., Dunne, E., Duplissy, J., Ehrhart, S., Flagan, R. C., Franchin, A., Guida, R., Hakala, J., Hansel, A., Heinritzi, M., Henschel, H., Jokinen, T., Junninen, H., Kajos, M., Kangasluoma, J., Keskinen, H., Kupc, A., Kurtén, T., Kvashin, A. N., Laaksonen, A., Lehtipalo, K., Leiminger, M., Leppä, J., Loukonen, V., Makhmutov, V., Mathot, S., McGrath, M. J., Nieminen, T., Olenius, T., Onnela, A., Petäjä, T., Riccobono, F., Riipinen, I., Rissanen, M., Rondo, L., Ruuskanen, T., Santos, F. D., Sarnela, N., Schallhart, S., Schnitzhofer, R., Seinfeld, J. H., Simon, M., Sipilä, M., Stozhkov, Y., Stratmann, F., Tomé, A., Tröstl, J., Tsagkogeorgas, G., Vaattovaara, P., Viisanen, Y., Virtanen, A., Vrtala, A., Wagner, P. E., Weingartner, E., Wex, H., Williamson, C., Wimmer, D., Ye, P., Yli-Juuti, T., Carslaw, K. S., Kulmala, M., Curtius, J., Baltensperger, U., Worsnop, D. R., Vehkamäki, H. and Kirkby, J.: Molecular understanding of sulphuric acid-amine particle nucleation in the atmosphere, Nature, doi:10.1038/nature12663, 2013.

Anderson, T. R., Spall, S. A., Yool, A., Cipollini, P., Challenor, P. G. and Fasham, M. J. R.: Global fields of sea surface dimethylsulfide predicted from chlorophyll, nutrients and light, J. Mar. Syst., doi:10.1016/S0924-7963(01)00028-8, 2001.

Baccarini, A., Karlsson, L., Dommen, J., Duplessis, P., Vüllers, J., Brooks, I. M., Saiz-lopez, A., Salter, M., Tjernström, M., Baltensperger, U., Zieger, P. and Schmale, J.: Arctic pack ice by enhanced iodine emissions, Nat. Commun., (2020), 1–11, doi:10.1038/s41467-020-18551-0, 2018.

Bandy, A. R., Thornton, D. C., Scott, D. L., Lalevic, M., Lewin, E. E. and Driedger, A. R.: A time series for carbonyl sulfide in the northern hemisphere, J. Atmos. Chem., doi:10.1007/BF00115256, 1992.

Bellouin, N., Quaas, J., Gryspeerdt, E., Kinne, S., Stier, P., Watson-Parris, D., Boucher, O., Carslaw, K. S., Christensen, M., Daniau, A. L., Dufresne, J. L., Feingold, G., Fiedler, S., Forster, P., Gettelman, A., Haywood, J. M., Lohmann, U., Malavelle, F., Mauritsen, T., McCoy, D. T., Myhre, G., Mülmenstädt, J., Neubauer, D., Possner, A., Rugenstein, M., Sato, Y., Schulz, M., Schwartz, S. E., Sourdeval, O., Storelvmo, T., Toll, V., Winker, D. and Stevens, B.: Bounding Global Aerosol Radiative Forcing of Climate Change, Rev. Geophys., doi:10.1029/2019RG000660, 2020.

Berndt, T., Herrmann, H., Sipilä, M. and Kulmala, M.: Highly Oxidized Second-Generation Products from the Gas-Phase Reaction of OH Radicals with Isoprene, J. Phys. Chem. A, doi:10.1021/acs.jpca.6b10987, 2016.

Bock, J., Michou, M., Nabat, P., Abe, M., Mulcahy, J. P., Olivié, D. J. L., Schwinger, J., Suntharalingam, P., Tjiputra, J., Van Hulten, M., Watanabe, M., Yool, A. and Séférian, R.: Evaluation of ocean dimethylsulfide concentration and emission in CMIP6 models, Biogeosciences, doi:10.5194/bg-18-3823-2021, 2021.

Bregonzio-Rozier, L., Giorio, C., Siekmann, F., Pangui, E., Morales, S. B., Temime-Roussel, B., Gratien, A., Michoud, V., Cazaunau, M., Dewitt, H. L., Tapparo, A., Monod, A. and Doussin, J. F.: Secondary organic aerosol formation from isoprene

photooxidation during cloud condensation-evaporation cycles, Atmos. Chem. Phys., doi:10.5194/acp-16-1747-2016, 2016.
Brock, C. A., Williamson, C., Kupc, A., Froyd, K. D., Erdesz, F., Wagner, N., Richardson, M., Schwarz, J. P., Gao, R. S., Katich, J. M., Campuzano-Jost, P., Nault, B. A., Schroder, J. C., Jimenez, J. L., Weinzierl, B., Dollner, M., Bui, T. and Murphy, D. M.: Aerosol size distributions during the Atmospheric Tomography Mission (ATom): Methods, uncertainties, and data products, Atmos. Meas. Tech., doi:10.5194/amt-12-3081-2019, 2019.
Brühl, C., Lelieveld, J., Crutzen, P. J. and Tost, H.: The role of carbonyl sulphide as a source of stratospheric sulphate aerosol and its impact on climate, Atmos. Chem. Phys., 12(3), 1239–1253, doi:10.5194/acp-12-1239-2012, 2012.
Carlton, A. G., Pinder, R. W., Bhave, P. V. and Pouliot, G. A.: To what extent can biogenic SOA be controlled?, Environ. Sci. Technol., doi:10.1021/es903506b, 2010.
Carslaw, K. S., Lee, L. A., Reddington, C. L., Pringle, K. J., Rap, A., Forster, P. M., Mann, G. W., Spracklen, D. V., Woodhouse, M. T., Regayre, L. A. and Pierce, J. R.: Large contribution of natural aerosols to uncertainty in indirect forcing, Nature, doi:10.1038/nature12674, 2013.
Chen, S., Jiang, N., Huang, J., Xu, X., Zhang, H., Zang, Z., Huang, K., Xu, X., Wei, Y., Guan, X., Zhang, X., Luo, Y., Hu, Z. and Feng, T.: Quantifying contributions of natural and anthropogenic dust emission from different climatic regions, Atmos. Environ., doi:10.1016/j.atmosenv.2018.07.043, 2018.
Christensen, M. W., Jones, W. K. and Stier, P.: Aerosols enhance cloud lifetime and brightness along the stratus-to-cumulus transition, Proc. Natl. Acad. Sci. U. S. A., 117(30), 17591–17598, doi:10.1073/pnas.1921231117, 2020.
Claeys, M., Graham, B., Vas, G., Wang, W., Vermeylen, R., Pashynska, V., Cafmeyer, J., Guyon, P., Andreae, M. O., Artaxo, P. and Maenhaut, W.: Formation of Secondary Organic Aerosols Through Photooxidation of Isoprene, Science (80-.)., doi:10.1126/science.1092805, 2004.
Clarke, A. D., Varner, J. L., Eisele, F., Mauldin, R. L., Tanner, D. and Litchy, M.: Particle production in the remote marine atmosphere: Cloud outflow and subsidence during ACE 1, J. Geophys. Res. Atmos., doi:10.1029/97JD02987, 1998.
Clarke, A. D., Eisele, F., Kapustin, V. N., Moore, K., Tanner, D., Mauldin, L., Litchy, M., Lienert, B., Carroll, M. A. and Albercook, G.: Nucleation in the equatorial free troposphere: Favorable environments during PEM-Tropics, J. Geophys. Res. Atmos., doi:10.1029/98JD02303, 1999.
Crutzen, P. J., Heidt, L. E., Krasnec, J. P., Pollock, W. H. and Seiler, W.: Biomass burning as a source of atmospheric gases CO, H2, N 2O, NO, CH3Cl and COS, Nature, doi:10.1038/282253a0, 1979.
Cuevas, C. A., Maffezzoli, N., Corella, J. P., Spolaor, A., Vallelonga, P., Kjær, H. A., Simonsen, M., Winstrup, M., Vinther, B., Horvat, C., Fernandez, R. P., Kinnison, D., Lamarque, J. F., Barbante, C. and Saiz-Lopez, A.: Rapid increase in atmospheric iodine levels in the North Atlantic since the mid-20th century, Nat. Commun., doi:10.1038/s41467-018-03756-1, 2018.
Dal Maso, M., Kulmala, M., Riipinen, I., Wagner, R., Hussein, T., Aalto, P. P. and Lehtinen, K. E. J.: Formation and growth of fresh atmospheric aerosols: Eight years of aerosol size distribution data from SMEAR II, Hyytiälä, Finland, Boreal Environ. Res., 2005.
Dee, D. P., Uppala, S. M., Simmons, A. J., Berrisford, P., Poli, P., Kobayashi, S., Andrae, U., Balmaseda, M. A., Balsamo, G., Bauer, P., Bechtold, P., Beljaars, A. C. M., van de Berg, L., Bidlot, J., Bormann, N., Delsol, C., Dragani, R., Fuentes, M., Geer, A. J., Haimberger, L., Healy, S. B., Hersbach, H., Hólm, E. V., Isaksen, L.,

Kållberg, P., Köhler, M., Matricardi, M., Mcnally, A. P., Monge-Sanz, B. M., Morcrette, J. J., Park, B. K., Peubey, C., de Rosnay, P., Tavolato, C., Thépaut, J. N. and Vitart, F.: The ERA-Interim reanalysis: Configuration and performance of the data assimilation system, Q. J. R. Meteorol. Soc., doi:10.1002/qj.828, 2011.
Donahue, N. M., Epstein, S. A., Pandis, S. N. and Robinson, A. L.: A two-dimensional volatility basis set: 1. organic-aerosol mixing thermodynamics, Atmos. Chem. Phys., doi:10.5194/acp-11-3303-2011, 2011.
Dunne, E. M., Gordon, H., Kürten, A., Almeida, J., Duplissy, J., Williamson, C., Ortega, I. K., Pringle, K. J., Adamov, A., Baltensperger, U., Barmet, P., Benduhn, F., Bianchi, F., Breitenlechner, M., Clarke, A., Curtius, J., Dommen, J., Donahue, N. M., Ehrhart, S., Flagan, R. C., Franchin, A., Guida, R., Hakala, J., Hansel, A., Heinritzi, M., Jokinen, T., Kangasluoma, J., Kirkby, J., Kulmala, M., Kupc, A., Lawler, M. J., Lehtipalo, K., Makhmutov, V., Mann, G., Mathot, S., Merikanto, J., Miettinen, P., Nenes, A., Onnela, A., Rap, A., Reddington, C. L. S., Riccobono, F., Richards, N. A. D., Rissanen, M. P., Rondo, L., Sarnela, N., Schobesberger, S., Sengupta, K., Simon, M., Sipilä, M., Smith, J. N., Stozkhov, Y., Tomé, A., Tröstl, J., Wagner, P. E., Wimmer, D., Winkler, P. M., Worsnop, D. R. and Carslaw, K. S.: Global atmospheric particle formation from CERN CLOUD measurements, Science (80-.)., doi:10.1126/science.aaf2649, 2016.
Ekman, A. M. L., Hermann, M., Gro, P., Heintzenberg, J., Kim, D. and Wang, C.: Sub-micrometer aerosol particles in the upper troposphere/lowermost stratosphere as measured by CARIBIC and modeled using the MIT-CAM3 global climate model, J. Geophys. Res. Atmos., doi:10.1029/2011JD016777, 2012.
Ervens, B.: Modeling the Processing of Aerosol and Trace Gases in Clouds and Fogs, Chem. Rev., 115(10), 4157–4198, doi:10.1021/cr5005887, 2015.
Ervens, B.: Progress and problems in modeling chemical processing in cloud droplets and wet aerosol particles, in ACS Symposium Series., 2018.
Ervens, B., Turpin, B. J. and Weber, R. J.: Secondary organic aerosol formation in cloud droplets and aqueous particles (aqSOA): A review of laboratory, field and model studies, Atmos. Chem. Phys., doi:10.5194/acp-11-11069-2011, 2011.
Ervens, B., Sorooshian, A., Aldhaif, A. M., Shingler, T., Crosbie, E., Ziemba, L., Campuzano-Jost, P., Jimenez, J. L. and Wisthaler, A.: Is there an aerosol signature of chemical cloud processing?, Atmos. Chem. Phys., doi:10.5194/acp-18-16099-2018, 2018.
Eyring, V., Bony, S., Meehl, G. A., Senior, C., Stevens, B., Stouffer, R. J. and Taylor, K. E.: Overview of the Coupled Model Intercomparison Project Phase 6 (CMIP6) experimental design and organisation, Geosci. Model Dev. Discuss., doi:10.5194/gmdd-8-10539-2015, 2015.
Faloona, I., Conley, S. A., Blomquist, B., Clarke, A. D., Kapustin, V., Howell, S., Lenschow, D. H. and Bandy, A. R.: Sulfur dioxide in the tropical marine boundary layer: Dry deposition and heterogeneous oxidation observed during the pacific atmospheric sulfur experiment, J. Atmos. Chem., doi:10.1007/s10874-010-9155-0, 2009.
Flossmann, A. I. and Wobrock, W.: A review of our understanding of the aerosol-cloud interaction from the perspective of a bin resolved cloud scale modelling, Atmos. Res., doi:10.1016/j.atmosres.2010.05.008, 2010.
FUCHS, N. A. and SUTUGIN, A. G.: HIGH-DISPERSED AEROSOLS, in Topics in Current Aerosol Research., 1971.
Gantt, B., Johnson, M. S., Meskhidze, N., Sciare, J., Ovadnevaite, J., Ceburnis, D. and O'Dowd, C. D.: Model evaluation of marine primary organic aerosol emission schemes, Atmos. Chem. Phys., doi:10.5194/acp-12-8553-2012, 2012.

Gao, R. S., Telg, H., McLaughlin, R. J., Ciciora, S. J., Watts, L. A., Richardson, M. S., Schwarz, J. P., Perring, A. E., Thornberry, T. D., Rollins, A. W., Markovic, M. Z., Bates, T. S., Johnson, J. E. and Fahey, D. W.: A light-weight, high-sensitivity particle spectrometer for PM2.5 aerosol measurements, Aerosol Sci. Technol., doi:10.1080/02786826.2015.1131809, 2016.
Ghan, S. J.: Technical note: Estimating aerosol effects on cloud radiative forcing, Atmos. Chem. Phys., doi:10.5194/acp-13-9971-2013, 2013.
Ginoux, P., Prospero, J. M., Gill, T. E., Hsu, N. C. and Zhao, M.: Global-scale attribution of anthropogenic and natural dust sources and their emission rates based on MODIS Deep Blue aerosol products, Rev. Geophys., doi:10.1029/2012RG000388, 2012.
Gordon, H., Kirkby, J., Baltensperger, U., Bianchi, F., Breitenlechner, M., Curtius, J., Dias, A., Dommen, J., Donahue, N. M., Dunne, E. M., Duplissy, J., Ehrhart, S., Flagan, R. C., Frege, C., Fuchs, C., Hansel, A., Hoyle, C. R., Kulmala, M., Kürten, A., Lehtipalo, K., Makhmutov, V., Molteni, U., Rissanen, M. P., Stozkhov, Y., Tröstl, J., Tsagkogeorgas, G., Wagner, R., Williamson, C., Wimmer, D., Winkler, P. M., Yan, C. and Carslaw, K. S.: Causes and importance of new particle formation in the present-day and preindustrial atmospheres, J. Geophys. Res. Atmos., doi:10.1002/2017JD026844, 2017.
Goto, D., Takemura, T. and Nakajima, T.: Importance of global aerosol modeling including secondary organic aerosol formed from monoterpene, J. Geophys. Res. Atmos., doi:10.1029/2007JD009019, 2008.
De Gouw, J. and Jimenez, J. L.: Organic aerosols in the earth's atmosphere, Environ. Sci. Technol., doi:10.1021/es9006004, 2009.
Gregory, D. and Rowntree, P. R.: A mass flux convection scheme with representation of cloud ensemble characteristics and stability-dependent closure, Mon. Weather Rev., doi:10.1175/1520-0493(1990)118<1483:AMFCSW>2.0.CO;2, 1990.
Guenther, A.: A global model of natural volatile organic compound emissions, J. Geophys. Res., doi:10.1029/94JD02950, 1995.
Guenther, A. B., Jiang, X., Heald, C. L., Sakulyanontvittaya, T., Duhl, T., Emmons, L. K. and Wang, X.: The model of emissions of gases and aerosols from nature version 2.1 (MEGAN2.1): An extended and updated framework for modeling biogenic emissions, Geosci. Model Dev., doi:10.5194/gmd-5-1471-2012, 2012.
Gurciullo, C. S. and Pandis, S. N.: Effect of composition variations in cloud droplet populations on aqueous-phase chemistry, J. Geophys. Res. Atmos., doi:10.1029/96jd03651, 1997.
Hallquist, M., Wenger, J. C., Baltensperger, U., Rudich, Y., Simpson, D., Claeys, M., Dommen, J., Donahue, N. M., George, C., Goldstein, A. H., Hamilton, J. F., Herrmann, H., Hoffmann, T., Iinuma, Y., Jang, M., Jenkin, M. E., Jimenez, J. L., Kiendler-Scharr, A., Maenhaut, W., McFiggans, G., Mentel, T. F., Monod, A., Prévôt, A. S. H., Seinfeld, J. H., Surratt, J. D., Szmigielski, R. and Wildt, J.: The formation, properties and impact of secondary organic aerosol: Current and emerging issues, Atmos. Chem. Phys., doi:10.5194/acp-9-5155-2009, 2009.
Hansen, J. and Nazarenko, L.: Soot climate forcing via snow and ice albedos, Proc. Natl. Acad. Sci. U. S. A., doi:10.1073/pnas.2237157100, 2004.
He, X. C., Tham, Y. J., Dada, L., Wang, M., Finkenzeller, H., Stolzenburg, D., Iyer, S., Simon, M., Kürten, A., Shen, J., Rörup, B., Rissanen, M., Schobesberger, S., Baalbaki, R., Wang, D. S., Koenig, T. K., Jokinen, T., Sarnela, N., Beck, L. J., Almeida, J., Amanatidis, S., Amorim, A., Ataei, F., Baccarini, A., Bertozzi, B., Bianchi, F., Brilke, S., Caudillo, L., Chen, D., Chiu, R., Chu, B., Dias, A., Ding, A., Dommen, J., Duplissy, J., Haddad, I. El, Carracedo, L. G., Granzin, M., Hansel, A.,

Heinritzi, M., Hofbauer, V., Junninen, H., Kangasluoma, J., Kemppainen, D., Kim, C., Kong, W., Krechmer, J. E., Kvashin, A., Laitinen, T., Lamkaddam, H., Lee, C. P., Lehtipalo, K., Leiminger, M., Li, Z., Makhmutov, V., Manninen, H. E., Marie, G., Marten, R., Mathot, S., Mauldin, R. L., Mentler, B., Möhler, O., Müller, T., Nie, W., Onnela, A., Petäjä, T., Pfeifer, J., Philippov, M., Ranjithkumar, A., Saiz-Lopez, A., Salma, I., Scholz, W., Schuchmann, S., Schulze, B., Steiner, G., Stozhkov, Y., Tauber, C., Tomé, A., Thakur, R. C., Väisänen, O., Vazquez-Pufleau, M., Wagner, A. C., Wang, Y., Weber, S. K., Winkler, P. M., Wu, Y., Xiao, M., Yan, C., Ye, Q., Ylisirniö, A., Zauner-Wieczorek, M., Zha, Q., Zhou, P., Flagan, R. C., Curtius, J., Baltensperger, U., Kulmala, M., Kerminen, V. M., Kurtén, T., et al.: Role of iodine oxoacids in atmospheric aerosol nucleation, Science (80-.)., doi:10.1126/science.abe0298, 2021.

Heald, C. L., Coe, H., Jimenez, J. L., Weber, R. J., Bahreini, R., Middlebrook, A. M., Russell, L. M., Jolleys, M., Fu, T. M., Allan, J. D., Bower, K. N., Capes, G., Crosier, J., Morgan, W. T., Robinson, N. H., Williams, P. I., Cubison, M. J., Decarlo, P. F. and Dunlea, E. J.: Exploring the vertical profile of atmospheric organic aerosol: Comparing 17 aircraft field campaigns with a global model, Atmos. Chem. Phys., doi:10.5194/acp-11-12673-2011, 2011.

Heintzenberg, J., Hermann, M., Weigelt, A., Clarke, A., Kapustin, V., Anderson, B., Thornhill, K., van Velthoven, P., Zahn, A. and Brenninkmeijer, C.: Near-global aerosol mapping in the upper troposphere and lowermost stratosphere with data from the CARIBIC project, Tellus, Ser. B Chem. Phys. Meteorol., doi:10.1111/j.1600-0889.2011.00578.x, 2011.

Herrmann, H., Schaefer, T., Tilgner, A., Styler, S. A., Weller, C., Teich, M. and Otto, T.: Tropospheric Aqueous-Phase Chemistry: Kinetics, Mechanisms, and Its Coupling to a Changing Gas Phase, Chem. Rev., doi:10.1021/cr500447k, 2015.

Hodshire, A. L., Campuzano-Jost, P., Kodros, J. K., Croft, B., Nault, B. A., Schroder, J. C., Jimenez, J. L. and Pierce, J. R.: The potential role of methanesulfonic acid (MSA) in aerosol formation and growth and the associated radiative forcings, Atmos. Chem. Phys., doi:10.5194/acp-19-3137-2019, 2019.

Hodzic, A., Kasibhatla, P. S., Jo, D. S., Cappa, C. D., Jimenez, J. L., Madronich, S. and Park, R. J.: Rethinking the global secondary organic aerosol (SOA) budget: Stronger production, faster removal, shorter lifetime, Atmos. Chem. Phys., doi:10.5194/acp-16-7917-2016, 2016.

Hodzic, A., Campuzano-Jost, P., Bian, H., Chin, M., Colarco, P. R., Day, D. A., Froyd, K. D., Heinold, B., Jo, D. S., Katich, J. M., Kodros, J. K., Nault, B. A., Pierce, J. R., Ray, E., Schacht, J., Schill, G. P., Schroder, J. C., Schwarz, J. P., Sueper, D. T., Tegen, I., Tilmes, S., Tsigaridis, K., Yu, P. and Jimenez, J. L.: Characterization of organic aerosol across the global remote troposphere: A comparison of ATom measurements and global chemistry models, Atmos. Chem. Phys., 20(8), 4607–4635, doi:10.5194/acp-20-4607-2020, 2020a.

Hodzic, A., Campuzano-Jost, P., Bian, H., Chin, M., Colarco, P. R., Day, D. A., Froyd, K. D., Heinold, B., Jo, D. S., Katich, J. M., Kodros, J. K., Nault, B. A., Pierce, J. R., Ray, E., Schacht, J., Schill, G. P., Schroder, J. C., Schwarz, J. P., Sueper, D. T., Tegen, I., Tilmes, S., Tsigaridis, K., Yu, P. and Jimenez, J. L.: Characterization of organic aerosol across the global remote troposphere: A comparison of ATom measurements and global chemistry models, Atmos. Chem. Phys., doi:10.5194/acp-20-4607-2020, 2020b.

Hoesly, R. M., Smith, S. J., Feng, L., Klimont, Z., Janssens-Maenhout, G., Pitkanen, T., Seibert, J. J., Vu, L., Andres, R. J., Bolt, R. M., Bond, T. C., Dawidowski, L., Kholod, N., Kurokawa, J. I., Li, M., Liu, L., Lu, Z., Moura, M. C. P., O'Rourke, P. R.

and Zhang, Q.: Historical (1750-2014) anthropogenic emissions of reactive gases and aerosols from the Community Emissions Data System (CEDS), Geosci. Model Dev., doi:10.5194/gmd-11-369-2018, 2018.
Hoffmann, E. H., Tilgner, A., Schrödner, R., Bräuer, P., Wolke, R. and Herrmann, H.: An advanced modeling study on the impacts and atmospheric implications of multiphase dimethyl sulfide chemistry, Proc. Natl. Acad. Sci. U. S. A., doi:10.1073/pnas.1606320113, 2016.
Hoyle, C. R., Boy, M., Donahue, N. M., Fry, J. L., Glasius, M., Guenther, A., Hallar, A. G., Huff Hartz, K., Petters, M. D., Petäjä, T., Rosenoern, T. and Sullivan, A. P.: A review of the anthropogenic influence on biogenic secondary organic aerosol, Atmos. Chem. Phys., doi:10.5194/acp-11-321-2011, 2011.
IPCC: Climate Change 2021, Phys. Sci. Basis. Contrib. Work. Gr. 1 to Sixth Assess. Rep. Intergov. Panel Clim. Chang., 2021.
Jacob, D. J., Crawford, J. H., Maring, H., Clarke, A. D., Dibb, J. E., Emmons, L. K., Ferrare, R. A., Hostetler, C. A., Russell, P. B., Singh, H. B., Thompson, A. M., Shaw, G. E., McCauley, E., Pederson, J. R. and Fisher, J. A.: The arctic research of the composition of the troposphere from aircraft and satellites (ARCTAS) mission: Design, execution, and first results, Atmos. Chem. Phys., doi:10.5194/acp-10-5191-2010, 2010.
Jacobson, M. Z., Turco, R. P., Jensen, E. J. and Toon, O. B.: Modeling coagulation among particles of different composition and size, Atmos. Environ., doi:10.1016/1352-2310(94)90280-1, 1994.
Jimenez, J. L., Canagaratna, M. R., Donahue, N. M., Prevot, A. S. H., Zhang, Q., Kroll, J. H., DeCarlo, P. F., Allan, J. D., Coe, H., Ng, N. L., Aiken, A. C., Docherty, K. S., Ulbrich, I. M., Grieshop, A. P., Robinson, A. L., Duplissy, J., Smith, J. D., Wilson, K. R., Lanz, V. A., Hueglin, C., Sun, Y. L., Tian, J., Laaksonen, A., Raatikainen, T., Rautiainen, J., Vaattovaara, P., Ehn, M., Kulmala, M., Tomlinson, J. M., Collins, D. R., Cubison, M. J., Dunlea, E. J., Huffman, J. A., Onasch, T. B., Alfarra, M. R., Williams, P. I., Bower, K., Kondo, Y., Schneider, J., Drewnick, F., Borrmann, S., Weimer, S., Demerjian, K., Salcedo, D., Cottrell, L., Griffin, R., Takami, A., Miyoshi, T., Hatakeyama, S., Shimono, A., Sun, J. Y., Zhang, Y. M., Dzepina, K., Kimmel, J. R., Sueper, D., Jayne, J. T., Herndon, S. C., Trimborn, A. M., Williams, L. R., Wood, E. C., Middlebrook, A. M., Kolb, C. E., Baltensperger, U. and Worsnop, D. R.: Evolution of organic aerosols in the atmosphere, Science (80-.)., doi:10.1126/science.1180353, 2009.
Johnson, B. T., Shine, K. P. and Forster, P. M.: The semi-direct aerosol effect: Impact of absorbing aerosols on marine stratocumulus, Q. J. R. Meteorol. Soc., doi:10.1256/qj.03.61, 2004.
Katich, J. M., Samset, B. H., Bui, T. P., Dollner, M., Froyd, K. D., Campuzano-Jost, P., Nault, B. A., Schroder, J. C., Weinzierl, B. and Schwarz, J. P.: Strong Contrast in Remote Black Carbon Aerosol Loadings Between the Atlantic and Pacific Basins, J. Geophys. Res. Atmos., doi:10.1029/2018JD029206, 2018.
Kazil, J., Stier, P., Zhang, K., Quaas, J., Kinne, S., O'Donnell, D., Rast, S., Esch, M., Ferrachat, S., Lohmann, U. and Feichter, J.: Aerosol nucleation and its role for clouds and Earth's radiative forcing in the aerosol-climate model ECHAM5-HAM, Atmos. Chem. Phys., doi:10.5194/acp-10-10733-2010, 2010.
Kerminen, V. M. and Kulmala, M.: Analytical formulae connecting the "real" and the "apparent" nucleation rate and the nuclei number concentration for atmospheric nucleation events, J. Aerosol Sci., doi:10.1016/S0021-8502(01)00194-X, 2002.
Kerminen, V. M., Chen, X., Vakkari, V., Petäjä, T., Kulmala, M. and Bianchi, F.: Atmospheric new particle formation and growth: Review of field observations,

Environ. Res. Lett., 13(10), doi:10.1088/1748-9326/aadf3c, 2018a.
Kerminen, V. M., Chen, X., Vakkari, V., Petäjä, T., Kulmala, M. and Bianchi, F.: Atmospheric new particle formation and growth: Review of field observations, Environ. Res. Lett., doi:10.1088/1748-9326/aadf3c, 2018b.
Kettle, A. J., Kuhn, U., Von Hobe, M., Kesselmeier, J. and Andreae, M. O.: Global budget of atmospheric carbonyl sulfide: Temporal and spatial variations of the dominant sources and sinks, J. Geophys. Res. Atmos., doi:10.1029/2002JD002187, 2002.
Kipling, Z., Stier, P., Schwarz, J. P., Perring, A. E., Spackman, J. R., Mann, G. W., Johnson, C. E. and Telford, P. J.: Constraints on aerosol processes in climate models from vertically-resolved aircraft observations of black carbon, Atmos. Chem. Phys., doi:10.5194/acp-13-5969-2013, 2013.
Kirkby, J., Curtius, J., Almeida, J., Dunne, E., Duplissy, J., Ehrhart, S., Franchin, A., Gagné, S., Ickes, L., Kürten, A., Kupc, A., Metzger, A., Riccobono, F., Rondo, L., Schobesberger, S., Tsagkogeorgas, G., Wimmer, D., Amorim, A., Bianchi, F., Breitenlechner, M., David, A., Dommen, J., Downard, A., Ehn, M., Flagan, R. C., Haider, S., Hansel, A., Hauser, D., Jud, W., Junninen, H., Kreissl, F., Kvashin, A., Laaksonen, A., Lehtipalo, K., Lima, J., Lovejoy, E. R., Makhmutov, V., Mathot, S., Mikkilä, J., Minginette, P., Mogo, S., Nieminen, T., Onnela, A., Pereira, P., Petäjä, T., Schnitzhofer, R., Seinfeld, J. H., Sipilä, M., Stozhkov, Y., Stratmann, F., Tomé, A., Vanhanen, J., Viisanen, Y., Vrtala, A., Wagner, P. E., Walther, H., Weingartner, E., Wex, H., Winkler, P. M., Carslaw, K. S., Worsnop, D. R., Baltensperger, U. and Kulmala, M.: Role of sulphuric acid, ammonia and galactic cosmic rays in atmospheric aerosol nucleation, Nature, doi:10.1038/nature10343, 2011.
Kirkby, J., Duplissy, J., Sengupta, K., Frege, C., Gordon, H., Williamson, C., Heinritzi, M., Simon, M., Yan, C., Almeida, J., Trostl, J., Nieminen, T., Ortega, I. K., Wagner, R., Adamov, A., Amorim, A., Bernhammer, A. K., Bianchi, F., Breitenlechner, M., Brilke, S., Chen, X., Craven, J., Dias, A., Ehrhart, S., Flagan, R. C., Franchin, A., Fuchs, C., Guida, R., Hakala, J., Hoyle, C. R., Jokinen, T., Junninen, H., Kangasluoma, J., Kim, J., Krapf, M., Kurten, A., Laaksonen, A., Lehtipalo, K., Makhmutov, V., Mathot, S., Molteni, U., Onnela, A., Perakyla, O., Piel, F., Petaja, T., Praplan, A. P., Pringle, K., Rap, A., Richards, N. A. D., Riipinen, I., Rissanen, M. P., Rondo, L., Sarnela, N., Schobesberger, S., Scott, C. E., Seinfeld, J. H., Sipila, M., Steiner, G., Stozhkov, Y., Stratmann, F., Tomé, A., Virtanen, A., Vogel, A. L., Wagner, A. C., Wagner, P. E., Weingartner, E., Wimmer, D., Winkler, P. M., Ye, P., Zhang, X., Hansel, A., Dommen, J., Donahue, N. M., Worsnop, D. R., Baltensperger, U., Kulmala, M., Carslaw, K. S. and Curtius, J.: Ion-induced nucleation of pure biogenic particles, Nature, doi:10.1038/nature17953, 2016.
Korhonen, H., Carslaw, K. S., Spracklen, D. V., Mann, G. W. and Woodhouse, M. T.: Influence of oceanic dimethyl sulfide emissions on cloud condensation nuclei concentrations and seasonality over the remote Southern Hemisphere oceans: A global model study, J. Geophys. Res. Atmos., doi:10.1029/2007JD009718, 2008.
Kreidenwies, S. M., Walcek, C. J., Feingold, G., Gong, W., Jacobson, M. Z., Kim, C. H., Liu, X., Penner, J. E., Nenes, A. and Seinfeld, J. H.: Modification of aerosol mass and size distribution due to aqueous-phase SO2 oxidation in clouds: Comparisons of several models, J. Geophys. Res. D Atmos., doi:10.1029/2002jd002697, 2003.
Kroll, J. H., Ng, N. L., Murphy, S. M., Flagan, R. C. and Seinfeld, J. H.: Secondary organic aerosol formation from isoprene photooxidation under high-NOx conditions, Geophys. Res. Lett., doi:10.1029/2005GL023637, 2005.
Kroll, J. H., Ng, N. L., Murphy, S. M., Flagan, R. C. and Seinfeld, J. H.: Secondary organic aerosol formation from isoprene photooxidation, Environ. Sci. Technol.,

doi:10.1021/es0524301, 2006.
Kulmala, M. and Kerminen, V. M.: On the formation and growth of atmospheric nanoparticles, Atmos. Res., doi:10.1016/j.atmosres.2008.01.005, 2008.
Kupc, A., Williamson, C., Wagner, N. L., Richardson, M. and Brock, C. A.: Modification, calibration, and performance of the Ultra-High Sensitivity Aerosol Spectrometer for particle size distribution and volatility measurements during the Atmospheric Tomography Mission (ATom) airborne campaign, Atmos. Meas. Tech., doi:10.5194/amt-11-369-2018, 2018.
Kürten, A., Williamson, C., Almeida, J., Kirkby, J. and Curtius, J.: On the derivation of particle nucleation rates from experimental formation rates, Atmos. Chem. Phys., doi:10.5194/acp-15-4063-2015, 2015.
Lamkaddam, H., Dommen, J., Ranjithkumar, A., Gordon, H., Wehrle, G., Krechmer, J., Majluf, F., Salionov, D., Schmale, J., Bjelić, S., Carslaw, K. S., El Haddad, I. and Baltensperger, U.: Large contribution to secondary organic aerosol from isoprene cloud chemistry, Sci. Adv., doi:10.1126/sciadv.abe2952, 2021.
Leck, C. and Bigg, E. K.: Comparison of sources and nature of the tropical aerosol with the summer high Arctic aerosol, Tellus, Ser. B Chem. Phys. Meteorol., doi:10.1111/j.1600-0889.2007.00315.x, 2008.
Lee, L. A., Pringle, K. J., Reddington, C. L., Mann, G. W., Stier, P., Spracklen, D. V., Pierce, J. R. and Carslaw, K. S.: The magnitude and causes of uncertainty in global model simulations of cloud condensation nuclei, Atmos. Chem. Phys., doi:10.5194/acp-13-8879-2013, 2013.
Lee, S. H., Uin, J., Guenther, A. B., de Gouw, J. A., Yu, F., Nadykto, A. B., Herb, J., Ng, N. L., Koss, A., Brune, W. H., Baumann, K., Kanawade, V. P., Keutsch, F. N., Nenes, A., Olsen, K., Goldstein, A. and Ouyang, Q.: Isoprene suppression of new particle formation: Potential mechanisms and implications, J. Geophys. Res., doi:10.1002/2016JD024844, 2016.
Lee, S. H., Gordon, H., Yu, H., Lehtipalo, K., Haley, R., Li, Y. and Zhang, R.: New Particle Formation in the Atmosphere: From Molecular Clusters to Global Climate, J. Geophys. Res. Atmos., doi:10.1029/2018JD029356, 2019.
Lehtinen, K. E. J., Dal Maso, M., Kulmala, M. and Kerminen, V. M.: Estimating nucleation rates from apparent particle formation rates and vice versa: Revised formulation of the Kerminen-Kulmala equation, J. Aerosol Sci., doi:10.1016/j.jaerosci.2007.06.009, 2007.
Lihavainen, H., Kerminen, V. M., Tunved, P., Aaltonen, V., Arola, A., Hatakka, J., Hyvärinen, A. and Viisanen, Y.: Observational signature of the direct radiative effect by natural boreal forest aerosols and its relation to the corresponding first indirect effect, J. Geophys. Res. Atmos., doi:10.1029/2009JD012078, 2009.
Liss, P. S. and Merlivat, L.: Air-sea gas exchange rates: Introduction and synthesis BT - The Role of Air-Sea Exchange in Geochemical Cycling, Role Air-Sea Exch. Geochemical Cycl., 1986.
Liu, Y., Monod, A., Tritscher, T., Praplan, A. P., Decarlo, P. F., Temime-Roussel, B., Quivet, E., Marchand, N., Dommen, J. and Baltensperger, U.: Aqueous phase processing of secondary organic aerosol from isoprene photooxidation, Atmos. Chem. Phys., doi:10.5194/acp-12-5879-2012, 2012.
Lovelock, J. E., Maggs, R. J. and Rasmussen, R. A.: Atmospheric dimethyl sulphide and the natural sulphur cycle, Nature, doi:10.1038/237452a0, 1972.
Lund, M. T., Samset, B. H., Skeie, R. B., Watson-Parris, D., Katich, J. M., Schwarz, J. P. and Weinzierl, B.: Short Black Carbon lifetime inferred from a global set of aircraft observations, npj Clim. Atmos. Sci., doi:10.1038/s41612-018-0040-x, 2018.
Määttänen, A., Merikanto, J., Henschel, H., Duplissy, J., Makkonen, R., Ortega, I. K.

and Vehkamäki, H.: New Parameterizations for Neutral and Ion-Induced Sulfuric Acid-Water Particle Formation in Nucleation and Kinetic Regimes, J. Geophys. Res. Atmos., doi:10.1002/2017JD027429, 2018.
Mann, G. W., Carslaw, K. S., Spracklen, D. V., Ridley, D. A., Manktelow, P. T., Chipperfield, M. P., Pickering, S. J. and Johnson, C. E.: Description and evaluation of GLOMAP-mode: A modal global aerosol microphysics model for the UKCA composition-climate model, Geosci. Model Dev., doi:10.5194/gmd-3-519-2010, 2010.
Van Marle, M. J. E., Kloster, S., Magi, B. I., Marlon, J. R., Daniau, A. L., Field, R. D., Arneth, A., Forrest, M., Hantson, S., Kehrwald, N. M., Knorr, W., Lasslop, G., Li, F., Mangeon, S., Yue, C., Kaiser, J. W. and Van Der Werf, G. R.: Historic global biomass burning emissions for CMIP6 (BB4CMIP) based on merging satellite observations with proxies and fire models (1750-2015), Geosci. Model Dev., doi:10.5194/gmd-10-3329-2017, 2017.
McCoy, D. T., Burrows, S. M., Wood, R., Grosvenor, D. P., Elliott, S. M., Ma, P. L., Rasch, P. J. and Hartmann, D. L.: Natural aerosols explain seasonal and spatial patterns of Southern Ocean cloud albedo, Sci. Adv., doi:10.1126/sciadv.1500157, 2015.
McDuffie, E. E., Smith, S. J., O'Rourke, P., Tibrewal, K., Venkataraman, C., Marais, E. A., Zheng, B., Crippa, M., Brauer, M. and Martin, R. V.: A global anthropogenic emission inventory of atmospheric pollutants from sector- And fuel-specific sources (1970-2017): An application of the Community Emissions Data System (CEDS), Earth Syst. Sci. Data, doi:10.5194/essd-12-3413-2020, 2020.
McMurry, P. H. and Friedlander, S. K.: New particle formation in the presence of an aerosol, Atmos. Environ., doi:10.1016/0004-6981(79)90322-6, 1979.
Merikanto, J., Spracklen, D. V., Mann, G. W., Pickering, S. J. and Carslaw, K. S.: Impact of nucleation on global CCN, Atmos. Chem. Phys., doi:10.5194/acp-9-8601-2009, 2009.
Metzger, A., Verheggen, B., Dommen, J., Duplissy, J., Prevot, A. S. H., Weingartner, E., Riipinen, I., Kulmala, M., Spracklen, D. V., Carslaw, K. S. and Baltensperger, U.: Evidence for the role of organics in aerosol particle formation under atmospheric conditions, Proc. Natl. Acad. Sci. U. S. A., doi:10.1073/pnas.0911330107, 2010.
Mihalopoulos, N., Putaud, J. P., Nguyen, B. C. and Belviso, S.: Annual variation of atmospheric carbonyl sulfide in the marine atmosphere in the Southern Indian Ocean, J. Atmos. Chem., doi:10.1007/BF00048101, 1991.
Montzka, S. A., Calvert, P., Hall, B. D., Elkins, J. W., Conway, T. J., Tans, P. P. and Sweeney, C. S.: On the global distribution, seasonality, and budget of atmospheric carbonyl sulfide (COS) and some similarities to CO2, J. Geophys. Res. Atmos., doi:10.1029/2006JD007665, 2007.
Morgenstern, O., Braesicke, P., O'Connor, F. M., Bushell, A. C., Johnson, C. E., Osprey, S. M. and Pyle, J. A.: Evaluation of the new UKCA climate-composition model-Part 1: The stratosphere, Geosci. Model Dev., doi:10.5194/gmd-2-43-2009, 2009.
Mulcahy, J., Johnson, C., Jones, C., Povey, A., Scott, C., Sellar, A., Turnock, S., Woodhouse, M., Andrews, M., Bellouin, N., Browse, J., Carslaw, K., Dalvi, M., Folberth, G., Glover, M., Grosvenor, D., Hardacre, C., Hill, R., Johnson, B., Jones, A., Kipling, Z., Mann, G., Mollard, J., O'Connor, F., Palmieri, J., Reddington, C., Rumbold, S., Richardson, M., Schutgens, N. A., Stier, P., Stringer, M., Tang, Y., Walton, J., Woodward, S. and Yool, A.: Description and evaluation of aerosol in UKESM1 and HadGEM3-GC3.1 CMIP6 historical simulations, Geosci. Model Dev. Discuss., doi:10.5194/gmd-2019-357, 2020.

Mulcahy, J. P., Jones, C., Sellar, A., Johnson, B., Boutle, I. A., Jones, A., Andrews, T., Rumbold, S. T., Mollard, J., Bellouin, N., Johnson, C. E., Williams, K. D., Grosvenor, D. P. and McCoy, D. T.: Improved Aerosol Processes and Effective Radiative Forcing in HadGEM3 and UKESM1, J. Adv. Model. Earth Syst., doi:10.1029/2018MS001464, 2018.
Myhre, G., Shindell, D., Bréon, F.-M., Collins, W. D., Fuglestvedt, J., Huang, J., Koch, D., Lamarque, J.-F., Lee, D., Mendoza, B., Nakajima, T., Robock, a., Stephens, G., Takemura, T. and Zhan, H.: IPCC AR5 (2013) Chapter 8: Anthropogenic and Natural Radiative Forcing, in Climate Change 2013: The Physical Science Basis. Contribution of Working Group I to the Fifth Assessment Report of the Intergovernmental Panel on Climate Change., 2013.
Nadykto, A. B. and Yu, F.: Uptake of neutral polar vapor molecules by charged clusters/particles: Enhancement due to dipole-charge interaction, J. Geophys. Res. D Atmos., doi:10.1029/2003jd003664, 2003.
O'Connor, F. M., Johnson, C. E., Morgenstern, O., Abraham, N. L., Braesicke, P., Dalvi, M., Folberth, G. A., Sanderson, M. G., Telford, P. J., Voulgarakis, A., Young, P. J., Zeng, G., Collins, W. J. and Pyle, J. A.: Evaluation of the new UKCA climate-composition model-Part 2: The troposphere, Geosci. Model Dev., doi:10.5194/gmd-7-41-2014, 2014.
O'Donnell, D., Tsigaridis, K. and Feichter, J.: Estimating the direct and indirect effects of secondary organic aerosols using ECHAM5-HAM, Atmos. Chem. Phys., doi:10.5194/acp-11-8635-2011, 2011.
O'Dowd, C. D., Facchini, M. C., Cavalli, F., Ceburnis, D., Mircea, M., Decesari, S., Fuzzi, S., Young, J. Y. and Putaud, J. P.: Biogenically driven organic contribution to marine aerosol, Nature, doi:10.1038/nature02959, 2004.
Pai, S. J., Heald, C. L., Pierce, J. R., Farina, S. C., Marais, E. A., Jimenez, J. L., Campuzano-Jost, P., Nault, B. A., Middlebrook, A. M., Coe, H., Shilling, J. E., Bahreini, R., Dingle, J. H. and Vu, K.: An evaluation of global organic aerosol schemes using airborne observations, Atmos. Chem. Phys., doi:10.5194/acp-20-2637-2020, 2020.
Petroff, A. and Zhang, L.: Development and validation of a size-resolved particle dry deposition scheme for application in aerosol transport models, Geosci. Model Dev., doi:10.5194/gmd-3-753-2010, 2010.
Pham, M., Boucher, O. and Hauglustaine, D.: Changes in atmospheric sulfur burdens and concentrations and resulting radiative forcings under IPCC SRES emission scenarios for 1990-2100, J. Geophys. Res. D Atmos., doi:10.1029/2004JD005125, 2005.
Pierce, J. R.: Cosmic rays, aerosols, clouds, and climate: Recent findings from the CLOUD experiment, J. Geophys. Res., doi:10.1002/2017JD027475, 2017.
Pierce, J. R. and Adams, P. J.: Efficiency of cloud condensation nuclei formation from ultrafine particles, Atmos. Chem. Phys., doi:10.5194/acp-7-1367-2007, 2007.
Pierce, J. R., Leaitch, W. R., Liggio, J., Westervelt, D. M., Wainwright, C. D., Abbatt, J. P. D., Ahlm, L., Al-Basheer, W., Cziczo, D. J., Hayden, K. L., Lee, A. K. Y., Li, S. M., Russell, L. M., Sjostedt, S. J., Strawbridge, K. B., Travis, M., Vlasenko, A., Wentzell, J. J. B., Wiebe, H. A., Wong, J. P. S. and MacDonald, A. M.: Nucleation and condensational growth to CCN sizes during a sustained pristine biogenic SOA event in a forested mountain valley, Atmos. Chem. Phys., doi:10.5194/acp-12-3147-2012, 2012.
Prein, A. F., Langhans, W., Fosser, G., Ferrone, A., Ban, N., Goergen, K., Keller, M., Tölle, M., Gutjahr, O., Feser, F., Brisson, E., Kollet, S., Schmidli, J., Van Lipzig, N. P. M. and Leung, R.: A review on regional convection-permitting climate modeling:

Demonstrations, prospects, and challenges, Rev. Geophys., doi:10.1002/2014RG000475, 2015.
Ranjithkumar, A., Gordon, H., Williamson, C., Rollins, A., Pringle, K., Kupc, A., Luke Abraham, N., Brock, C. and Carslaw, K.: Constraints on global aerosol number concentration, SO2and condensation sink in UKESM1 using ATom measurements, Atmos. Chem. Phys., doi:10.5194/acp-21-4979-2021, 2021.
Rap, A., Scott, C. E., Spracklen, D. V., Bellouin, N., Forster, P. M., Carslaw, K. S., Schmidt, A. and Mann, G.: Natural aerosol direct and indirect radiative effects, Geophys. Res. Lett., doi:10.1002/grl.50441, 2013.
Regayre, L., Schmale, J., Johnson, J., Tatzelt, C., Baccarini, A., Henning, S., Yoshioka, M., Stratmann, F., Gysel-Beer, M. and Carslaw, K.: The value of remote marine aerosol measurements for constraining radiative forcing uncertainty, Atmos. Chem. Phys., doi:10.5194/acp-2019-1085, 2019.
Regayre, L., Schmale, J., Johnson, J., Tatzelt, C., Baccarini, A., Henning, S., Yoshioka, M., Stratmann, F., Gysel-Beer, M. and Carslaw, K.: The value of remote marine aerosol measurements for constraining radiative forcing uncertainty, Atmos. Chem. Phys., 1–11, doi:10.5194/acp-2019-1085, 2020.
Regayre, L. A., Johnson, J. S., Yoshioka, M., Pringle, K. J., Sexton, D. M. H., Booth, B. B. B., Lee, L. A., Bellouin, N. and Carslaw, K. S.: Aerosol and physical atmosphere model parameters are both important sources of uncertainty in aerosol ERF, Atmos. Chem. Phys., doi:10.5194/acp-18-9975-2018, 2018.
Riccobono, F., Schobesberger, S., Scott, C. E., Dommen, J., Ortega, I. K., Rondo, L., Almeida, J., Amorim, A., Bianchi, F., Breitenlechner, M., David, A., Downard, A., Dunne, E. M., Duplissy, J., Ehrhart, S., Flagan, R. C., Franchin, A., Hansel, A., Junninen, H., Kajos, M., Keskinen, H., Kupc, A., Kürten, A., Kvashin, A. N., Laaksonen, A., Lehtipalo, K., Makhmutov, V., Mathot, S., Nieminen, T., Onnela, A., Petäjä, T., Praplan, A. P., Santos, F. D., Schallhart, S., Seinfeld, J. H., Sipilä, M., Spracklen, D. V., Stozhkov, Y., Stratmann, F., Tomé, A., Tsagkogeorgas, G., Vaattovaara, P., Viisanen, Y., Vrtala, A., Wagner, P. E., Weingartner, E., Wex, H., Wimmer, D., Carslaw, K. S., Curtius, J., Donahue, N. M., Kirkby, J., Kulmala, M., Worsnop, D. R. and Baltensperger, U.: Oxidation products of biogenic emissions contribute to nucleation of atmospheric particles, Science (80-.)., doi:10.1126/science.1243527, 2014.
Ridley, J. K., Blockley, E. W., Keen, A. B., Rae, J. G. L., West, A. E. and Schroeder, D.: The sea ice model component of HadGEM3-GC3.1, Geosci. Model Dev., doi:10.5194/gmd-11-713-2018, 2018.
Rollins, A. W., Thornberry, T. D., Ciciora, S. J., McLaughlin, R. J., Watts, L. A., Hanisco, T. F., Baumann, E., Giorgetta, F. R., Bui, T. V. and Fahey, D. W.: A laser-induced fluorescence instrument for aircraft measurements of sulfur dioxide in the upper troposphere and lower stratosphere, Atmos. Meas. Tech., doi:10.5194/amt-9-4601-2016, 2016.
Russell, L. M., Hawkins, L. N., Frossard, A. A., Quinn, P. K. and Bates, T. S.: Carbohydrate-like composition of submicron atmospheric particles and their production from ocean bubble bursting, Proc. Natl. Acad. Sci. U. S. A., doi:10.1073/pnas.0908905107, 2010.
Samset, B. H., Myhre, G., Herber, A., Kondo, Y., Li, S. M., Moteki, N., Koike, M., Oshima, N., Schwarz, J. P., Balkanski, Y., Bauer, S. E., Bellouin, N., Berntsen, T. K., Bian, H., Chin, M., Diehl, T., Easter, R. C., Ghan, S. J., Iversen, T., Kirkeväg, A., Lamarque, J. F., Lin, G., Liu, X., Penner, J. E., Schulz, M., Seland, Skeie, R. B., Stier, P., Takemura, T., Tsigaridis, K. and Zhang, K.: Modelled black carbon radiative forcing and atmospheric lifetime in AeroCom Phase II constrained by aircraft

observations, Atmos. Chem. Phys., 14(22), 12465–12477, doi:10.5194/acp-14-12465-2014, 2014.
Samset, B. H., Stjern, C. W., Andrews, E., Kahn, R. A., Myhre, G., Schulz, M. and Schuster, G. L.: Aerosol Absorption: Progress Towards Global and Regional Constraints, Curr. Clim. Chang. Reports, doi:10.1007/s40641-018-0091-4, 2018.
Schill, G. P., Froyd, K. D., Bian, H., Kupc, A., Williamson, C., Brock, C. A., Ray, E., Hornbrook, R. S., Hills, A. J., Apel, E. C., Chin, M., Colarco, P. R. and Murphy, D. M.: Widespread biomass burning smoke throughout the remote troposphere, Nat. Geosci., doi:10.1038/s41561-020-0586-1, 2020.
Schmidt, G. A., Ruedy, R. A., Miller, R. L. and Lacis, A. A.: Attribution of the present-day total greenhouse effect, J. Geophys. Res. Atmos., 115(20), 1–6, doi:10.1029/2010JD014287, 2010.
Schutgens, N. A. J., Gryspeerdt, E., Weigum, N., Tsyro, S., Goto, D., Schulz, M. and Stier, P.: Will a perfect model agree with perfect observations? The impact of spatial sampling, Atmos. Chem. Phys., doi:10.5194/acp-16-6335-2016, 2016.
Scott, C. E., Rap, A., Spracklen, D. V., Forster, P. M., Carslaw, K. S., Mann, G. W., Pringle, K. J., Kivekäs, N., Kulmala, M., Lihavainen, H. and Tunved, P.: The direct and indirect radiative effects of biogenic secondary organic aerosol, Atmos. Chem. Phys., doi:10.5194/acp-14-447-2014, 2014.
Seinfeld, J. H. and Pandis, S. N.: Atmospheric Chemistry and physics, From air Pollution to Climate Change, , Third edit, 465, 2016.
Sellar, A. A., Jones, C. G., Mulcahy, J., Tang, Y., Yool, A., Wiltshire, A., O'Connor, F. M., Stringer, M., Hill, R., Palmieri, J., Woodward, S., Mora, L., Kuhlbrodt, T., Rumbold, S., Kelley, D. I., Ellis, R., Johnson, C. E., Walton, J., Abraham, N. L., Andrews, M. B., Andrews, T., Archibald, A. T., Berthou, S., Burke, E., Blockley, E., Carslaw, K., Dalvi, M., Edwards, J., Folberth, G. A., Gedney, N., Griffiths, P. T., Harper, A. B., Hendry, M. A., Hewitt, A. J., Johnson, B., Jones, A., Jones, C. D., Keeble, J., Liddicoat, S., Morgenstern, O., Parker, R. J., Predoi, V., Robertson, E., Siahaan, A., Smith, R. S., Swaminathan, R., Woodhouse, M. T., Zeng, G. and Zerroukat, M.: UKESM1: Description and evaluation of the UK Earth System Model, J. Adv. Model. Earth Syst., doi:10.1029/2019ms001739, 2019.
Sengupta, K., Pringle, K., Johnson, J. S., Reddington, C., Browse, J., Scott, C. E. and Carslaw, K.: A global model perturbed parameter ensemble study of secondary organic aerosol formation, Atmos. Chem. Phys., doi:10.5194/acp-21-2693-2021, 2021.
Sherwood, S. C., Webb, M. J., Annan, J. D., Armour, K. C., Forster, P. M., Hargreaves, J. C., Hegerl, G., Klein, S. A., Marvel, K. D., Rohling, E. J., Watanabe, M., Andrews, T., Braconnot, P., Bretherton, C. S., Foster, G. L., Hausfather, Z., von der Heydt, A. S., Knutti, R., Mauritsen, T., Norris, J. R., Proistosescu, C., Rugenstein, M., Schmidt, G. A., Tokarska, K. B. and Zelinka, M. D.: An Assessment of Earth's Climate Sensitivity Using Multiple Lines of Evidence, Rev. Geophys., doi:10.1029/2019RG000678, 2020a.
Sherwood, S. C., Webb, M. J., Annan, J. D., Armour, K. C., Forster, P. M., Hargreaves, J. C., Hegerl, G., Klein, S. A., Marvel, K. D., Rohling, E. J., Watanabe, M., Andrews, T., Braconnot, P., Bretherton, C. S., Foster, G. L., Hausfather, Z., von der Heydt, A. S., Knutti, R., Mauritsen, T., Norris, J. R., Proistosescu, C., Rugenstein, M., Schmidt, G. A., Tokarska, K. B. and Zelinka, M. D.: An Assessment of Earth's Climate Sensitivity Using Multiple Lines of Evidence, Rev. Geophys., 58(4), 1–92, doi:10.1029/2019RG000678, 2020b.
Sindelarova, K., Granier, C., Bouarar, I., Guenther, A., Tilmes, S., Stavrakou, T., Müller, J. F., Kuhn, U., Stefani, P. and Knorr, W.: Global data set of biogenic VOC

emissions calculated by the MEGAN model over the last 30 years, Atmos. Chem. Phys., doi:10.5194/acp-14-9317-2014, 2014.
Singh, H. B., Brune, W. H., Crawford, J. H., Jacob, D. J. and Russell, P. B.: Overview of the summer 2004 Intercontinental Chemical Transport Experiment-North America (INTEX-A), J. Geophys. Res. Atmos., doi:10.1029/2006JD007905, 2006.
Spiro, P. A., Jacob, D. J. and Logan, J. A.: Global inventory of sulfur emissions with 1° × 1° resolution, J. Geophys. Res., doi:10.1029/91JD03139, 1992.
Spracklen, D. V., Carslaw, K. S., Kulmala, M., Kerminen, V. M., Mann, G. W. and Sihto, S. L.: The contribution of boundary layer nucleation events to total particle concentrations on regional and global scales, Atmos. Chem. Phys., doi:10.5194/acp-6-5631-2006, 2006.
Storkey, D., Blaker, A. T., Mathiot, P., Megann, A., Aksenov, Y., Blockley, E. W., Calvert, D., Graham, T., Hewitt, H. T., Hyder, P., Kuhlbrodt, T., Rae, J. G. L. and Sinha, B.: UK Global Ocean GO6 and GO7: A traceable hierarchy of model resolutions, Geosci. Model Dev., doi:10.5194/gmd-11-3187-2018, 2018.
T Archibald, A., M O'Connor, F., Luke Abraham, N., Archer-Nicholls, S., P Chipperfield, M., Dalvi, M., A Folberth, G., Dennison, F., S Dhomse, S., T Griffiths, P., Hardacre, C., J Hewitt, A., S Hill, R., E Johnson, C., Keeble, J., O Köhler, M., Morgenstern, O., P Mulcahy, J., Ordóñez, C., J Pope, R., T Rumbold, S., R Russo, M., H Savage, N., Sellar, A., Stringer, M., T Turnock, S., Wild, O. and Zeng, G.: Description and evaluation of the UKCA stratosphere-troposphere chemistry scheme (StratTrop vn 1.0) implemented in UKESM1, Geosci. Model Dev., doi:10.5194/gmd-13-1223-2020, 2020.
Telford, P. J., Braesicke, P., Morgenstern, O. and Pyle, J. A.: Technical note: Description and assessment of a nudged version of the new dynamics Unified Model, Atmos. Chem. Phys., doi:10.5194/acp-8-1701-2008, 2008.
Teng, A. P., Crounse, J. D. and Wennberg, P. O.: Isoprene Peroxy Radical Dynamics, J. Am. Chem. Soc., doi:10.1021/jacs.6b12838, 2017.
Tröstl, J., Chuang, W. K., Gordon, H., Heinritzi, M., Yan, C., Molteni, U., Ahlm, L., Frege, C., Bianchi, F., Wagner, R., Simon, M., Lehtipalo, K., Williamson, C., Craven, J. S., Duplissy, J., Adamov, A., Almeida, J., Bernhammer, A. K., Breitenlechner, M., Brilke, S., Dias, A., Ehrhart, S., Flagan, R. C., Franchin, A., Fuchs, C., Guida, R., Gysel, M., Hansel, A., Hoyle, C. R., Jokinen, T., Junninen, H., Kangasluoma, J., Keskinen, H., Kim, J., Krapf, M., Kürten, A., Laaksonen, A., Lawler, M., Leiminger, M., Mathot, S., Möhler, O., Nieminen, T., Onnela, A., Petäjä, T., Piel, F. M., Miettinen, P., Rissanen, M. P., Rondo, L., Sarnela, N., Schobesberger, S., Sengupta, K., Sipilä, M., Smith, J. N., Steiner, G., Tomè, A., Virtanen, A., Wagner, A. C., Weingartner, E., Wimmer, D., Winkler, P. M., Ye, P., Carslaw, K. S., Curtius, J., Dommen, J., Kirkby, J., Kulmala, M., Riipinen, I., Worsnop, D. R., Donahue, N. M. and Baltensperger, U.: The role of low-volatility organic compounds in initial particle growth in the atmosphere, Nature, doi:10.1038/nature18271, 2016.
Tsigaridis, K., Daskalakis, N., Kanakidou, M., Adams, P. J., Artaxo, P., Bahadur, R., Balkanski, Y., Bauer, S. E., Bellouin, N., Benedetti, A., Bergman, T., Berntsen, T. K., Beukes, J. P., Bian, H., Carslaw, K. S., Chin, M., Curci, G., Diehl, T., Easter, R. C., Ghan, S. J., Gong, S. L., Hodzic, A., Hoyle, C. R., Iversen, T., Jathar, S., Jimenez, J. L., Kaiser, J. W., Kirkeväg, A., Koch, D., Kokkola, H., H Lee, Y., Lin, G., Liu, X., Luo, G., Ma, X., Mann, G. W., Mihalopoulos, N., Morcrette, J. J., Müller, J. F., Myhre, G., Myriokefalitakis, S., Ng, N. L., O'donnell, D., Penner, J. E., Pozzoli, L., Pringle, K. J., Russell, L. M., Schulz, M., Sciare, J., Seland, Shindell, D. T., Sillman, S., Skeie, R. B., Spracklen, D., Stavrakou, T., Steenrod, S. D., Takemura, T., Tiitta, P., Tilmes, S., Tost, H., Van Noije, T., Van Zyl, P. G., Von Salzen, K., Yu, F., Wang,

Z., Wang, Z., Zaveri, R. A., Zhang, H., Zhang, K., Zhang, Q. and Zhang, X.: The AeroCom evaluation and intercomparison of organic aerosol in global models, Atmos. Chem. Phys., doi:10.5194/acp-14-10845-2014, 2014.
Tsui, W. G., Woo, J. L. and McNeill, V. F.: Impact of aerosol-cloud cycling on aqueous secondary organic aerosol formation, Atmosphere (Basel)., doi:10.3390/atmos10110666, 2019.
Twomey, S.: The Influence of Pollution on the Shortwave Albedo of Clouds, J. Atmos. Sci., doi:10.1175/1520-0469(1977)034<1149:tiopot>2.0.co;2, 1977.
Vehkamäki, H. and Riipinen, I.: Thermodynamics and kinetics of atmospheric aerosol particle formation and growth, Chem. Soc. Rev., doi:10.1039/c2cs00002d, 2012.
Vehkamäki, H., Kulmala, M., Napari, I., Lehtinen, K. E. J., Timmreck, C., Noppel, M. and Laaksonen, A.: An improved parameterization for sulfuric acid-water nucleation rates for tropospheric and stratospheric conditions, J. Geophys. Res. Atmos., doi:10.1029/2002JD002184, 2002.
Veres, P. R., Andrew Neuman, J., Bertram, T. H., Assaf, E., Wolfe, G. M., Williamson, C. J., Weinzierl, B., Tilmes, S., Thompson, C. R., Thames, A. B., Schroder, J. C., Saiz-Lopez, A., Rollins, A. W., Roberts, J. M., Price, D., Peischl, J., Nault, B. A., Møller, K. H., Miller, D. O., Meinardi, S., Li, Q., Lamarque, J. F., Kupc, A., Kjaergaard, H. G., Kinnison, D., Jimenez, J. L., Jernigan, C. M., Hornbrook, R. S., Hills, A., Dollner, M., Day, D. A., Cuevas, C. A., Campuzano-Jost, P., Burkholder, J., Paul Bui, T., Brune, W. H., Brown, S. S., Brock, C. A., Bourgeois, I., Blake, D. R., Apel, E. C. and Ryerson, T. B.: Global airborne sampling reveals a previously unobserved dimethyl sulfide oxidation mechanism in the marine atmosphere, Proc. Natl. Acad. Sci. U. S. A., doi:10.1073/pnas.1919344117, 2020.
Walters, D., Boutle, I., Brooks, M., Melvin, T., Stratton, R., Vosper, S., Wells, H., Williams, K., Wood, N., Allen, T., Bushell, A., Copsey, D., Earnshaw, P., Edwards, J., Gross, M., Hardiman, S., Harris, C., Heming, J., Klingaman, N., Levine, R., Manners, J., Martin, G., Milton, S., Mittermaier, M., Morcrette, C., Riddick, T., Roberts, M., Sanchez, C., Selwood, P., Stirling, A., Smith, C., Suri, D., Tennant, W., Luigi Vidale, P., Wilkinson, J., Willett, M., Woolnough, S. and Xavier, P.: The Met Office Unified Model Global Atmosphere 6.0/6.1 and JULES Global Land 6.0/6.1 configurations, Geosci. Model Dev., doi:10.5194/gmd-10-1487-2017, 2017.
Wang, M., Kong, W., Marten, R., He, X. C., Chen, D., Pfeifer, J., Heitto, A., Kontkanen, J., Dada, L., Kürten, A., Yli-Juuti, T., Manninen, H. E., Amanatidis, S., Amorim, A., Baalbaki, R., Baccarini, A., Bell, D. M., Bertozzi, B., Bräkling, S., Brilke, S., Murillo, L. C., Chiu, R., Chu, B., De Menezes, L. P., Duplissy, J., Finkenzeller, H., Carracedo, L. G., Granzin, M., Guida, R., Hansel, A., Hofbauer, V., Krechmer, J., Lehtipalo, K., Lamkaddam, H., Lampimäki, M., Lee, C. P., Makhmutov, V., Marie, G., Mathot, S., Mauldin, R. L., Mentler, B., Müller, T., Onnela, A., Partoll, E., Petäjä, T., Philippov, M., Pospisilova, V., Ranjithkumar, A., Rissanen, M., Rörup, B., Scholz, W., Shen, J., Simon, M., Sipilä, M., Steiner, G., Stolzenburg, D., Tham, Y. J., Tomé, A., Wagner, A. C., Wang, D. S., Wang, Y., Weber, S. K., Winkler, P. M., Wlasits, P. J., Wu, Y., Xiao, M., Ye, Q., Zauner-Wieczorek, M., Zhou, X., Volkamer, R., Riipinen, I., Dommen, J., Curtius, J., Baltensperger, U., Kulmala, M., Worsnop, D. R., Kirkby, J., Seinfeld, J. H., El-Haddad, I., Flagan, R. C. and Donahue, N. M.: Rapid growth of new atmospheric particles by nitric acid and ammonia condensation, Nature, 581(7807), 184–189, doi:10.1038/s41586-020-2270-4, 2020.
Ward, D. S., Shevliakova, E., Malyshev, S., Lamarque, J. F. and Wittenberg, A. T.: Variability of fire emissions on interannual to multi-decadal timescales in two Earth System models, Environ. Res. Lett., doi:10.1088/1748-9326/11/12/125008, 2016.

Warren, S. G. and Wiscombe, W. J.: A model for the spectral albedo of snow. II: snow containing atmospheric aerosols., J. Atmos. Sci., doi:10.1175/1520-0469(1980)037<2734:AMFTSA>2.0.CO;2, 1980.
Watson-Parris, D., Schutgens, N., Reddington, C., Pringle, K. J., Liu, D., Allan, J. D., Coe, H., Carslaw, K. S. and Stier, P.: In situ constraints on the vertical distribution of global aerosol, Atmos. Chem. Phys., doi:10.5194/acp-19-11765-2019, 2019.
Williamson, C., Kupc, A., Wilson, J., Gesler, D. W., Michael Reeves, J., Erdesz, F., McLaughlin, R. and Brock, C. A.: Fast time response measurements of particle size distributions in the 3-60ĝ€nm size range with the nucleation mode aerosol size spectrometer, Atmos. Meas. Tech., doi:10.5194/amt-11-3491-2018, 2018.
Williamson, C. J., Kupc, A., Axisa, D., Bilsback, K. R., Bui, T. P., Campuzano-Jost, P., Dollner, M., Froyd, K. D., Hodshire, A. L., Jimenez, J. L., Kodros, J. K., Luo, G., Murphy, D. M., Nault, B. A., Ray, E. A., Weinzierl, B., Wilson, J. C., Yu, F., Yu, P., Pierce, J. R. and Brock, C. A.: A large source of cloud condensation nuclei from new particle formation in the tropics, Nature, doi:10.1038/s41586-019-1638-9, 2019.
Wilson, D. R., Bushell, A. C., Kerr-Munslow, A. M., Price, J. D. and Morcrette, C. J.: PC2: A prognostic cloud fraction and condensation scheme. I: Scheme description, Q. J. R. Meteorol. Soc., doi:10.1002/qj.333, 2008.
Wofsy, S. C. and S. Afshar, H.M. Allen, E.C. Apel, E.C. Asher, B. Barletta, J. Bent, H. Bian, B.C. Biggs, D.R. Blake, N. Blake, I. Bourgeois, C.A. Brock, W.H. Brune, J.W. Budney, T.P. Bui, A. Butler, P. Campuzano-Jost, C.S. Chang, M. Chin, R. Commane, G. Corr, and L. H. Z.: ATom: merged atmospheric chemistry, trace gases, and aerosols, ORNL DAAC, https://da, 2018.
Wood, R., Mechoso, C. R., Bretherton, C. S., Weller, R. A., Huebert, B., Straneo, F., Albrecht, B. A., Coe, H., Allen, G., Vaughan, G., Daum, P., Fairall, C., Chand, D., Gallardo Klenner, L., Garreaud, R., Grados, C., Covert, D. S., Bates, T. S., Krejci, R., Russell, L. M., De Szoeke, S., Brewer, A., Yuter, S. E., Springston, S. R., Chaigneau, A., Toniazzo, T., Minnis, P., Palikonda, R., Abel, S. J., Brown, W. O. J., Williams, S., Fochesatto, J., Brioude, J. and Bower, K. N.: The VAMOS ocean-cloud-atmosphere-land study regional experiment (VOCALS-REx): Goals, platforms, and field operations, Atmos. Chem. Phys., doi:10.5194/acp-11-627-2011, 2011.
Woodward, S.: Modeling the atmospheric life cycle and radiative impact of mineral dust in the Hadley Centre climate model, J. Geophys. Res. Atmos., doi:10.1029/2000JD900795, 2001.
Yin, Y., Carslaw, K. S. and Parker, D. J.: Redistribution of trace gases by convective clouds - Mixed-phase processes, Atmos. Chem. Phys., doi:10.5194/acp-2-293-2002, 2002.
Yoshioka, M., Regayre, L. A., Pringle, K. J., Johnson, J. S., Mann, G. W., Partridge, D. G., Sexton, D. M. H., Lister, G. M. S., Schutgens, N., Stier, P., Kipling, Z., Bellouin, N., Browse, J., Booth, B. B. B., Johnson, C. E., Johnson, B., Mollard, J. D. P., Lee, L. and Carslaw, K. S.: Ensembles of Global Climate Model Variants Designed for the Quantification and Constraint of Uncertainty in Aerosols and Their Radiative Forcing, J. Adv. Model. Earth Syst., doi:10.1029/2019MS001628, 2019.
Yu, F. and Luo, G.: Simulation of particle size distribution with a global aerosol model: Contribution of nucleation to aerosol and CCN number concentrations, Atmos. Chem. Phys., doi:10.5194/acp-9-7691-2009, 2009.
Yu, P., Froyd, K. D., Portmann, R. W., Toon, O. B., Freitas, S. R., Bardeen, C. G., Brock, C., Fan, T., Gao, R. S., Katich, J. M., Kupc, A., Liu, S., Maloney, C., Murphy, D. M., Rosenlof, K. H., Schill, G., Schwarz, J. P. and Williamson, C.: Efficient In-Cloud Removal of Aerosols by Deep Convection, Geophys. Res. Lett., doi:10.1029/2018GL080544, 2019.

Yu, S., Eder, B., Dennis, R., Chu, S.-H. and Schwartz, S. E.: New unbiased symmetric metrics for evaluation of air quality models, Atmos. Sci. Lett., doi:10.1002/asl.125, 2006.
Zeng, L., Zhang, A., Wang, Y., Wagner, N. L., Katich, J. M., Schwarz, J. P., Schill, G. P., Brock, C., Froyd, K. D., Murphy, D. M., Williamson, C. J., Kupc, A., Scheuer, E., Dibb, J. and Weber, R. J.: Global Measurements of Brown Carbon and Estimated Direct Radiative Effects, Geophys. Res. Lett., doi:10.1029/2020GL088747, 2020.
Zhang, K., Wan, H., Liu, X., Ghan, S. J., Kooperman, G. J., Ma, P. L., Rasch, P. J., Neubauer, D. and Lohmann, U.: Technical note: On the use of nudging for aerosol-climate model intercomparison studies, Atmos. Chem. Phys., doi:10.5194/acp-14-8631-2014, 2014.